



5-2007

Bioengineering of Protein Nanotubes and Protein Nanomaterial Composites

Thilak Kumara Mudalige
Western Michigan University

Follow this and additional works at: <https://scholarworks.wmich.edu/dissertations>



Part of the Chemistry Commons

Recommended Citation

Mudalige, Thilak Kumara, "Bioengineering of Protein Nanotubes and Protein Nanomaterial Composites" (2007). *Dissertations*. 899.

<https://scholarworks.wmich.edu/dissertations/899>

This Dissertation-Open Access is brought to you for free and open access by the Graduate College at ScholarWorks at WMU. It has been accepted for inclusion in Dissertations by an authorized administrator of ScholarWorks at WMU. For more information, please contact wmu-scholarworks@wmich.edu.



BIOENGINEERING OF PROTEIN NANOTUBES AND PROTEIN-
NANOMATERIAL COMPOSITES

by

Thilak Kumara Mudalige

A Dissertation
Submitted to the
Faculty of The Graduate College
in partial fulfillment of the
requirements for the
Degree of Doctor of Philosophy
Department of Chemistry

Western Michigan University
Kalamazoo, Michigan
May 2007

UMI Number: 3265909

INFORMATION TO USERS

The quality of this reproduction is dependent upon the quality of the copy submitted. Broken or indistinct print, colored or poor quality illustrations and photographs, print bleed-through, substandard margins, and improper alignment can adversely affect reproduction.

In the unlikely event that the author did not send a complete manuscript and there are missing pages, these will be noted. Also, if unauthorized copyright material had to be removed, a note will indicate the deletion.

UMI[®]

UMI Microform 3265909

Copyright 2007 by ProQuest Information and Learning Company.

All rights reserved. This microform edition is protected against unauthorized copying under Title 17, United States Code.

ProQuest Information and Learning Company
300 North Zeeb Road
P.O. Box 1346
Ann Arbor, MI 48106-1346

Copyright by
Thilak Kumara Mudalige
2007

ACKNOWLEDGMENTS

First, I would like to thank my research advisors Professor Subra Muralidharan and Professor Brian C. Tripp for their guidance, support, dedication and patience through my research.

Next, I would like to gratefully thank my committee members Professor Yirong Mo, Professor Dongil Lee and Professor Nora Berrah for taking time to review my work and for valuable advice. I would also like to thank the help and advice from Professor Karim Essani and Professor Robert Eversole of the Biological Sciences Department. This work would not have been possible without the love and affection of my parents and my wife Sulari.

This research was supported by the Nanotechnology Research and Computation Center at Western Michigan University, Michigan Life Science Corridor, W. M. Keck Foundation, and Western Michigan University President's Innovation Fund.

Thilak Kumara Mudalige

TABLE OF CONTENTS

ACKNOWLEDGMENTS	ii
LIST OF TABLES	ix
LIST OF FIGURES.....	x
CHAPTER	
I. INTRODUCTION	1
Central Hypothesis	1
Scope of This Research Dissertation	1
Bionanotube in Nanotechnology	2
Advantages of Bacterial Flagella over Other Systems	3
Structure of Bacterial Flagella.....	6
II. GENERATION AND CHARACTERIZATION OF INORGANIC AND ORGANIC NANOTUBES ON BIOENGINEERED FLAGELLA OF MESOPHILIC BACTERIA	11
Introduction	11
Experimental Methods	12
Materials and Methods.....	12
Preparation of FliTrx Engineered Loop Peptide Flagella for Use as Nanotube Scaffolds	13
Synthesis of Silica Nanotubes on Cationic Arginine-Lysine Loop Flagella Scaffold.....	17
Synthesis of Titanium Dioxide Nanotubes on Tyrosine- Serine-Glycine Loop Flagella Scaffold.....	18

Table of Content—Continued

CHAPTER		
	Synthesis of Hydroxyapatite Nanotubes on Anionic Aspartate-Glutamate Loop Flagella Scaffold.....	18
	Synthesis of Polyaniline Nanowires on Anionic Aspartate-Glutamate Loop Flagella Scaffold	19
	Results and Discussion.....	20
	Silica Biomineralization on Cationic Arginine-Lysine Loop Flagella Scaffolds.....	20
	Titania Biomineralization on Phenolic Tyrosine Loop Flagella Scaffold	23
	Hydroxyapatite Biomineralization on Anionic-Aspartate-Glutamate Flagella Scaffold.....	26
	Polyaniline Biomineralization on Anionic Aspartate-Glutamate Flagella Scaffold.....	29
	Conclusion.....	29
III.	EXCITON ENERGY TRANSFER IN SELF-ASSEMBLED QUANTUM DOTS ON BIOENGINEERED BACTERIAL FLAGELLA NANOTUBES	32
	Introduction	32
	Materials and Methods	34
	Results and Discussion.....	37
	Conclusion.....	45
IV.	SELF-ASSEMBLY OF METAL NANOPARTICLES AND NANOTUBES ON BIOENGINEERED FLAGELLA SCAFFOLDS.....	46
	Introduction	46
	Experimental Methods	49

Table of Content—Continued

CHAPTER

Materials	49
Engineering of FliTrx Flagella Loop Peptide Variants for Use as Bionanotube Scaffolds and Templates	49
Generation of Nanoparticle Arrays and Nanotubes on Flagella with Peptide Loops.....	51
Generation of Gold Nanoparticle Arrays on Histidine Loop Flagella.....	51
Covalent Attachment of Gold Nanoparticles to Arginine- Lysine Loop Flagella.....	52
Generation of Copper Nanoparticle Arrays and Nanowires on Histidine Loop Flagella.....	53
Generation of Copper Nanoparticle Arrays and Nanowires on Histidine Loop Flagella.....	53
Generation of Palladium and Cadmium Nanoparticles on Aspartic Acid-Glutamic Acid Loop Flagella	55
Generation of Silver Nanowires on Aspartic Acid-Glutamic Acid Loop Flagella.....	55
Results and Discussion.....	55
Generation of Gold Nanoparticle Arrays on Histidine Loop Flagella	56
Covalent Attachment of Gold Nanoparticles to Arginine- Lysine Loop Flagella.....	60
Generation of Copper Nanoparticle Arrays and Nanowires on Histidine Loop Flagella.....	63
Generation of Cobalt Nanoparticles on Histidine Loop Flagella.....	66

Table of Content—Continued

CHAPTER		
	Generation of Palladium and Cadmium Nanoparticles on Aspartic Acid-Glutamic Acid Loop Flagella	68
	Generation of Silver Nanowires on Aspartic Acid-Glutamic Acid Loop Flagella.....	69
	Conclusion.....	70
V.	BIOENGINEERED FLAGELLA PROTEIN NANOTUBES WITH CYSTEINE LOOPS: SELF-ASSEMBLY AND MANIPULATION IN AN OPTICAL TRAP	74
	Introduction	74
	Experimental Methods	75
	Materials	75
	Construction of FliTrx Polycysteine Loop Display Vector.....	76
	Construction of FliTrx Peptide Loop Variants	78
	FliTrx Flagellin Protein Expression and Purification	79
	Fluorescence Imaging and Laser Tweezer Manipulation of Flagella Bundle	80
	Isolation and Expression Tolerance of Flagellin Loop Variants.....	82
	Optical Trapping of Flagella Bundles.....	88
	Conclusion.....	90
VI.	LAYER BY LAYER ASSEMBLY OF BIOENGINEERED FLAGELLA NANOTUBE FILM AND BIOMINERALIZATION	92
	Introduction	92
	Experimental Procedures	94

Table of Content—Continued

CHAPTER		
	Materials	94
	Preparation of amine terminated mixed self-assembled monolayers on Au(111) surface	95
	Biotinylation of thiol self assembled monolayers	95
	Biotinylation of flagella	96
	Layer-by-Layer Assembly of Streptavidin and Flagella.....	96
	Layer-by-Layer Assembly of Polyamines and Flagella.....	97
	CaCO ₃ Mineralization on Flagella	98
	Results and Discussion.....	98
VII.	FUTURE DIRECTIONS	105
	Assembly of Multifunctional Bio-Nanotubes and Their Applications	105
	Display of Gold, Silver, and Titanium Binding Peptides and Generation of Gold Nanowires.....	106
	Synthesis and Applications of Transition Metal Alloy Nanoparticles on Flagella Scaffold.....	106
	Application of Self-Assembled Nanoparticles on Flagella as an Optical Waveguide System	107
	Synthesis of Doped Semiconductor Quantum Dots on Flagella Scaffold and Study of Their Properties with Fluorescence and Electron Spin Resonance.....	107
	Fluorescence Detection of Flagella Self-Assembly Process and Use of Dye and Quantum Dots Labeled Flagella as Antenna for Harvesting Solar Light.....	108

Table of Content—Continued

CHAPTER	
	Generation of Millimeter Length Flagella Wires with a Microfluidic System and Characterization of its Mechanical Properties..... 109
REFERENCES	111
APPENDIX	
	DNA PRIMERS AND RESULTED DNA SEQUENCES 129

LIST OF TABLES

4.1 Summary of Nanomaterials Prepared in This Study Using Engineered Flagella Nanotubes as Scaffolds.....	72
--	----

LIST OF FIGURES

1.1 TEM image of flagella and part of bacteria stained with 2% neutral phosphotungstic acid	5
1.2 Diagram of flagellin protein monomer structure	8
2.1 Silica biomineralization on flagella scaffold with tetraethoxysilane as silica source	21
2.2 Silica biomineralization on flagella scaffold with sodium silicate as silica source	22
2.3 TiO ₂ nanotube synthesized on flagella scaffold.....	24
2.4 Schematic illustration synthesis of titania nanotube by sol-gel process	25
2.5 Apatite nanocrystals synthesized on flagella scaffold after 10 minutes exposure to mineralization solution.....	26
2.6 Apatite nanocrystals synthesized on flagella scaffold after 20 minutes exposure to mineralization solution.....	27
2.7 TEM images of polyaniline synthesized on flagella scaffold.....	30
2.8 SEM images of Polyaniline synthesized on flagella scaffold.....	31
3.1 TEM image of ZnS:Mn nanoparticles immobilized on histidine loop flagella scaffold	39
3.2 Normalized absorbance and emission spectra of ZnS:Mn QDs nanoparticles self-assembled on His-loop flagella nanotubes	40
3.3 Absorbance spectra of free L-cysteine capped CdTe quantum dots in solution and the same quantum dots immobilized on His-loop flagella nanotubes	41
3.4 Emission spectra of quantum dots in solution and self-assembled on Flagella. Inset shows emission spectra of normalized for absorbance at the excitation wave length	43

List of Figures—Continued

3.5 Emission intensity decay as a function of time for free CdTe in solution and those bound to His-loop flagella.....	44
4.1 Gold nanoparticle-flagella nanotube composite materials obtained by reduction of Au.....	57
4.2 Visible absorbance spectra of gold nanoparticles on histidine-loop peptide flagella	59
4.3 Gold nanoparticle-flagellin nanotube composite materials prepared by covalent attachment of pre-made gold nanoparticles	61
4.4 Diagram of covalent immobilization of pre-made gold nanoparticles on flagella by amide bond formation with arginine-lysine peptide loops	62
4.5 Copper-flagellin composite nanomaterials	64
4.6 Cobalt-flagella composite nanomaterials	67
4.7 Palladium-flagellin nanocomposites.....	68
4.8 Silver-flagellin and cadmium-flagellin nanocomposite materials.....	71
5.1 Post-induction whole-cell lysate of twelve cysteine loop variants.....	81
5.2 Post-induction exported sheared flagella of six cysteine loop variant	81
5.3 TEM imaging of disulfide cross-linked cysteine-loop FliTrx flagellin bundles.....	83
5.4 SEM image of Cys-loop flagella bundles on carbon grid.....	84
5.5 Formation of disulfide bonds between cysteine loops in the presence of oxygen	86
5.6 TEM images of cysteine loop FliTrx flagella monomeric fibers after 12 h incubation with 50 mM TCEP.....	87
5.7 Fluorescence image of Cys-loop flagella bundles adsorbed on surface of glass slide.....	88
5.8 Image of lasers tweezers with inverted microscope	90

List of Figures—Continued

6.1 AFM images of a biotin-functionalized gold surface and a subsequent streptavidin assembled surface	98
6.2 AFM images of the assembled flagella layer.....	100
6.3 AFM images of the streptavidin layer assembled on flagella.....	100
6.4 Schematic representation of layer-by-layer assembly of biotinylated flagella nanotubes	102
6.5 Electrostatic layer-by-layer assembly of flagella electrostatic layer-by-layer assembly of flagella	102
6.6 Schematic illustration of electrostatic layer-by-layer assembly.....	103
6.7 Absorbance spectra of electrostatic assembly of flagella on quartz	103
6.8 AFM images of CaCO ₃ mineralized on flagella.....	104

CHAPTER I

INTRODUCTION

Central Hypothesis

The central hypothesis of the research undertaken is that bioengineered flagella protein nanotubes of mesophilic bacteria provide a facile and inexpensive approach for the generation of a variety of monodisperse inorganic and organic nanotubes and nanoparticle arrays in high yields. This is distinctly different from and better than chemical synthetic methods which require harsh conditions and result in polydisperse materials often in poor yields.

Scope of This Research Dissertation

Bacterial flagella provide natural protein nanotube, which can be utilized to generate nanostructures with genetically controlled functionality. The scope of this dissertation is application of bioengineered flagella nanotube as scaffolds and templates for generation of useful inorganic and organic nanotubes (conductive and nonconductive), and generation of inorganic nanoparticle arrays.

Bionanotube in Nanotechnology

Nanotechnology is inspired by biological systems and biomineralized structures; thus naturally available biological systems are widely mimicked and utilized in nanotechnology. As recently reviewed, biological materials represent novel templates and scaffolds for the development of new fabrication methods for microelectronic devices, microelectromechanical systems, sensor platforms, highly selective catalysts and novel biomaterials and integrated nanoparticle-biomolecule hybrid systems (1). Nanotubes are one of the important fields of study in nanotechnology, in part because they have several interesting advantages over spherical nanoparticles. Some of the major advantages of nanotubes over nanoparticles include the large aspect ratio of a hollow tube, which results in a much larger internal volume that can be used to encapsulate small drug molecules and larger proteins, such as enzymes, and the ability to separately modify the inner and outer surfaces with designed functional groups (2, 3). Self-assembling nanotubes are an emerging field of nanotechnology and have been proposed for use as antibiotics, reaction media, drug delivery devices, catalyst and conductors in microcircuits (4, 5). Self-assembling protein, peptide, and lipid nanotubes have previously been described by several research groups and employed as templates for metal, silica, and semiconductor nanotubes (4-10). Two recently described self-assembling protein nanotube systems include tobacco mosaic virus and bacterial pili, have been used extensively as self assembly nanotubes (7, 11-13). Peptide bionanotube systems were developed as antibacterial materials, wound healing materials, supporting substrate for tissue engineering, sensors and scaffold for

biomineralization of inorganic materials (14-19). Unfortunately, the cost of synthesis of peptides is high which prohibits the large scale application in industry. Bacteriophage and tobacco mosaic virus are systems that have been studied in some detail, where peptide displayed virus have been used as template and scaffold for inorganic and organic materials (7, 20-22). Recently, application of engineered virus as coating materials for fibers in sensor application, supporting materials in lithium ion battery, liquid crystal, and digital memory devices were explored (23-26). Protein and peptide tobacco mosaic virus were employed as bionanotube and chemical modification of surface functionality increased diversity of resultant nanostructures (27).

Advantages of Bacterial Flagella over Other Systems

Here, we describe an investigation of bioengineered bacterial flagella that contain loops of amino acids in the D3 domain and the reactive formation of nanotube bundles to demonstrate the importance of these systems for biomaterial research. Like other biological protein nanotube systems, flagella self-assemble in a “bottom-up” fashion and form nanotubes with uniform diameters. However, flagella may have a number of potential advantages over other previously investigated self-assembling protein systems, as detailed below.

1. Large peptides (28-30) and entire proteins such as *E. coli* thioredoxin (109 residues, 12 kDa) have been successfully inserted into the solvent-accessible

hypervariable domain of flagellin (FliTrx) (31, 32) and displayed in high copy number, although the rational design of such insertions remains to be demonstrated.

2. Up to 100% incorporation into the flagella fiber can be attained for engineered flagellins containing mutations, fusion peptides or proteins, vs. 20% incorporation for the M13 virus.

3. Flagella can readily form single bionanotubes with much longer dimensions of 10-15 μm *in vivo* vs. dimensions of less than 1 μm (500-900 nm) for the M13 virus and 300 nm for tobacco mosaic virus (TMV). This is because flagella have significantly more monomers than viruses, with 20,000-30,000 flagellin monomers (33) vs. 2700 monomers of the gP8 protein for M13 bacteriophage virus particles and 2100 monomers for the capsid protein of tobacco mosaic virus (TMV).

4. Some flagella have a dynamic structure; flagellins from peritrichously flagellated bacteria such as *E. coli* and *Salmonella* have a two-state conformational switch and can form helical or straight filaments. This protein switch may be engineered to function as a sensor or control element for a novel helical “smart” nanomaterial.

5. Flagellins are naturally produced at high levels in *E. coli* and *Salmonella* (up to 8% of total protein), do not require the use of viruses and can be expressed at even higher levels using an inducible promoter system. Flagellin monomers can also be purified from inclusion bodies by liquid chromatography and refolded *in vitro*. Thus, flagella can be economically produced by fermentation processes in large quantities, using bacteria typically used for bioproduction, such as *E. coli*.

6. Flagellins have highly conserved self-assembly properties and can reversibly self-assemble *in vitro*. Furthermore, flagellins from different mesophilic bacterial species can be combined *in vitro* into heterogeneous flagella through interactions of the highly conserved terminal domains (34-37). Thus, two or more types of flagellins with different engineered surface functionalities could be expressed *in vivo* or recombined *in vitro* to form multifunctional heterogeneous flagella.

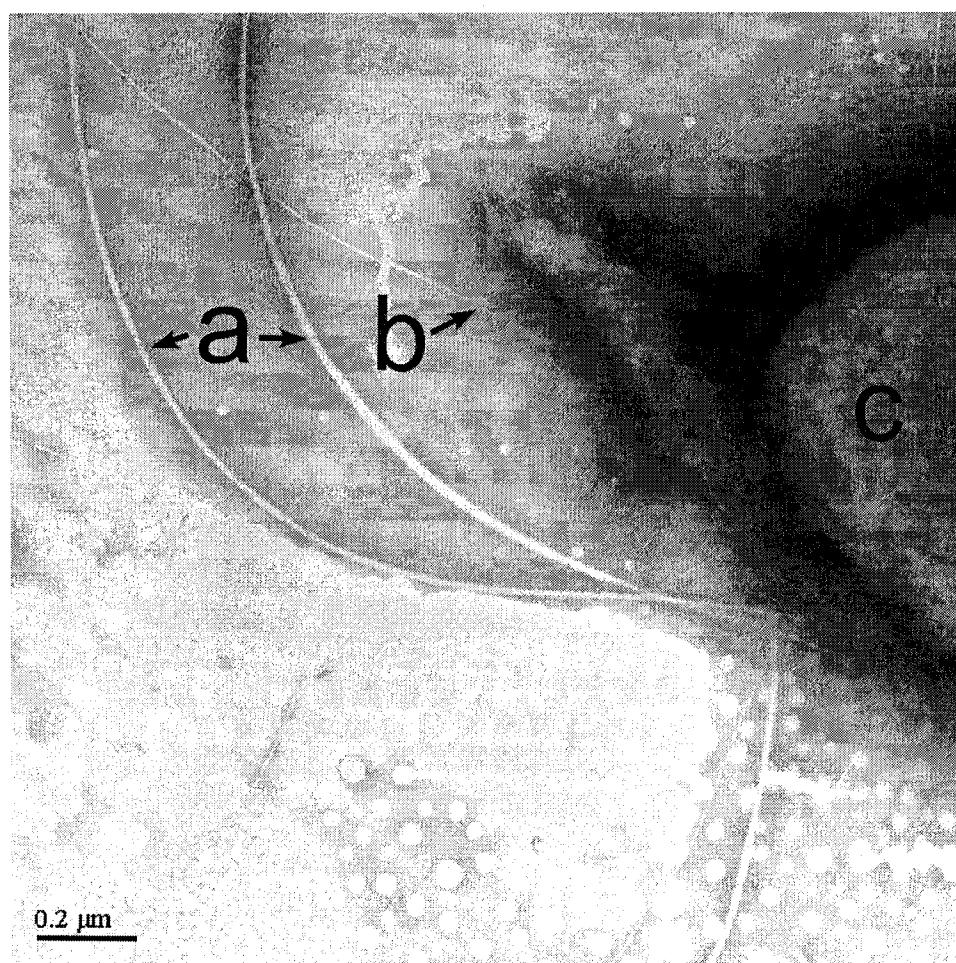


Figure 1.1 TEM image of flagella and part of bacteria stained with 2% neutral phosphotungstic acid (a) flagella, (b)-pili and (c) bacteria. TEM image was recorded with JEOL 1230 model transmission electron microscope (TEM) operating at 80 kV.

Structure of Bacterial Flagella

Bacterial flagella are a naturally-occurring, self-assembling protein nanotube that enable bacteria to swim in aqueous environments (38-41). Flagella are composed of a membrane-bound proton gradient driven motor (42-44), a universal joint hook structure (45, 46) with one end attached to the motor and a long helical fiber attached to the other end of the hook structure that can be 10-15 μm or longer. When all flagellar motors in a motile *E. coli* cell rotate counterclockwise, the hydrodynamic interaction can lead to bundling of the individual flagella filaments into a larger helical fiber (47). Up to 30,000 monomers of the flagellin protein, encoded by the *fliC* gene product in *E. coli*, self-assemble to form a flagellar filament (48-50). A typical flagellar filament has an outer diameter of 12-25 nm and an inner diameter of 2-3 nm (51), depending on the bacterial species. In the process of self-assembly of flagella on bacteria surface, flagellin monomers are recognized and transported by a type III export apparatus in the basal body, diffuse through the hook structure and the inner pore of the flagellar fiber and assemble at the distal end of flagella filament (50, 52, 53). It is believed that flagellin monomers are exported in a partially unfolded state because the 2 nm pore size of the flagellin is too small to allow diffusion of the folded flagellin structure (51). The distal end, furthest from the cell surface, is protected by a pentameric cap of the FliD/Hap2 protein, which functions as a chaperone to assist in folding and self-assembly of flagellin monomers and also forms a barrier to prevent loss of flagellin monomers to the surrounding environment (54, 55). Inside the cell, flagellin aggregation into inclusion bodies or self-assembly into oligomeric flagella is

prevented by association with the FliS chaperonin protein, which binds to flagellin with 2:1 ratio and forms a soluble trimer (51, 56). Flagellin monomers can self-assemble to form flagella in vitro at physiological pH and ionic strength. This self-assembly reaction can be promoted by providing nucleation seeds, *i.e.*, small flagellar fragments. Flagellin was proposed as an object for molecular engineering by Fedorov in 1990 (57), and a number of peptides and proteins have been successfully inserted into flagella for use as a display tool for investigating molecular interactions (30, 31, 58).

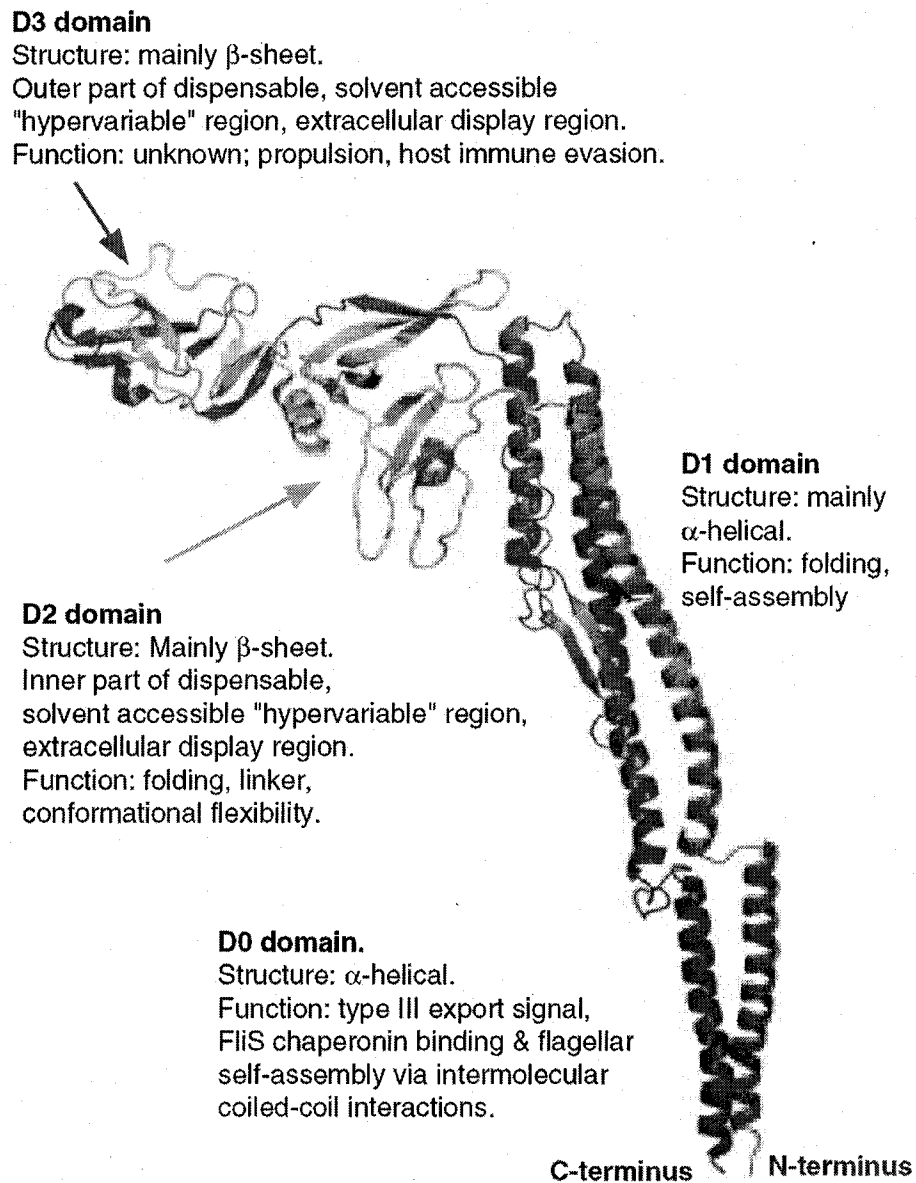


Figure 1.2 Diagram of flagellin protein monomer structure. Image was generated with PyMol software using the Protein Data Bank flagellin structure coordinate file 1UCU.

In this study, a genetically engineered fusion protein of *E. coli* flagellin protein (*fliC* gene product) and thioredoxin (*trxA* gene product), termed FliTrx(31), was used as a scaffold for the engineering of self-assembling nanotube bundles. The globular FliC

protein consists of four domains, termed D0, D1, D2 and D3, and has been structurally characterized (51, 59, 60). Flagellin monomers self-assemble via non-covalent interactions between alpha-helical, coiled-coil motifs that compose the majority of the D0 and D1 domains, forming a helical fiber with a repeat of 11 monomers per turn. The structural core of the flagellar protein nanotube is composed of the D0 and D1 domains and the outer solvent-exposed region of the fiber is composed of the D2 and D3 domains, which form a knob-like structure on the fiber surface. In FliTrx, the 109 residue thioredoxin protein was internally fused at its N- and C-termini between *E. coli* flagellin residues Gly243 and Ala352, corresponding to regions of the D2 and D3 domains, after removing approximately 50% of the wild-type D2 and D3 domains (35). The active site of fused thioredoxin is solvent accessible, has a disulfide-constrained loop, and is an ideal site to insert genetically encoded peptides for display purposes (31). In these studies, DNA oligonucleotide cassettes encoding several types of designed loop peptides, including were inserted in the thioredoxin active site and the engineered proteins were expressed, purified and characterized. Surface modification of carbon nanotubes can be achieved by doping and adding functional groups (61-67), but distribution of functional groups on the surface of nanotubes is not homogenous. Surface modification of the FliTrx protein, unlike carbon nanotubes, can be performed by genetically inserting amino acids with functional side chains into the thioredoxin active site, achieving precise control of the type and extent of homogeneous surface modification. It should also be noted that the flagella nanotube is a fixed structure formed by self-assembly of smaller *fliC* proteins,

resulting in fixed outer and inner diameters, unlike carbon nanotubes. Computational simulation of self-assembly of nanoscale building blocks as function of temperature have been studied by several research groups; the distribution of intersubunit interaction sites and shape complementarity to select interacting particles determines the shape of assembled structures (68). Flagellin proteins with engineered cysteine loops on the outer D3 domain can be considered as “sticky-patch” helical building blocks. Flagella have eleven flagellin subunits per 360° turn, yielding eleven sticky patches per turn. Each patch can theoretically form up to six disulfide bonds with neighboring flagella or other molecules and surfaces. This provides interesting possibilities for obtaining nanostructures through self-assembly. Careful reduction of transition metal ion complex on histidine looped flagella generate metal nanotubes and one dimensional nanoparticles assemblies (69). Histidine looped flagella were use as scaffold for self assembly of semiconductor quantum dots and template for synthesis of semiconductor quantum dots (70). Several conductive/nonconductive inorganic and organic nanotubes were generated using flagella as templates (71). The ordered assembly of cysteine-rich proteins by covalent disulfide bonds was previously investigated by several groups (6, 72). Here, the oxidative self-assembly of bacterial flagella nanotubes into macroscopic fibrous bundles by covalent disulfide bond formation is presented. Molecular recognition and electrostatic interaction were used to layer by layer assembly of flagella nanotubes and assembled flagella were use as template for biomineralization of calcium carbonates. These results are discussed in following chapters (69-71, 73).

CHAPTER II

GENERATION AND CHARACTERIZATION OF INORGANIC AND ORGANIC
NANOTUBES ON BIOENGINEERED FLAGELLA OF
MESOPHILIC BACTERIA

Introduction

A number of naturally occurring and synthetic materials being investigated for use as nanomaterials might also be incorporated into bionanotubes, using engineered flagella as a nucleation scaffold. Silica is a major biomaterial utilized by some plants; diatoms, a type of algae, are a leading organism involved in silica biomineralization (74). Diatoms uptake dissolved silica in water and generate a silicate shell in a process that involves phosphoproteins with polyamine side chains known as silaffins (75, 76). This process of silica biomineralization is currently being investigated using engineered peptides, polymers and proteins (76-87). Titania nanotube synthesis on biological scaffolds such as DNA, virus, protein and lipid nanotubes has also been recently studied. In most cases a titanium alkoxide precursor was reacted on the surface of the scaffold by a sol-gel process to generate titania nanostructures (24, 88-90). Applications of titania nanotubes as a catalyst for photocleavage of water, harvesting sunlight in dye sensitized solar cells, sensors, lithium storage in batteries and function as electrodes, have recently been described by several research groups (91-97). Apatite is the major constituent of bone tissue; understanding the process of apatite biomineralization is important in development of artificial bones (98).

Biom mineralization of apatite on self-assembling peptides and functionalized carbon nanotubes has also been recently investigated (15, 99, 100). Polyaniline is yet another nanomaterial that has recently been investigated as a conductive coating for development of electrically conductive nanowires, manipulating DNA conformation and sensing application (101-104). Biomaterial scaffolds were extensively used in the fabrication of polyaniline nanotubes; anilinium ions are attracted and bind to the negatively charged scaffold by ionic interactions and π - π stacking (105, 106). Here, we describe the synthesis and characterization of silica, titania, hydroxyapatite and polyaniline nanotubes on bioengineered flagella scaffolds. The flagella bionanotubes displayed several different types of rationally designed loop peptides with a variety of chemical recognition properties for different types of ions, such as positive or negative charge or aromatic moieties (71).

Experimental Methods

Materials and Methods

The commonly employed chemicals and their sources and the instrumental techniques are listed here. More specific methods, chemicals and instruments are described under appropriate sections. All chemicals were reagent grade or better and were obtained from Sigma-Aldrich (St. Louis, MO), unless otherwise noted. Tris(2-carboxyethyl)phosphine hydrochloride (TCEP) was obtained from Fluka (Sigma-Aldrich). *E. coli* strain GI 826, the pFliTrx peptide display plasmid and all custom

DNA oligonucleotides primers were obtained from Invitrogen Corp. (Carlsbad, CA). RsrII restriction enzyme, T4 DNA ligase and alkaline phosphatase were obtained from New England Biolabs (Beverly, MA). The QuikChange site-directed mutagenesis kit, including PfuTurbo DNA polymerase, 10X reaction buffer, Dpn I restriction enzyme and dNTP mix, were purchased from Stratagene (La Jolla, CA). DNA gel extraction and purification kits were obtained from QIAGEN, Inc. (Valencia, CA). Polyacrylamide gels were prepared and run using a Bio-Rad (Hercules, CA) Mini-Protean 3 gel apparatus. All transmission electron microscope (TEM) Formvar sample imaging grids were obtained from Electron Microscopy Science (Fort Washington, PA). TEM images were taken with a JEOL model JEM 1230 transmission electron microscope operating at 80 kV and scanning electron microscope (SEM) images were taken with a Hitachi S-4700 PC FESEM operating at 1 kV.

Preparation of FliTrx Engineered Loop Peptide Flagella for Use as Nanotube Scaffolds

The development of the FliTrx system for the display of constrained peptide loops on the surface of *E. coli* flagella fibers has been previously described (31, 32). The chimeric FliTrx protein consists of *E. coli* thioredoxin, (107) the 109 residue *trxA* gene product, inserted as an internal fusion into the solvent-exposed hypervariable region of an *E. coli* flagellin, the ~500 residue *fliC* gene product. This bacterial flagellin expression system, available from Invitrogen (Carlsbad, CA), was designed

to allow genetically encoded insertion and extracellular display of constrained loop peptides on the surface of bacterial flagella fibers and is an alternative to phage display (31, 32, 108). The fusion peptides are inserted into the solvent-accessible active site region of thioredoxin, which has the peptide sequence: -Cys₃₂-Gly₃₃-*-Pro₃₄-Cys₃₅- (109, 110). The pFliTrx plasmid is used with either motile GI724 or non-motile GI826 strains of *E. coli* to express engineered FliTrx flagella fibers. This genetically encoded display system has been used to identify various peptides with affinity for specific metal and protein ligands (111-113) and material surfaces, (114) including selection of a peptide that exhibited zinc-dependent-antibody recognition . In a recent study, we demonstrated that the FliTrx system can also be engineered to display reactive thiol cysteine loop peptides which readily crosslink to form protein nanobundles, nanoparticles and nanotubes (69, 73).

Three of the FliTrx loop peptide variants used in this study were previously described (69, 73). To summarize, molecular biology procedures involved insertion of double-stranded synthetic oligonucleotide cassettes (i.e., “cassette mutagenesis”) encoding desired peptides at a unique RsrII restriction site in a modified version of the pFliTrx plasmid. These procedures yielded modified FliTrx flagellin proteins that displayed peptide loops composed of one or more repeats of rationally designed peptide sequences on their outer surface. An anionic “Asp-Glu” loop peptide with six carboxylate side chain groups composed of one histidine residue, three glutamic acid residues, three aspartic acid residues and one glycine residue (His-Asp-Glu-Asp-Glu-Asp-Glu-Gly; HDEDEDEG), was encoded by the forward oligonucleotide, 5'-GT

CAC GAC GAA GAT GAG GAC GAA G-3', and the reverse oligonucleotide, 5'-G ACC TTC GTC CTC ATC TTC GTC GT-3'. A cationic "Arg-Lys" loop peptide encoding four arginine residues with guanido side chain groups and three lysine residues with amine side chain groups (Arg-Lys-Arg-Lys-Arg-Lys-Arg; RKRKRKR) was encoded by the forward oligonucleotide, 5'-GTC GCA AGC GTA AGC GCA AGC-3' and the reverse oligonucleotide, 5'-GAC GCT TGC GCT TAC GCT TGC-3'. The same cassette mutagenesis approach was used to prepare a polytyrosine loop ("Tyr loop") peptide version of the FliTrx protein with one histidine residue and six tyrosine residues with phenol side chains groups, alternating with three serine and glycine residues: His-Tyr-Ser-Tyr-Gly-Tyr-Ser-Tyr-Gly-Tyr-Ser-Tyr; HYSYGYSYGYSY. This peptide was encoded by the forward oligonucleotide, 5'-GT CAC TAT AGC TAC GGT TAC TCC TAC GGC TAC TCT TAT G-3' and the reverse oligonucleotide, 5'-G ACC ATA AGA GTA GCC GTA GGA GTA ACC GTA GCT ATA GT-3'. All resulting modified pFliTrx plasmids were electrotransformed into GI 826 E. coli cells, single colonies were picked and cultured and plasmid DNA was isolated and sequenced (15). Due to the nature of the self-complementary ends of DNA cassettes encoding loop peptides, both single and multiple loop peptide inserts were isolated in the resulting plasmids. The presence of one or more loop inserts in the expressed FliTrx protein was also verified in a qualitative manner by sodium dodecyl sulfate-polyacrylamide gel electrophoresis (SDS-PAGE) analysis of post-induction whole cell lysates. Polyacrylamide gels with

15% cross-linking were run at constant current with an initial voltage of 130 volts for 1.5 h and were stained with Coomassie brilliant blue R-250 dye.

The engineered pFliTrx plasmids were transformed into GI826 *E. coli* cells and plated on RMG media-Ampicillin (Amp) agar plates. Individual colonies were picked and used to inoculate 50 ml IMC-Amp media at 30 °C with shaking (225 rpm) for 16 h. These overnight cultures were then used to inoculate one liter volumes of IMC-Amp media to give an initial optical density at 550 nm (OD_{550}) of 0.05. The cell cultures were grown at 30 °C with shaking (225 rpm) to an OD_{550} of 0.5 and protein expression was induced with 100 mg/l L-tryptophan at 37 °C with slow shaking (22 rpm) for 3 h. Cells were harvested by centrifugation at $4000 \times g$ for 15 minutes at 4 °C. Cells harvested from 4 liters of culture were resuspended in 50 ml of 150 mM NaCl and the solution pH was adjusted to 2.5 with 0.1 M HCl and stirred for 25 min to disassemble the flagella. The pH of the resultant solution was adjusted to pH 7 with 0.1 M NaOH and cells were pelleted by centrifugation at $10000 \times g$ for 20 min. The supernatant was dialysed against 5 liters of pH 7.5, 20 mM Tris-HCl buffer for 24 h using 10 kDa molecular weight cutoff (MWCO) cellulose dialysis membrane to lower the concentration of NaCl. Flagellin was purified by anion exchange chromatography using a Q Sepharose Fast Flow column, with a gradient of 0-1.0 M NaCl in 20 mM Tris-HCl, pH 7.5 buffer on an Äkta Fast Protein Liquid Chromatography (FPLC) instrument (Amersham Biosciences/GE Healthcare, Piscataway, NJ). Flagella seeds, small fragments of flagella generated by polymerization of monomers in 0.8 M ammonium sulfate, were added to purified flagellin monomers and incubated at 4 °C

for 24 h to allow polymerization. Polymerized flagella were precipitated by the addition of ammonium sulfate to obtain 1.8 M final concentration and stored at 4 °C overnight. Precipitated flagella were isolated by centrifugation at $10,000 \times g$ at 4 °C and suspended in 20 mM NaCl solution. The flagella suspension was dialyzed against one liter of 100 mM NaCl using a 50 kDa MWCO cellulose dialysis membrane for 24 h with one buffer change. The flagellin concentration was determined by absorbance measurements at 280 nm in 6.0 M guanidine hydrochloride, 0.02 M phosphate buffer at pH 6.5, using molar absorptivity values of $30495 \text{ M}^{-1} \text{ cm}^{-1}$ for the Tyr loop variant and $21555 \text{ M}^{-1} \text{ cm}^{-1}$ for the Arg-Lys loop variant and the Asp-Glu loop variant. These values were computed from the variant amino acid sequences using the ProtParam tool at the ExPASy Proteomics Server at <http://www.expasy.org>.

Synthesis of Silica Nanotubes on Cationic Arginine-Lysine Loop Flagella Scaffold

A 500 μl volume of cationic Arg-Lys loop flagella (0.5 mg/ml in 100 mM NaCl) with the single loop insert sequence, RKRKRKR, was mixed with 20 μl of 50 mM sodium silicate solution and incubated at 4 °C for 12 h. Then, 50 μl of 0.1 M HCl was added and mixed with this solution. A 10 μl volume of the resulting solution was placed on a carbon coated Formvar/copper grid and the excess solvent was removed by blotting with filter paper. A 200 μl volume of cationic Arg-Lys loop flagella in 100 mM NaCl was incubated with 1 μl of tetraethyl orthosilicate ($\text{Si}(\text{OC}_2\text{H}_5)_4$) at 30 °C for

12 hours. A 10 μ l volume of the resulting solution was placed on a TEM grid, the excess solution was removed after one min and TEM images were recorded. Control experiments were also performed using the same experimental procedures with FliTrx flagella that did not have any loop peptide inserts and also without any flagella.

Synthesis of Titanium Dioxide Nanotubes on Tyrosine-Serine-Glycine Loop Flagella Scaffold

A 10 μ l volume of purified flagella (0.5 mg/ml in 100 mM NaCl) with a single Tyr-loop insert (HYSYGYSYGYSY) was placed on a carbon coated Formvar/Cu TEM grid for three min. The excess solution was removed by blotting with a piece of filter paper. The grid was then allowed to dry for 10 min under nitrogen flow. A 5 μ l volume of 5 mM titanium(IV) ethoxide solution in ethanol was placed on the grid and removed with filter paper after 30 s and the grid was washed with ethanol. Then, a 10 μ l volume of millipore water was placed on the grid and removed after 5 min. The grid was dried under nitrogen flow and these steps were repeated up to three times. The samples were then characterized by TEM imaging.

Synthesis of Hydroxyapatite Nanotubes on Anionic Aspartate-Glutamate Loop Flagella Scaffold

Biomineralization of hydroxyapatite nanocrystals on flagella scaffolds displaying a loop peptide encoding three repeats of the anionic Asp-Glu loop sequence (HDEDEDEG-HDEDEDEG-HDEDEDEG) was carried out as described in elsewhere

(115). A volume of 10 μl of flagella (0.5 mg/ml in 100 mM NaCl) with anionic aspartic acid and glutamic acid peptide loops was placed on a holey carbon/Ni(200 mesh) grid for 5 min and the excess solution was removed by blotting with a piece of filter paper. The grid was then allowed to dry for 10 min. A volume of 5 μl of 10 mM freshly prepared CaCl_2 solution was then placed on the grid and incubated in a water vapor-saturated chamber for 5 min. Then the grid was carefully turned so that the side with the flagella and CaCl_2 solution faced downwards. A volume of 5 μl of 10 mM Na_2HPO_4 solution was then placed on the opposite side of the grid (opposite side from CaCl_2 solution) and the grid was placed in a water vapor saturated chamber for another 10-20 min. The solvent was carefully removed and TEM images were collected.

Synthesis of Polyaniline Nanowires on Anionic Aspartate-Glutamate Loop Flagella Scaffold

A volume of 10 μl of flagella solution (0.5 mg/ml in 100 mM NaCl) with a triple repeat Asp-Glu loop peptide (HDEDEDEG-HDEDEDEG-HDEDEDEG) was placed on a carbon coated Formvar TEM grid for 3 min. This was the same anionic Asp-Glu loop sequence peptide used for hydroxyapatite synthesis. The excess flagella solution was removed by blotting with a piece of filter paper. The grid was allowed to dry for another 10 min. A 10 μl volume of 10 mM aniline solution at pH 4.2 (pH adjusted with 0.1 M HCl) was placed on the grid for one min and removed by blotting with filter paper. Then, 10 μl of 0.5 mM Tris(2,2'-bipyridine)dichlororuthenium(II)

hexahydrate solution at pH 4.2 were placed on the grid. The grid was placed in a glass vial saturated with water vapor and exposed to a 40 W tungsten bulb for 20 min. The ruthenium complex adsorbs light at a wavelength of 450 nm and initiates polymerization by oxidative electron transfer (75, 76, 81, 83, 85, 116-119). Excess solvent was removed by blotting with filter paper and TEM and SEM images were collected.

Results and Discussion

Silica Biomineralization on Cationic Arginine-Lysine Loop Flagella Scaffolds

Silica biomineralization on cationic Arg-Lys loop peptide flagella bionanotubes was performed with two different silica precursors, Na_2SiO_3 and $\text{Si}(\text{OEt})_4$. The morphology of the resulting silica nanotube structures formed using these two silica precursors were different; the Na_2SiO_3 generated very separated nanotubes while $\text{Si}(\text{OEt})_4$ generated silica nanotubes which were clumped together with further silica mineralization. Typical TEM images of silica nanotubes formed on flagella using $\text{Si}(\text{OEt})_4$ as the soluble silicate ion precursor are indicated in Figure 2.1 (a) (b) and (c), where Figure 2.1 (d) is the control sample prepared without the cationic Arg-Lys loop flagella. Figure 2.2 (a) and (b) show typical TEM images of silica nanotubes formed on Arg-Lys loop flagella using Na_2SiO_3 as the source of silicate ions.

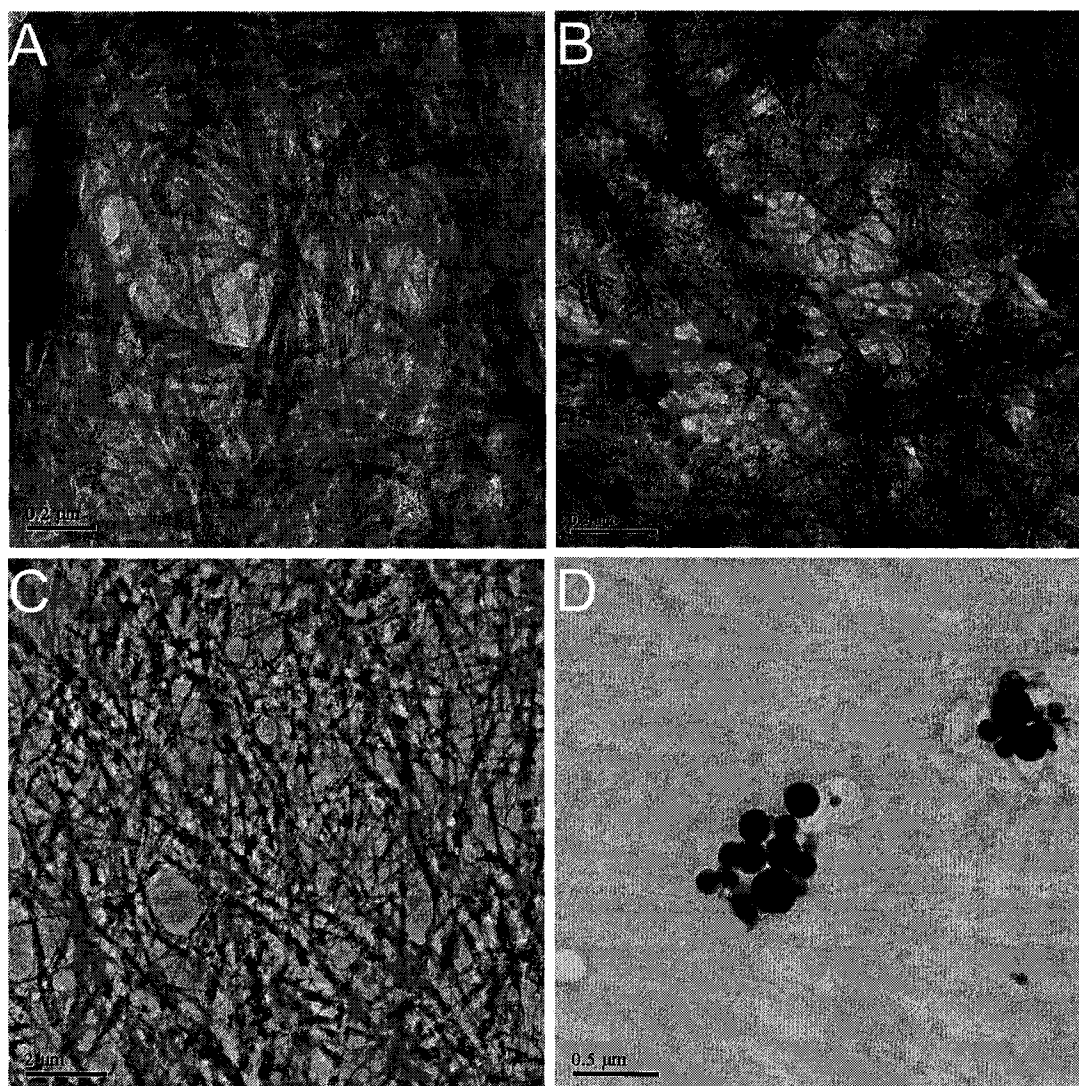


Figure 2.1 (a), (b) and (c) Silica biomineralization on flagella scaffold with tetraethoxysilane as silica source. (d) Without flagella. (JEOL 1230)

The observed biomineralization of silica flagella bionanotubes mimics the natural biomineralization process in diatoms, where catalytic proteins known as silaffins are involved in the biomineralization process. Lysine and arginine-rich proteins with polyamine modification on the lysine residues were investigated by several groups for their ability to initiate *in vitro* silica biomineralization (24, 87-90,

120-124). Biom mineralization by loop-less wild-type flagella or biom mineralization without flagella generated silica nanospheres with a large size distribution. Thus, the positively charged arginine and lysine residues that are displayed in a localized region on the Arg-Lys loop flagella surface appear to play a key role in silica biom mineralization. There are an estimated 66 of these positively charged residues per 5 nm length of flagella. These cationic residues may generate a positively charged surface on the protein fibers, which then attracts and binds the first layer of silicate ions on the flagella surface during the initial state of biom mineralization. Further mineralization of silicate ions on the initial layer of silica may lead to a thick coating of silica on the flagella surface.

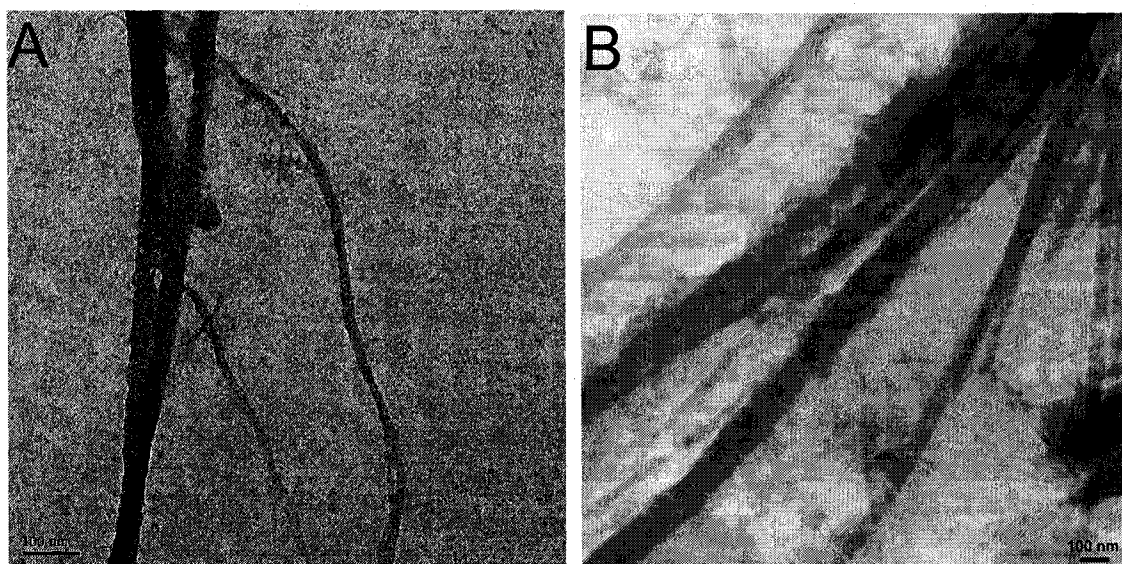


Figure 2.2 (a) and (b) Silica biom mineralization on flagella scaffold with sodium silicate as silica source. (JOEL JEM 1230)

Titania Biomineralization on Phenolic Tyrosine Loop Flagella Scaffold

It may be possible to use the previously described anionic Asp-Glu loop flagella to nucleate formation of titania from Ti(IV) ions. However, a review of literature describing titania synthesis indicated that Ti(IV) ions have a higher affinity for hydroxyl groups (R-O) than carboxylate groups (RCOO⁻); (99, 125) titanium ions more readily form TiO₂ versus Ti(CO₃)₂. Thus, we designed another loop peptide that contained tyrosine and serine groups with phenolic and aliphatic hydroxyl moieties for use with Ti(IV) ions. The resulting flagella displaying this loop peptide were successfully used to nucleate formation of titania nanotubes. Typical TEM images of titania nanotubes formed on flagella scaffold are indicated in Figure 2.3 (a), (b) and (c); the control experiment is shown in Figure 2.3 (d). The TEM image shows that the low electron density protein nanotube is surrounded by titania composite. Both hydroxyl groups from tyrosine residue phenolic side chains on the surface of flagella and water molecules adsorbed on the flagella may play a critical role in titania biomineralization. As indicated in the previously described mechanism of the sol-gel process depicted in Figure 2.4, an initial layer of titania is formed on the flagella surface, followed by further growth of titania on the initial layers.

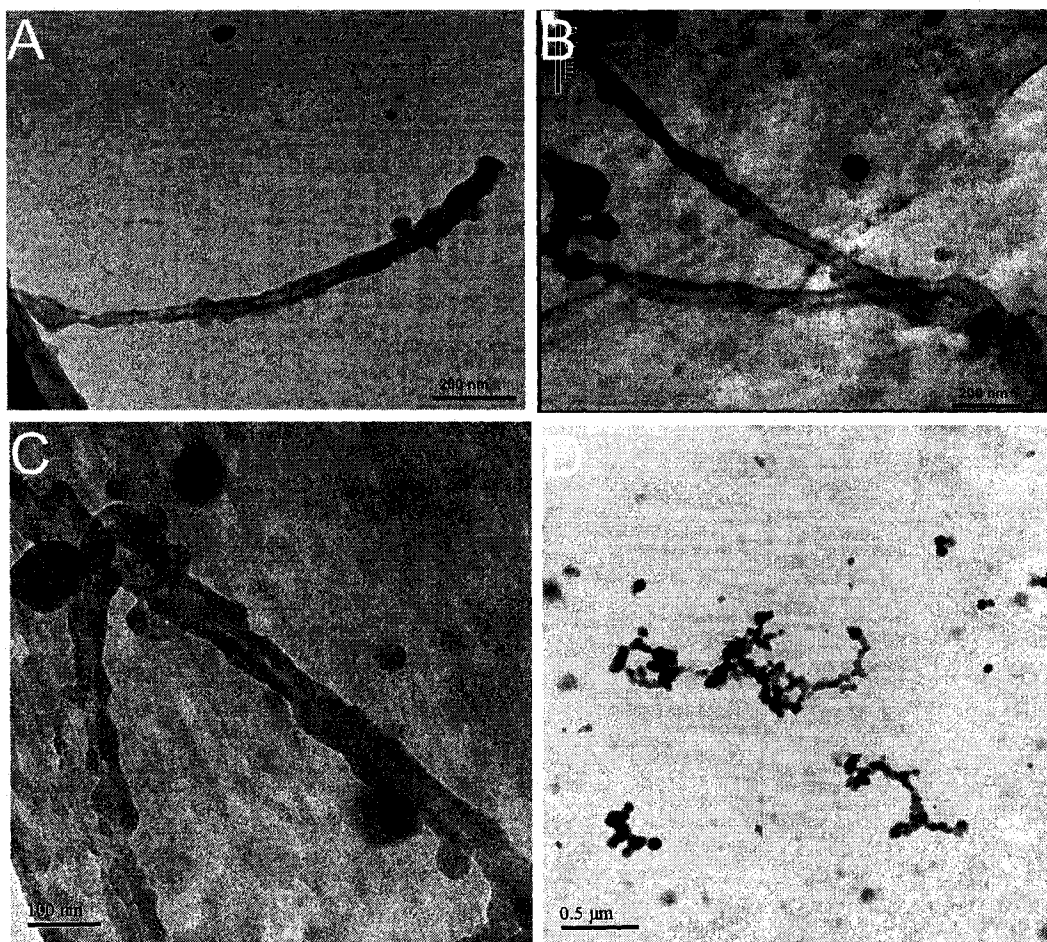


Figure 2.3 (a), (b) and (c) TiO₂ nanotube synthesized on flagella scaffold (d) without flagella. (JOEL JEM 1230)

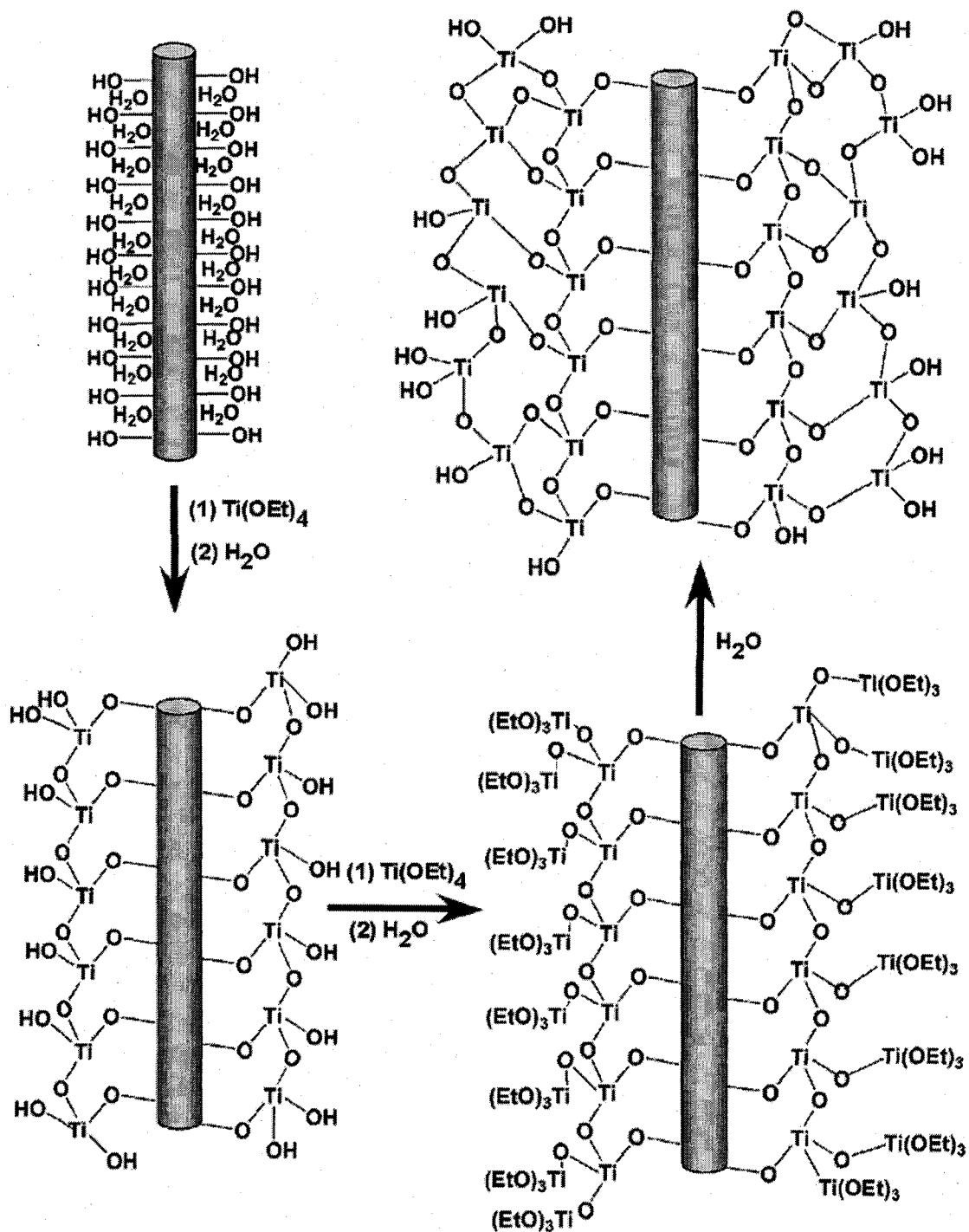


Figure 2.4 Schematic illustration synthesis of titania nanotube by sol-gel process.

Hydroxyapatite Biomineralization on Anionic-Aspartate-Glutamate Flagella Scaffold

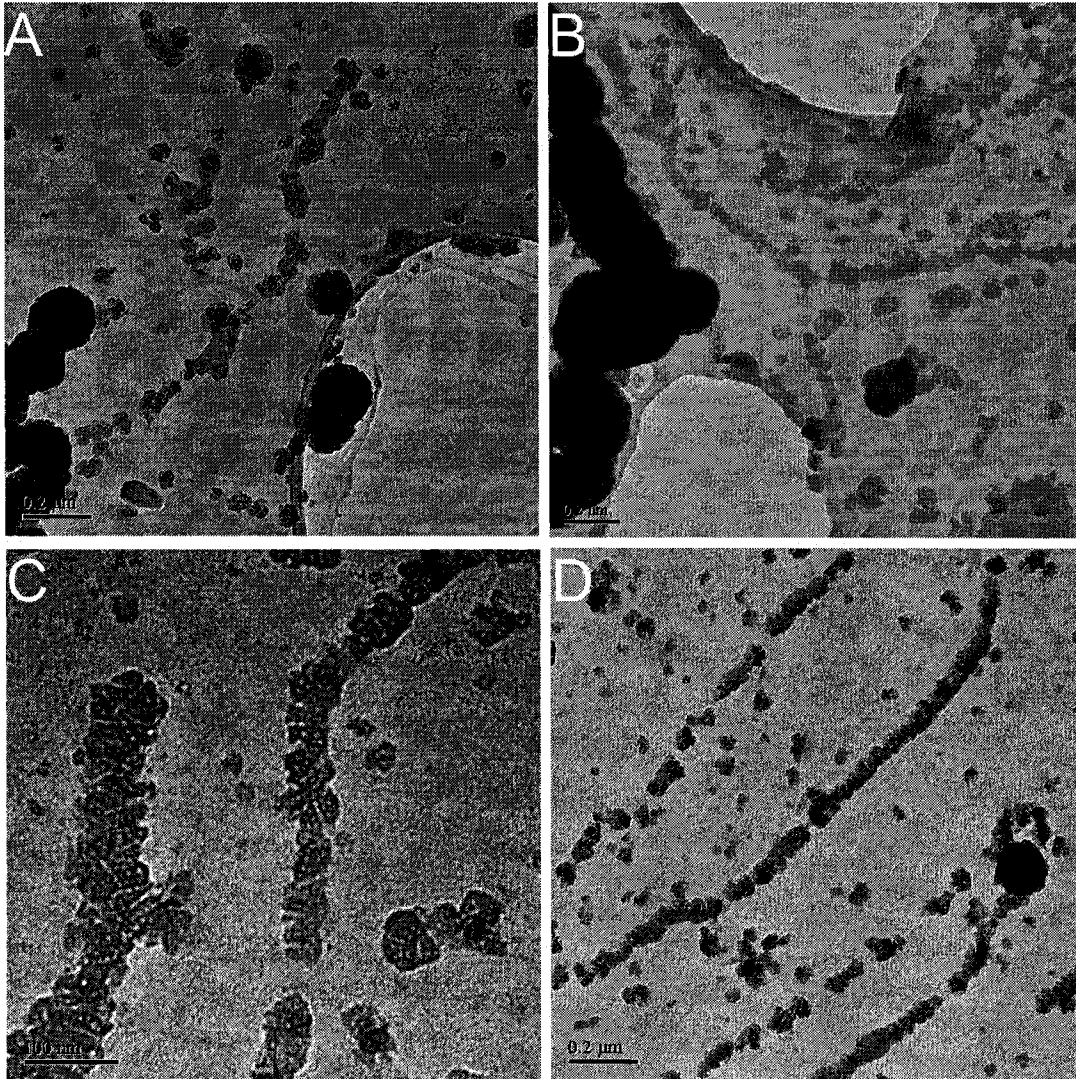


Figure 2.5 Apatite nanocrystals synthesized on flagella scaffold after 10 minutes exposure to mineralization solution. (JOEL JEM 1230)

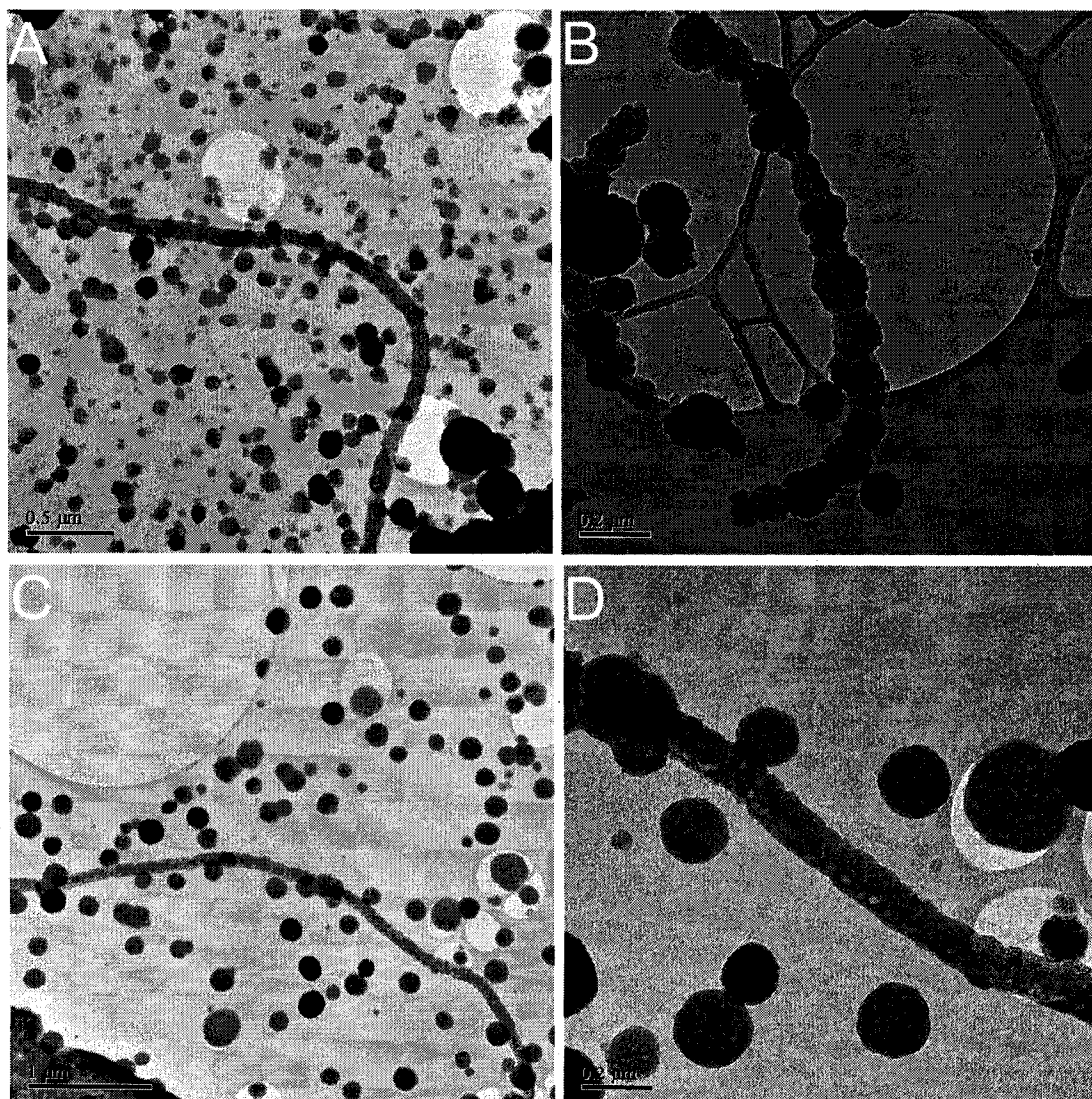


Figure 2.6 Apatite nanocrystals synthesized on flagella scaffold after 20 minutes exposure to mineralization solution. (JEOL JEM 1230)

Biom mineralization processes that involve the controlled precipitation of calcium ions to form biological structures composed of calcium carbonates, phosphates and oxalates are common in nature (126, 127) and have been investigated in vivo with acidic proteins and lipid monolayers (15, 100, 128-130). Furthermore, a number of studies have demonstrated the biom mineralization of hydroxyapatite, a key mineral

component of bones, on various types of peptide, carbon and inorganic nanotube scaffolds (104-106, 131-138). In this study we have demonstrated the biomineralization of hydroxyapatite on flagella bionanotubes. Hydroxyapatite formation was performed on a porous holey carbon grid, where small pores on the grid allowed slow diffusion of ions to generate controlled rates of biomineralization. Typical TEM images of hydroxyapatite nanocrystals formed on flagella are indicated in Figures 2.5 and 2.6. Association of Ca^{2+} ions with the closely spaced carboxylic acid groups of aspartate and glutamate loop residues on the surface of flagella should lead to a higher concentration of Ca^{2+} on the surface of flagella compared to bulk solution. This will eventually result in supersaturation and subsequent localized precipitation of hydroxyapatite on the surface of flagella. As indicated in the TEM images, the tubular apatite structures formed on flagella consist of arrays of mineral nanocrystals; their packing density and approximate size depended on the exposure time to the mineralization solution. As indicated in Figure 2.6, a 20 min exposure generated larger and more densely packed nanocrystals on the surface of flagella than the 10 min exposure time. All TEM images indicated that the nanocrystals were randomly oriented on the flagella scaffold. Each D3 domain may nucleate a single nanocrystal, which eventually grow together to form a continuous assemblage of nanocrystals after longer exposure to the ion source solution.

Polyaniline Biomineralization on Anionic Aspartate-Glutamate Flagella Scaffold

The construction of conductive polyaniline nanowires and spherical nanostructures with redox-active ligands has been investigated with a variety of inorganic and biological polymers and nanoparticle structures and reaction conditions. We were able to demonstrate the preparation of an organic coating of polyaniline on anionic Asp-Glu loop peptide flagella, which could potentially be used as conductive nanowires. In the case of the aniline polymerization process, anilinium ions may assemble on flagella by ionic interactions and π - π stacking of the aromatic rings. The ruthenium complex absorbs visible light around 450 nm and the resulting photoexcited complex oxidizes aniline. This, in turn, leads to initiation and propagation polyaniline flagella nanowires due to the low electron density of this carbon-rich material; only thicker tubes were visible in TEM images, as indicated in Figure 2.7 (a), (b) and (c). As indicated in Figure 2.8, the polyaniline nanotubes immobilized on a copper grid were more readily visualized by SEM due to the high conductivity of copper, which improved the contrast of the images.

Conclusion

These initial studies have demonstrated the feasibility of using genetically engineered bacterial flagella as a scaffold for the biomineralization of various inorganic minerals, including materials with catalytic potential, and a conductive organic matrix that could potentially be used as a conductive nanowire. It may be possible to fine tune the

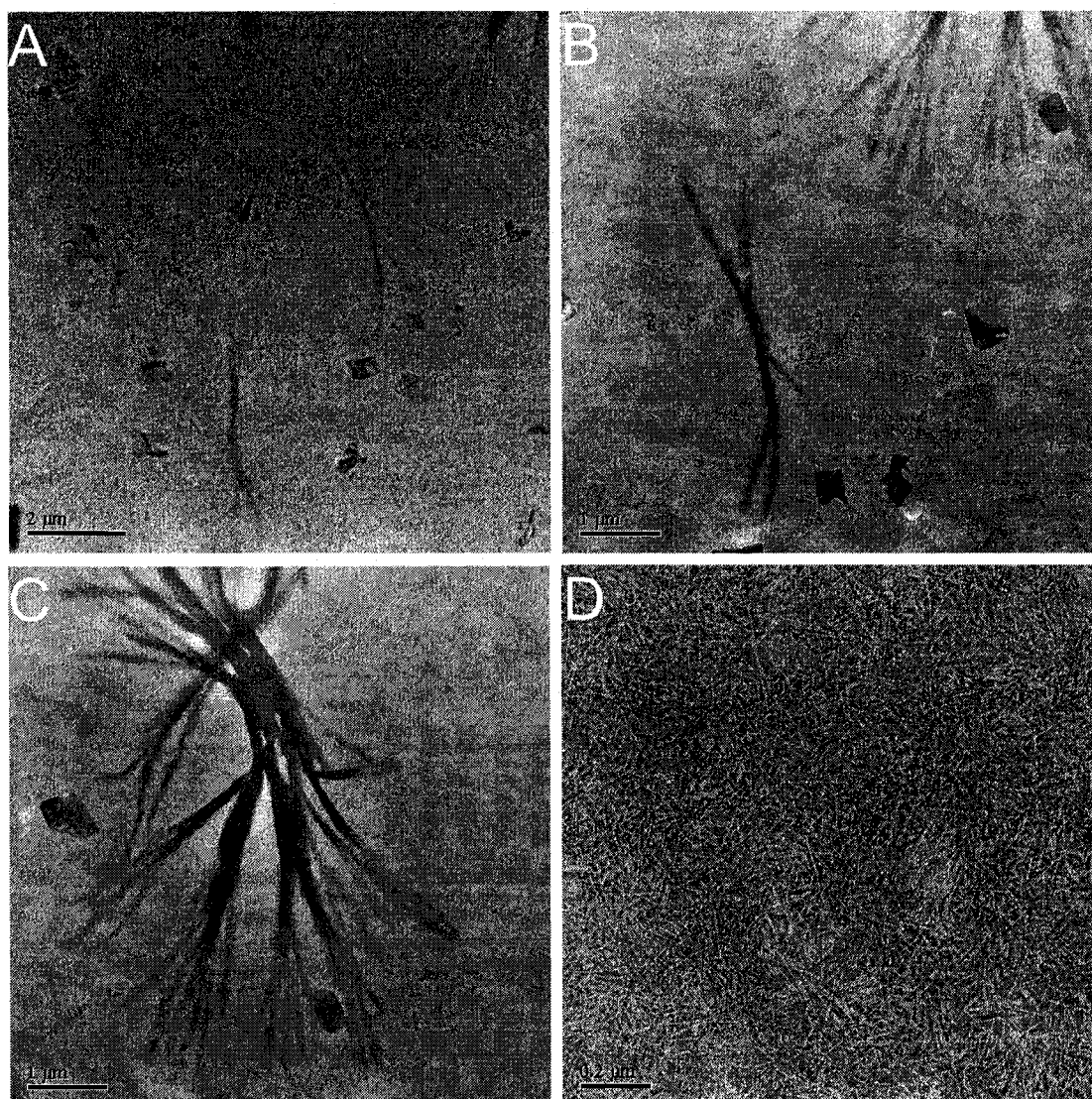


Figure 2.7 (a), (b) and (c) TEM images of polyaniline synthesized on flagella scaffold (d) Flagella stained with phosphotungstic acid. (JOEL JEM 1230)

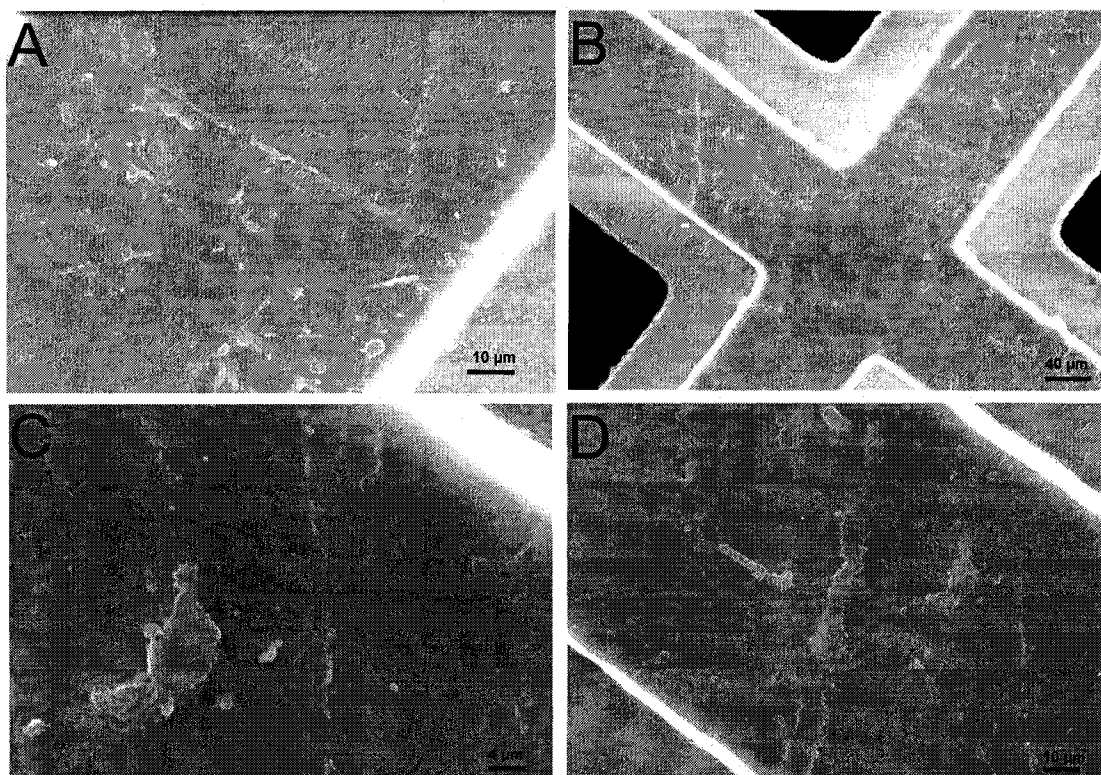


Figure 2.8 (a), (b), (c) and (d) SEM images of polyaniline synthesized on flagella scaffold.

nucleation properties and morphology of the resulting bionanotubes by systematically varying the size and composition of the loop peptide sequences with resulting changes in the net charge, polarity, hydrophobicity and affinity for specific ions or other small molecules. Furthermore, chemical modification of the resulting peptide loops, to incorporate other functional groups not encoded in the twenty common amino acids, also remains to be explored.

CHAPTER III

EXCITON ENERGY TRANSFER IN SELF-ASSEMBLED QUANTUM DOTS
ON BIOENGINEERED BACTERIAL FLAGELLA NANOTUBES

Introduction

Biological molecules such as peptides, proteins, lipids, and DNA are being investigated as templates and scaffolds for the assembly and biomineralization of semiconductor nanoparticles and nanowires. These bio-inspired approaches are interesting because they employ a bottom-up approach to manufacturing which has certain advantages, including reproducibility at the molecular level, selectivity, e.g., high affinity for certain ions or small molecules and not others, and the ability of biomaterials to direct crystal morphology in biomineralization; these approaches could surpass current lithographic capabilities (7, 21, 139-142). Tunable optical properties, photo-stability, relatively high quantum yields, and the ability for doping with other elements make semiconductor QDs increasingly useful in various applications, such as imaging, sensors, lasers, light emitting diodes, solar cells, photon guide, and molecular electronics (26, 71, 143-155). The combination of biomineralization and/or assembly of semiconductor materials on engineered biological scaffolds and templates can yield novel bottom-up nanoscale systems with unique properties that can address limitations of current top-down approaches to manufacturing electronic devices.

Our research program is focused on gaining a fundamental understanding of protein nanotubes derived from bacterial flagella (69-71, 73) and QDs doped with magnetic nuclei (156-158). An integral part of these efforts is the investigation of flagella-quantum dot nanocomposites. In this work, the two-dimensional assembly of ZnS:Mn and CdTe QDs on the surface of bioengineered flagella and their exciton energy transfer (EET) are presented. We recently demonstrated assembly and manipulation in an optical trap of bioengineered flagella protein nanotubes with cysteine loops, (73) biomineralization of transition metals, (69) silica, titania, and apatite and application of flagella as a template for polyaniline nanowires (71). In these studies, we used the FliTrx fusion protein, composed of *E. coli* flagellin (FliC) and thioredoxin (TrxA), where sections of the FliC D2 and D3 domains were replaced with thioredoxin. Thioredoxin, in turn, has a disulfide bond-constrained active site region on the surface of the protein that is suitable for insertion and display of loop peptides (71, 73). As previously described, a DNA cassette encoding a loop peptide of twenty one amino acid residues was removed from the FliTrx thioredoxin domain and a new DNA cassette encoding histidine (His) residues with imidazole side chain groups, the seven amino acid "His-loop" peptide (Gly-His-His-His-His-His-His; GHHHHHH), was inserted, using standard molecular biology methods. FliTrx variants containing inserts with 1-6 repeats of the His-loop peptide were isolated and characterized with respect to their intracellular protein expression and competence for extracellular export and assembly into flagella nanotubes. Although expression levels were high for all six unique FliTrx His-loop variants, export and assembly of His-loop

variants with 5 and 6 inserts was very low. Therefore, the His-loop variant with the largest loop peptide that was still efficiently exported and assembled into flagella nanotubes was used in this study, the 4X insert variant with 24 histidine residues (GHHHHHHH-GHHHHHHH-GHHHHHHH-GHHHHHHH). The FliC protein does not have any tryptophan (Trp) residues, while the inserted thioredoxin protein has two Trp residues, Trp28 and Trp31 in native thioredoxin, corresponding to residues Trp272 and Trp275 in the FliTrx protein. These two Trp residues are located in the thioredoxin active site region near the base of the peptide loop. These two Trp residues were replaced with tyrosine residues by site-directed mutagenesis (Trp272→Tyr, Trp275→Tyr) to minimize possible absorbance and excitation of the Trp indole ring side chain when attached ZnS QDs were excited at 300 nm.

Materials and Methods

Protein expression, purification and self-assembly of the 4X repeat His-loop FliTrx variant into flagella protein nanotubes was carried out as previously described (159). Synthesis of Mn-doped ZnS nanoparticles was carried out as described in detail elsewhere and the significant aspects are provided here. A 45 mL volume of HPLC-grade ethanol was bubbled with nitrogen for 15 minutes and 990 μ L of 1 M zinc acetate and 10 μ L of manganese(II) acetate were added to the ethanol (160). A 1 mL volume of 1 M sodium sulfide solution was added drop-wise and the mixture was stirred for five minutes. The resulting ZnS:Mn nanoparticles that formed were washed

with nitrogen-saturated ethanol 3 times, isolated by centrifugation for 10 minutes at 5000g and suspended in deionized (DI) water for assembly on flagella. A calculated volume of ZnS:Mn quantum dots to yield an absorbance value of 0.2 at 300 nm with a Lambda 20 spectrophotometer (Perkin Elmer, Wellesley, MA) was mixed with 500 μ L of 1 mg/mL flagella solution in 100 mM NaCl, made up to 1 mL with DI water and equilibrated for 30 min at room temperature. The fluorescence lifetime and emission intensity were measured for ZnS:Mn QDs with excitation at 300 nm and emission at 590 nm on an FLS 920 spectrophotometer (Edinburgh Instruments, Livingston, UK), using a 395 nm cutoff filter. A 10 μ L volume of this solution was placed on carbon coated Formvar/400 mesh transmission electron microscopy (TEM) grid for one min and excess water was removed by blotting with a piece of filter paper. The CdTe quantum dots capped with L-cysteine were synthesized as described elsewhere (51). A 2 mg quantity of nanoparticles capped with L-cysteine was dispersed in 2 mL volume of water by sonicating for 30 min and the absorbance of the nanoparticles at 400 nm was measured. A volume of nanoparticles calculated to yield an absorbance value of 0.2 at 400 nm was mixed with a mixture of 500 μ L of 1 mg/mL flagella in 100 mM NaCl, 20 μ L of 1 M borate buffer (pH 8.2) and 50 μ L 1 M NaCl, and the volume was adjusted to 1 mL with DI water. Absorbance spectra were measured for the appropriate blank solution without QDs and fluorescence spectra were recorded with excitation at 400 nm. The fluorescence lifetime for CdTe nanoparticles was measured with excitation at 400 nm and emission at 580 nm. A 10 μ L volume of this solution was placed on a carbon coated Formvar/400 mesh TEM

grid for one min and excess solvent was removed by blotting with filter paper. The average lifetime for the entire decay process was calculated with FAST software (Edinburgh Instruments, Livingston, UK) using reconvolution fit with instrumental response.

The ZnS nanoparticles were also synthesized by immobilizing His-loop flagella on a holey carbon TEM grid. For synthesis of ZnS QDs on flagella, a 10 μL volume of 0.25 mg/mL flagella solution was placed on holey carbon grid and excess solvent was removed by blotting with filter paper. A 5 μL volume of 5 mM ZnSO_4 was placed on the flagella-coated TEM grid and 5 μL of 5 mM Na_2S solution was placed on the other side of the TEM grid. After 5 min, the excess solution was removed by blotting with filter paper. Typical TEM images of previously synthesized ZnS:Mn QDs immobilized on the His-loop flagella scaffold are shown in Figure 3.1(a) and a TEM image of ZnS QDs synthesized on the His-loop flagella template is shown in Figure 1(b). The ZnS QDs nanoparticles synthesized on the flagella scaffold yielded an electron diffraction pattern indicative of Wurtzite structure (Figure 3.1(b) inset). In contrast, control experiments performed using FliTrx flagella without any inserted histidine loop peptides on the thioredoxin domain did not result in formation of any QDs, under the same conditions. During the synthesis of QDs on flagella, the high local concentration of Zn^{2+} ions, which are complexed to the imidazole groups of His residue on the flagella surface, may initiate the nucleation process and generate nanoparticles on flagella scaffolds. Figure 3.1(c) shows the assembly of cysteine-capped CdTe QDs on His-loop flagella. In the case of assembly of QDs on His-loop

flagella, the imidazole groups of histidine residues most likely play a critical role through coordination with Zn (II) and Cd(II) ions of the QD nano-crystals.

Results and Discussion

The histidine loops on the flagella are present on the D3 domain of the flagella nanotube, where each segment is a helical self-assembly of 11 flagellin protein monomers. This results in a distance of about 5.4 nm between consecutive D3 domains (147). The procedures for synthesizing ZnS:Mn and CdTe nanoparticles were optimized to obtain QDs with an average size of 3 nm and a polydispersity of 10%. The ZnS:Mn QDs did not have a capping agent while the CdTe QDs were capped with L-cysteine. The cooperative binding of the peptide loop histidine ligands displaced the cysteine ligands from the CdTe surface to facilitate their binding to the flagella (161). The solvent exposed surfaces of the flagella-bound CdTe QDs most likely are still covered with cysteine. Thus, in effect, the CdTe QDs bound to the flagella nanotubes are coordinated to both histidine and cysteine ligands. The organized assembly of 3 nm (average size) QDs on flagella nanotubes shown in Figure 3.1 (c) are, on average separated by 2.4 nm. This separation distance is much larger than the corresponding distances typically encountered in QD and nanoparticle systems linked with organic molecules (161, 162). The CdTe QDs have band gaps that are sensitive to their size; excitation with photons in their band gap yields excitons which emit at wavelengths characteristic of the band gap (156, 163). By

contrast, the fluorescence emission maximum from the ZnS:Mn QDs that is centered at 590 nm is due to the dopant Mn(II), corresponding to the transition from 4T_1 to 6A_1 . This emission is due to energy transfer from the exciton to the dopant and its position and intensity are not very sensitive to the size of the QD. However, the emission is sensitive to the concentration and location of the dopant, namely, surface vs. lattice doping (161, 162, 164-167). The CdTe QDs, in addition to possessing size-dependent band gaps and emission wavelengths for excitons, are also capable of undergoing interparticle exciton energy transfer and electronic coupling when they are closely assembled (166, 168-173). The exciton energy transfer can occur over longer ranges for various size nanoparticles while the electronic coupling, which requires an overlap of electron wave functions, typically occurs for small organically linked or electrostatically interacting QDs over a short range. Similar processes have also been observed for CdSe and InP QDs and QD-metal nanoparticle composites (163). The QDs self-assembled on the histidine loops of flagella provide an excellent system to explore exciton energy transfer and electronic coupling for these systems. We have investigated the absorption and emission spectra and emission lifetimes of ZnS:Mn and CdTe QDs self-assembled on the His-loop flagella to determine if interparticle interaction leading to exciton energy transfer or electronic coupling could be observed.

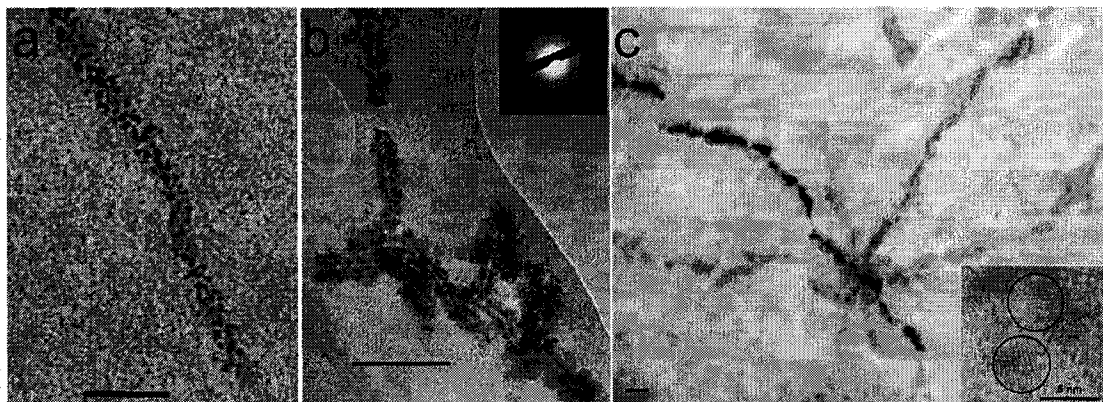


Figure 3.1 (a) TEM image of ZnS:Mn nanoparticles immobilized on histidine loop.

flagella scaffold (scale bar 50 nm). (b) TEM image of ZnS nanoparticles synthesized on flagella scaffold (scale bar 100 nm). (b, inset) Electron diffraction pattern indicating Wurtzite structure. (c) TEM image of CdTe nanoparticles immobilized on histidine loop flagella scaffold (scale 100 nm). (c, inset) High resolution TEM image of CdTe nanoparticles immobilized on flagella template (scale bar 5 nm). The quantum dots had an average size of 3 nm and TEM images were recorded with a JEOL 1230 TEM instrument operating at 80 kV (a and b) and a JEOL 3011 TEM instrument operating at 300 kV (c).

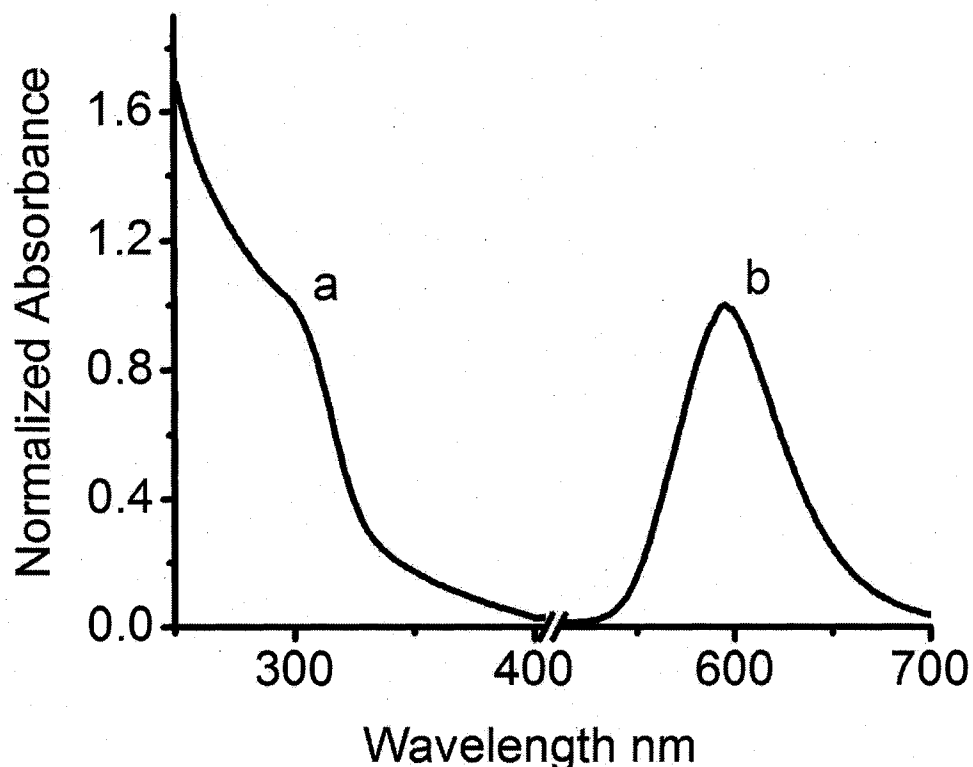


Figure 3.2 Normalized absorbance (a) and emission (b) spectra of ZnS:Mn QDs nanoparticles self-assembled on His-loop flagella nanotubes. Emission spectra were recorded with excitation at 300 nm.

The normalized absorbance and emission spectra of ZnS:Mn nanoparticles assembled on His-loop flagella are shown in Figure 3.2. The absorption and emission spectra of ZnS:Mn QDs did not exhibit any change between the QDs suspended in solution and bound to His-loop flagella. The luminescence decay of Mn^{2+} showed biexponential decay, with emission lifetimes of 2.00 ms and 0.28 ms, which did not change between the free and bound QDs. The longer emission lifetime was due to Mn^{2+} ions in slightly distorted tetrahedral sites in the crystal lattice, while the shorter

emission life time was due to Mn^{2+} ions adsorbed on the surface of the quantum dots (157). The metal centered emission was insensitive to binding by histidine and long-range interparticle interactions on the His-loop flagella. We have observed emission intensity and lifetime changes for the ZnS:Mn QDs when capped with L-cysteine, which binds much more strongly than does histidine (161, 162).

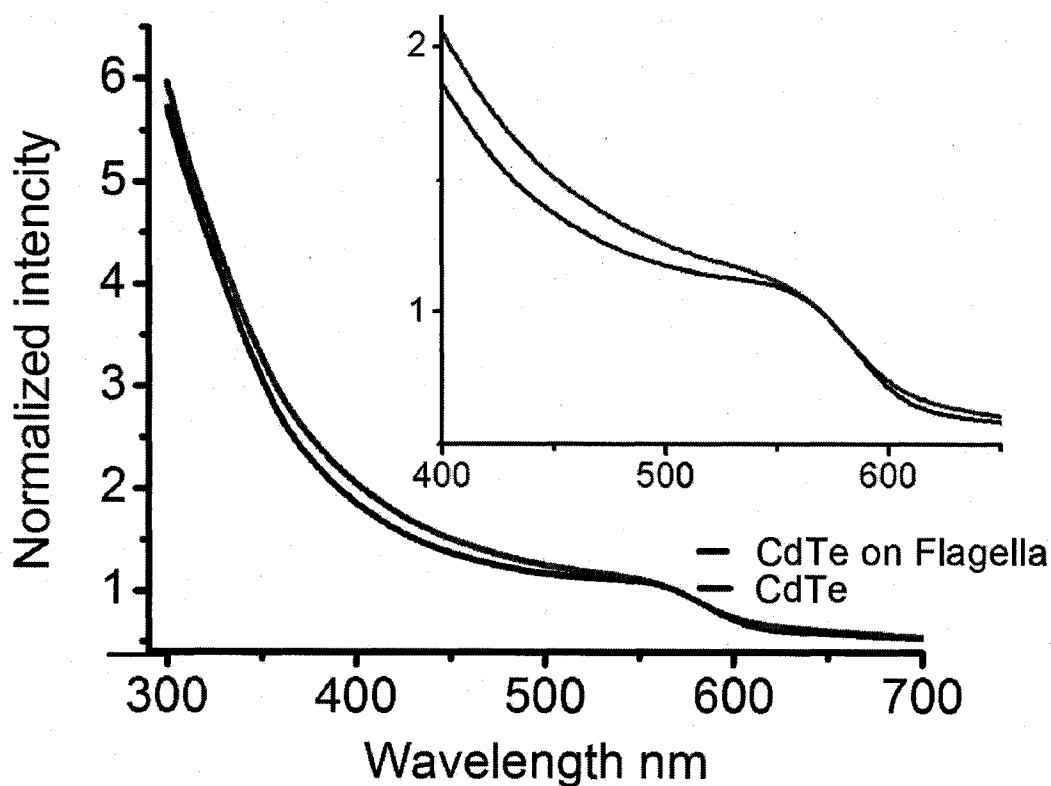


Figure 3.3 Absorbance spectra of free L-cysteine capped CdTe quantum dots in solution and the same quantum dots immobilized on His-loop flagella nanotubes.

A different behavior was observed for the CdTe QDs on the His-loop flagella compared to CdTe QDs in solution. The normalized absorbance spectrum for the CdTe QDs on His-loop flagella, as seen in Figure 3.3, showed an increase in

absorbance and a slight red shift, compared to the CdTe QDs in solution, which indicates possible electronic coupling between closely packed CdTe QDs on the His-loop flagella. The emission spectrum of CdTe QDs on His-loop flagella showed a reduction in their fluorescence intensity and a 5 nm red shift from 578 nm to 583 nm, as seen in Figure 3.4, compared to CdTe QDs in solution. The spectrum for CdTe QDs on the flagella exhibited a 5 nm red shift corresponding to an energy difference of 18.4 meV between the free QDs in solution and those bound to the flagella. This corresponds to a change in the exciton energy level for the flagella bound QDs which could be due to exciton energy transfer from the smaller (larger band gap) to the larger (smaller band gap) QDs bound to the flagella, given the 10% polydispersity in their size. Such a transfer is facilitated on the flagella due to the organized self-assembly of the QDs, while in solution the random orientation of the various QDs results in an average emission spectrum. The emission peak width at half peak maximum for the CdTe nanoparticles on the flagella scaffold was 52 nm compared to 55.5 nm for the QDs in solution, which is also indicative of the exciton energy transfer.

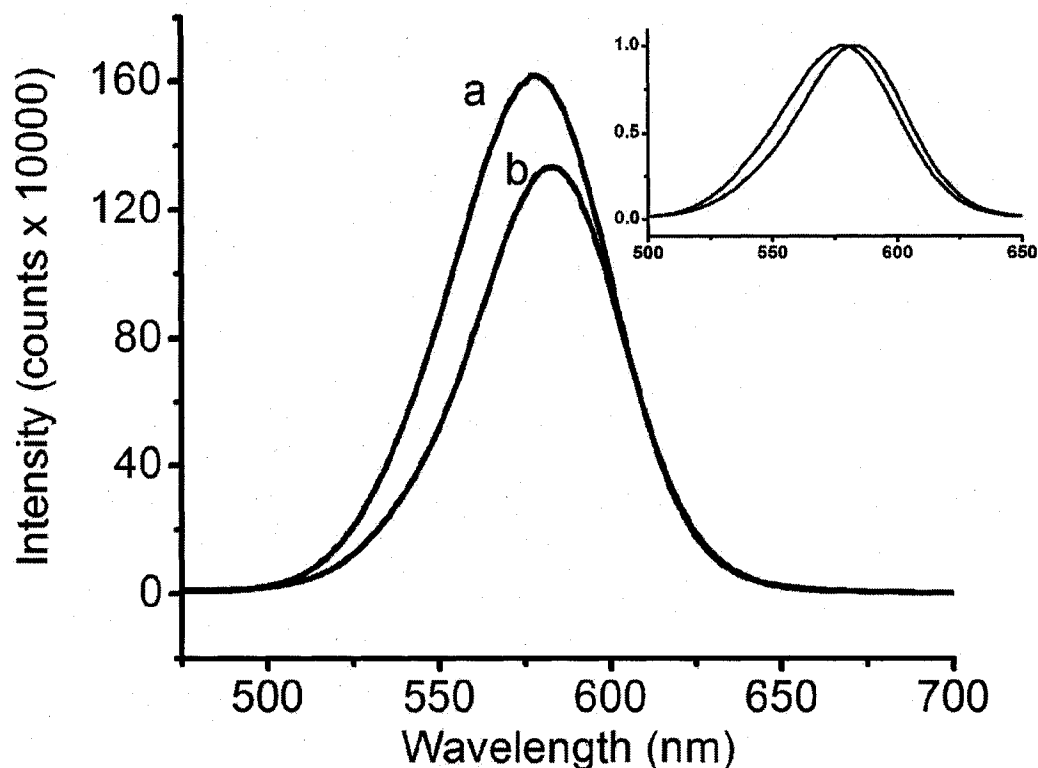


Figure 3.4 Emission spectra of quantum dots (a) in solution and (b) self-assembled on Flagella. Inset shows emission spectra of normalized for absorbance at the excitation wave length.

These observations are similar to those of Meijerink for CdTe QDs linked by thiol ligands and theoretical calculations of Forchel for exciton energy transfer between CdTe QDs as a function of their separation. The 18.4 meV energy change is consistent with the average interparticle distance of 2.4 nm for the CdTe QDs on the His-loop flagella. Further evidence for the exciton energy transfer among CdTe quantum dots is also obtained from emission lifetime measurements by monitoring the emission intensity as a function of time shown in Figure 3.5. The exciton lifetime of the cysteine capped nanoparticles of CdTe QDs in solution was determined to be

18.1 ns and those for the CdTe QDs on His-loop flagella to be 15.5 ns. The difference in the lifetimes of the free and flagella-bound nanoparticles is evident from the inset in Figure 3.5 displaying the emission intensity for the initial 30 ns. The approximately 2.5 ns reduction in the lifetime of the CdTe excitation can be rationalized as arising from the exciton energy transfer from small to large flagella bound CdTe quantum dots.

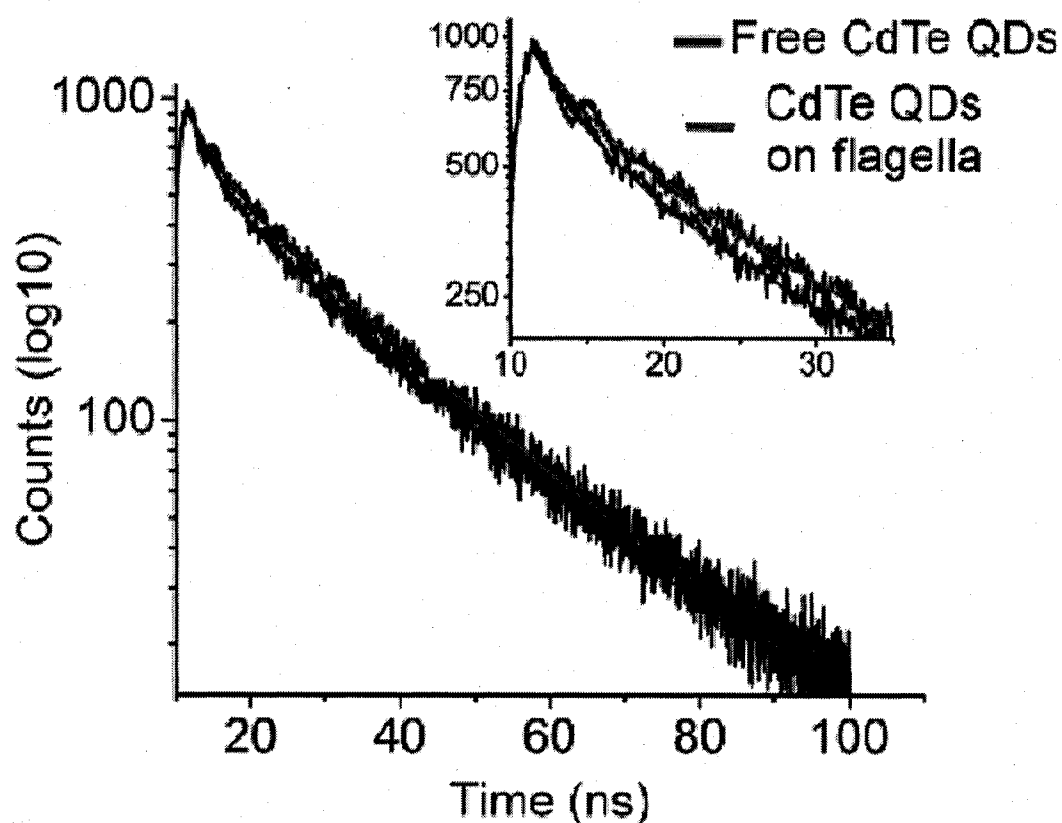


Figure 3.5 Emission intensity decay as a function of time for free CdTe in solution and those bound to His-loop flagella. The jagged lines represent the experimental data and the solid lines the fit from which the exciton lifetimes were obtained. The inset shows the data from 10 – 30 ns to indicate differences in the lifetimes of the quantum dots free in solution and those bound to the His-loop flagella. Decay curves were collected at 580 nm with excitation at 400 nm using hydrogen filled nF900 nanosecond flash lamp operating at 40 kHz.

Conclusion

We have successfully self-assembled ZnS:Mn and CdTe QDs on flagella nanotubes displaying histidine peptide loops on their outer domain regions. The interparticle interaction of the QDs separated by about 2.4 nm does not lead to shift in the emission wavelength maximum and lifetime change for the Mn-centered emission of the ZnS:Mn QDs. Such an interaction for CdTe QDs resulted in exciton energy transfer from smaller to larger QDs, resulting in a 5 nm red shift (18.4 meV energy) of the exciton emission peak and a shortening of the exciton lifetime by about a 2.5 ns. The flagella-quantum dot composites are fundamentally interesting and important bionanostructures and further investigations with other engineered peptide loops are underway.

CHAPTER IV

SELF-ASSEMBLY OF METAL NANOPARTICLES AND NANOTUBES ON
BIOENGINEERED FLAGELLA SCAFFOLDS

Introduction

The utilization of self-assembling biological systems in nanofabrication is attractive because of their genetically controlled reproducibility at the molecular level; they have the property of controlled self-assembly, often leading to the generation of less polydisperse nanoscale materials compared to chemical synthetic procedures. In addition, biomaterials are environmentally friendly and have a higher probability for biocompatibility. Peptide and protein assemblies are being actively investigated as nanotube templates for casting metal nanowires and nanotubes, and as scaffolds for the self-assembly of nanoparticles (174, 175). One example of a self-assembling protein nanotube is the M13 virus, which has been genetically engineered to display peptides on its surface (176-178). These phage-displayed peptides may be selected for specific affinity for inorganic materials (179, 180) and used as scaffolds for the controlled assembly or generation of inorganic nanoparticles and nanowires (7, 21, 26, 139, 140, 181, 182). Furthermore, self-assembling beta-amyloid peptides, composed of a fragment of a Sup35p prion determinant from *Saccharomyces cerevisiae*, have also been demonstrated for the assembly of gold and silver nanowires (183). Microtubules and peptide nanotubes have also been used as scaffolds for binding nanoparticles and as templates for the synthesis of monodisperse

nanoparticles and metal nanotubes (4, 9, 174, 184-192). The resulting nanostructures prepared with these biomaterials and other organic and inorganic materials have been proposed to function as conducting wires for use in microcircuits, optical signal enhancing cuvettes, lithium ion batteries, catalysts, and as tool kits for the fabrication of nanoparticles (193-195).

Gold nanoparticles and composite structures, e.g., nanowires, have been proposed to have applications as small capacitors, biosensors and conductors (196). The ordered assembly of gold nanoparticles is important because their optical properties depend on particle shape, size, the dielectric constant of the surrounding media, and the interparticle distance. Synthesis and assembly of gold nanoparticles and nanowires on carbon nanotubes, (197-199) silica nanotubes, (139, 200, 201) lipids, (202-204) virus particles, (4, 9, 188-192) DNA, (203, 204) and self-assembling peptide nanotubes (205-210) have been described by several research groups. However, these methods may generate randomly distributed nanoparticles without consistent diameters and inter-particle distances on the peptide or protein scaffolds (211). Similarly, Cu nanotubes have been generated by vapor deposition, electrodeposition, and chemical methods (212) on carbon nanotubes, (213) by supercritical fluid decomposition on silica, (9, 185) on DNA, (214) and on peptide nanotubes (215). Studies have also been reported on the formation of Co nanoparticles and nanotubes on silica, (26, 182) on carbon fibers for use as Fischer-Tropsch catalysts, (216) and on M13 virus particles (217). Nanoparticles and nanotubes composed of the platinum group metals Pd and Pt have been synthesized

by chemical methods, (218) in supercritical fluids, (219) on carbon nanotubes, (192, 220, 221) on DNA, (200) on protein and peptide nanotubes, (222, 223) and on tobacco mosaic virus particles (224). The generation of Ag nanoparticles and nanotubes has also been examined to a limited extent by chemical deposition methods on aluminum and polycarbonate membranes, (225, 226) on DNA, (200) on peptide nanotubes and on tobacco mosaic virus particles (227). Thus, biomolecules such as DNA, viruses, peptides, and proteins, as exemplified by these studies, are attractive and useful as scaffolds and templates for the generation of the nanoparticles and nanotubes of a variety of metals.

Flagella nanotubes are complementary to the various biological scaffolds that are being investigated for the generation of uniform array of nanoparticles and nanotubes. Each segment of the flagella nanotube contains a flagellin protein 11-mer. Introduction of peptide loops in the D3 domain of the flagellin protein yields an extremely ordered array of binding sites for cations and anions which can be used as precursors for the generation of nanoparticles and nanotubes. Flagella nanotubes represent a system that can be manipulated for the generation of ordered nanomaterials for catalysis, molecular electronics, and other applications. In this study, FliTrx flagella engineered to display constrained peptide loops containing imidazole groups, cationic amine and guanido groups, and anionic carboxylic acid groups were used as scaffolds for the self-assembly of metal nanoparticles and nanotubes, as summarized in Table 4.1. The transition metal ion Co(II), the Group IB ions Cu(II), Ag(I), and Au(I), the Group IIB ion Cd(II), and the platinum group metal

Pd(II) were complexed with histidine, arginine, lysine, aspartic acid and glutamic acid residues in loop peptides and reduced with NaBH₄ or hydroquinone, in the case of Ag(I). These studies are complementary to other research efforts to exploit biological molecules as scaffolds and templates for the bottom-up construction of ordered nanomaterials (51)

Experimental Methods

Materials

The commonly employed chemicals and their sources and the instrumental techniques are listed here. More specific methods, chemicals and instruments are described under appropriate sections. All chemicals were reagent grade or better and were obtained from Sigma-Aldrich (St. Louis, MO), unless otherwise noted. All transmission electron microscope (TEM) Formvar sample-imaging grids were obtained from Electron Microscopy Science (Fort Washington, PA). TEM images were taken with a JEOL model JEM 1230 TEM operating at 80 kV or a JEOL model 3011 TEM operating at 300 kV.

Engineering of FliTrx Flagella Loop Peptide Variants for Use as Bionanotube Scaffolds and Templates

The development of the FliTrx system for the display of constrained peptide loops on the surface of *E. coli* flagella fibers has been previously described (70, 71, 73). As detailed in a previous publication, (215) the multiple cloning site region of the

commercially available pFliTrx plasmid, which encoded a foreign peptide, was removed and replaced with the wild-type thioredoxin active-site DNA sequence, which encoded a unique RsrII restriction site. Furthermore, a non-native cysteine residue with a thiol side chain was mutated to serine to minimize the potential for intermolecular disulfide bond formation. The resulting modified pFliTrx plasmid is suitable for insertion of DNA oligonucleotide cassettes that encode displayed loop peptides in the solvent-exposed thioredoxin active site on the surface of FliTrx flagella.

The loop peptides chosen for this study were primarily composed of histidine, glutamic acid and aspartic acid, or arginine and lysine amino acid residues. Oligonucleotides encoding the loop peptides used in this study are described in Supporting Information; the modified plasmid DNA was isolated and insertional mutations were confirmed by DNA sequencing (see Supporting Information). The three loop peptides consisted of a 4X insert of a one glycine, six histidine loop (“His-loop”) peptide containing imidazole groups (-Gly-His-His-His-His-His-His-; GHHHHHH), a 3X insert of an anionic “Asp-Glu loop” peptide composed of one histidine residue, three glutamic acid residues, and three aspartic acid residues, and one glycine residue (-His-Asp-Glu-Asp-Glu-Asp-Glu-; HDEDEDE), and a single insert of a cationic “Arg-Lys loop” peptide encoding four arginine residues with guanido side chain groups and three lysine residues with amine side chain groups (-Arg-Lys-Arg-Lys-Arg-Lys-Arg-; RKRKRKR). Plasmids encoding the loop peptides were used to express FliTrx flagella fibers with peptide loops displayed on their surface and

purified from *E. coli*.

Generation of Nanoparticle Arrays and Nanotubes on Flagella with Peptide Loops

In general an appropriate metal ion or its complex was bound to the suitable peptide loop followed by controlled reduction to generate metal nanoparticle arrays and nanotubes on the flagella. Control experiments were performed with the wild-type (unmodified) flagella with all metal ions studied to demonstrate that they did not bind to the flagella and metal nanoparticles and nanotubes were not generated on the flagella when they were reduced, as indicated by TEM images. Examples of TEM images from control experiments have been included in the figures demonstrating the generation of nanoparticles and nanotubes on flagella with peptide loops.

Generation of Gold Nanoparticle Arrays on Histidine Loop Flagella

Gold nanoparticles were synthesized using the His-loop flagella as a nucleation template. Control experiments were also performed with the wild type flagella to clearly indicate the role of the peptide loops in generating Au nanoparticle arrays on peptide modified flagella. A volume of 500 μL of 2 mg/mL solution of flagella with a 28-mer His-loop peptide composed of four repeats of the Gly-His-His-His-His-His heptapeptide sequence (for a total of 24 histidines) was mixed with 10 μL of saturated chloro(trimethylphosphine)gold(I) in deionized water at 4 °C. The Au complex was incubated with flagella for 24 h at 4 °C and reduced with 25 μL of 50

mM sodium borohydride solution at room temperature. TEM samples were prepared by placing 10 μ L of the resulting solution on a carbon coated Formvar copper grid for 2 min; excess solution was removed by blotting with a piece of filter paper.

Covalent Attachment of Gold Nanoparticles to Arginine-Lysine Loop Flagella

A different approach was used to covalently attach gold nanoparticles to an Arg-Lys loop flagella scaffold. Two sizes of 10-thioldecanoic acid-coated Au nanoparticles, 3 nm and 12 nm, were coupled to lysine amine groups in the Arg-Lys loop flagella. Synthesis of 3 nm and 12 nm diameter gold nanoparticles, protected by citrate, is described elsewhere. The sizes of the nanoparticles were determined by TEM and showed a 10% polydispersity. The citrate coating on the Au nanoparticles was replaced with 10-thioldecanoic acid, and the carboxylic groups were further modified to sulfo-succinamide esters by reaction with 1-ethyl-3-(3-dimethylaminopropyl)-carbodiimide and sulfo-N-hydroxysuccinamide at pH 7 in 50 mM HEPES buffer. The resulting surface modified Au nanoparticles were well dispersed in water and the excess reactants were removed by diafiltration with a Centricon 3 kDa MWCO centrifugal filter unit (Millipore, Billerica, MA), using excess buffer. The Au nanoparticles, with amine-reactive surface groups, were dispersed in 100 μ L of 20 mM HEPES buffer, and 10 μ L of this suspension was mixed with 200 μ L of 2 mg/mL of flagella with a single insert of the Arg-Lys loop peptide (RKRKRKR). After 30 min, 10 μ L of this mixture was placed on a carbon

coated Formvar copper grid and allowed to settle on the grid for 1 min. Excess solution was removed by blotting with filter paper and TEM images were collected.

Generation of Copper Nanoparticle Arrays and Nanowires on Histidine Loop Flagella

Cu(II) ions in a 5 mM solution of CuCl_2 , CuSO_4 , or $\text{Cu}(\text{NO}_3)_2$ were allowed to complex with the imidazole side chains of the His-loop flagellin histidine residues and wild type flagella for control experiments for 24 h at 4 °C at pH 7.0. Immobilized Cu(II) ions were reduced by successive addition of 20 μL of freshly prepared 100 mM NaBH_4 solution at 4 °C. The same procedure was followed to synthesize copper nanoparticles on the His-loop flagella template using a 0.05 mM Cu(II) solution. The resulting Cu nanoparticle or Cu nanotube flagella composites were immobilized on a carbon coated Formvar copper TEM grid by placing 10 μL of the resulting solution on the grid. After one minute, excess solution was removed by blotting with filter paper and TEM images were recorded.

Generation of Cobalt Nanoparticles on Histidine Loop Flagella

These studies were extended to the transition metal Co, the Group IB metal Ag, the Group IIB metal Cd and the platinum group metal Pd. In all cases, suitable divalent metal ions (Co(II), Cd(II), Pd(II)) were complexed to imidazole groups on His-loop flagella and wild type flagella for control experiments and reduced in a controlled

manner with NaBH_4 . In the case of Ag(I) and Co(II) ions, complexation with Asp-Glu peptide loops and subsequent Ag(I) reduction with a hydroquinone solution at a pH of 10.5, and Co(II) reduction with NaBH_4 were also studied. The immobilization and subsequent reduction of Co(II) , Cd(II) , Pd(II) , and Ag(I) ions had to be carried out on a TEM grid and immediately characterized. This was in contrast to the studies with Cu(II) and Au(I) described above, where the immobilization and reduction studies were conducted in bulk solution in vials, and nanotube samples were subsequently placed on carbon coated Formvar copper TEM grids for image characterization.

Cobalt nanoparticles were generated by careful reduction of Co^{2+} ions complexed with histidine imidazole groups on the 4X insert His-loop FliTrx variant (with 24 histidine residues), or aspartic acid and glutamic acid carboxylic acid groups on the Asp-Glu loop flagella. The Asp-Glu variant used in this study had an insert of three repeats of the anionic Asp-Glu loop sequence (HDEDEDEG-HDEDEDEG-HDEDEDEG), for a total of 18 carboxylate groups, and three histidine groups. Flagella with His-loop or Asp-Glu loop peptides were immobilized on a carbon coated Formvar copper TEM grid and 10 μL of 50 mM CoCl_2 solution was placed on the grid for one min. Excess solvent was removed by blotting with a piece of filter paper and followed by a 5 min reduction with 10 μL of 10 mM NaBH_4 solution and collection of TEM images.

Generation of Palladium and Cadmium Nanoparticles on Aspartic Acid-Glutamic Acid Loop Flagella

Palladium and cadmium nanoparticles were generated on His-loop flagella using the same procedure used for cobalt. A 50 mM CdCl₂ solution and a saturated solution of palladium acetate, prepared by sonicating excess palladium acetate in deionized water followed by centrifugation to remove insoluble residues, were used as precursors for the formation of metal nanostructures.

Generation of Silver Nanowires on Aspartic Acid-Glutamic Acid Loop Flagella

Silver nanowires were generated by immobilizing Ag(I) on anionic Asp-Glu loop flagella and wild type flagella (control) deposited on a carbon coated Formvar copper grid and careful reduction with NaBH₄. A 10 μL volume of 20 mM AgNO₃ solution (pH adjusted to 10.5 with ammonium hydroxide) was placed on the TEM grid with immobilized flagella for one min and excess solution was removed by blotting with filter paper. Immobilized silver ions were reduced with 10 μL of 10 mM hydroquinone solution (pH adjusted to 10.5 with ammonium hydroxide) for five min and TEM images were collected.

Results and Discussion

The various types of FliTrx loop-nanomaterial systems used in this study are summarized in Table 4.1, including the FliTrx peptide loop composition, the use of

pre-synthesized nanoparticles vs. templated synthesis in situ, and the resulting type of hybrid nanomaterial, i.e., nanoparticle arrays or continuous nanotubes.

Generation of Gold Nanoparticle Arrays on Histidine Loop Flagella

This procedure yielded 5.93 (± 1.48) nm diameter Au nanoparticles attached to the surface of the flagella scaffold as determined by TEM. Representative TEM images are shown in Figure 4.1, where images a and b were taken with flagella on a carbon coated Formvar copper grid, image c is a high resolution image of gold nanoparticles and image d is the result of Au nanoparticle generation on wild type flagella. The Au nanoparticles define the outer edge of the flagella nanotubes as they are bound to the solvent exposed D3 domain. The Au nanoparticles are not bound to the wild type flagella which lack the histidine loops as evident from Figure 4.1d. The process of Au nanoparticle formation is proposed to first involve binding of Au(I) ions by imidazole groups of the solvent-exposed loop peptide histidine residues, followed by reduction of Au(I) ions to Au(0) by controlled addition of NaBH₄. These histidine bound Au(0) centers serve as nucleating sites for the growth of Au nanoparticles by the reduction of unbound Au(I). In the absence of histidine loops with wild type flagella free Au nanoparticles are formed in solution as seen in Figure 4.1d.

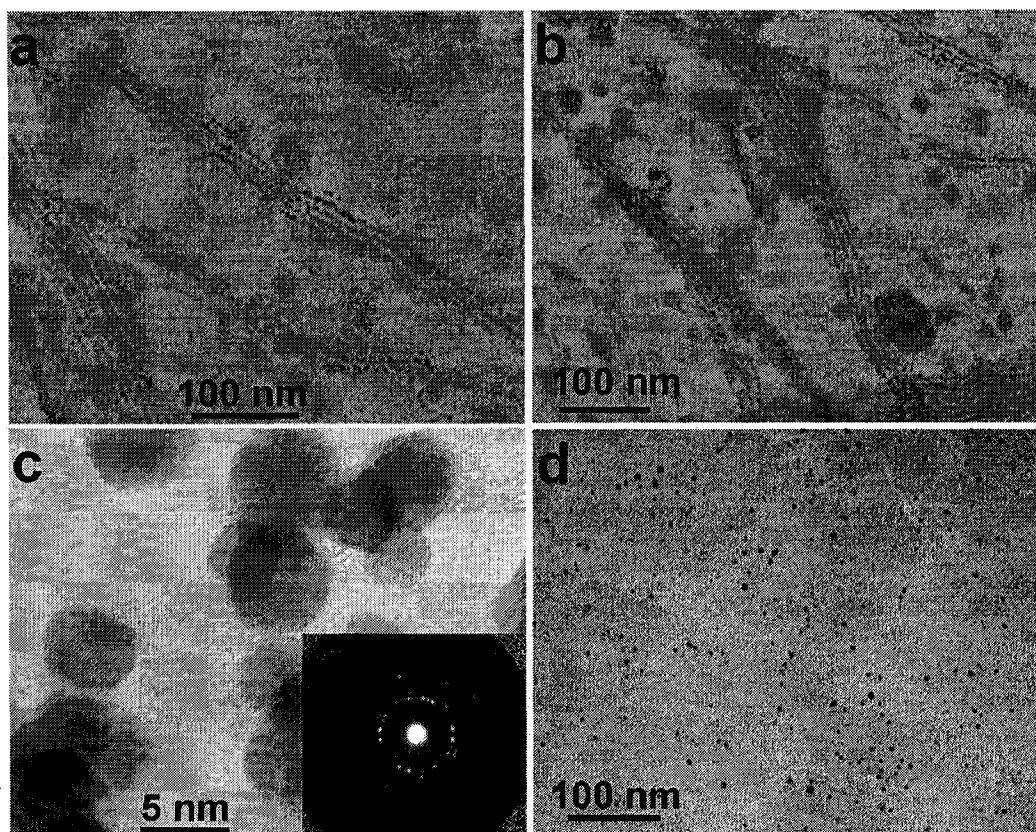


Figure 4.1 Gold nanoparticle-flagella nanotube composite materials obtained by reduction of Au(I). (a) and (b) TEM images of gold nanoparticles that were synthesized by reduction of Au(I) on a histidine-loop peptide flagella scaffold. (c) High resolution TEM image of individual gold nanoparticles on flagella; (Inset) electron diffraction pattern of gold nanoparticles on flagella indicative of metallic gold nanoparticles. (d) TEM image of control experiment of the reduction of Au(I) on wild type (without histidine loops) flagella indicating no attachment of Au and only random distribution of Au nanoparticles.

The visible absorption spectrum of the 6 nm Au nanoparticles on the His-loop flagella scaffold is shown in Figure 4.2 a. The Au-flagellin nanocomposite exhibited

an absorption maximum (λ_{max}) at 522.5 nm due to surface plasmon resonance of the Au nanoparticles. The TEM image of the flagella indicated an ordered array of Au nanoparticles on the flagella backbone. The Au nanoparticles are presumably bound to the histidine peptide loops on the flagellin D2-D3 outer domain region. The longitudinal axial distance between two consecutive D3 domains of flagella is approximately 5 nm. Thus, the ordered arrangement of the Au nanoparticles is probably a direct result of the ordered display of the peptide loops at regular intervals on the flagella scaffold surface. Some lateral association of flagella with Au nanoparticles occurred, as observed in Figures 1a and b, where bundled assemblies of two and three flagella fibers can be seen. However, the aggregation was not so extensive as to adversely affect the surface plasmon resonance, as shown in Figure 4.2 a.

The effect of disassembly of the flagella scaffold on the Au nanoparticle surface plasmon resonance was also investigated. The aggregated flagella nanotubes with bound Au nanoparticles were dissociated by heating them to 80 °C for 5 min and cooling to 25 °C. The mesophilic FliTrx *E. coli* flagella oligomers will dissociate into flagellin protein monomers over the temperature range of 50-60 °C. The heated and cooled Au-flagellin solution exhibited a 16% increase in absorbance intensity and a ~5 nm shift in λ_{max} to 527 nm (Figure 4.2b). The heating and cooling process, in addition to breaking up multimeric nanotube assemblies, also resulted in the formation of monomeric flagella and free gold nanoparticles as discerned from TEM images; dissociated Au nanoparticles precipitated from this heated solution within 2

h. Thus, the absorbance increase was likely due to disassembly of the flagella aggregates and dissociation of Au nanoparticles from the flagella nanotubes, with the small red shift in λ_{max} due to aggregation of disassembled nanoparticles.

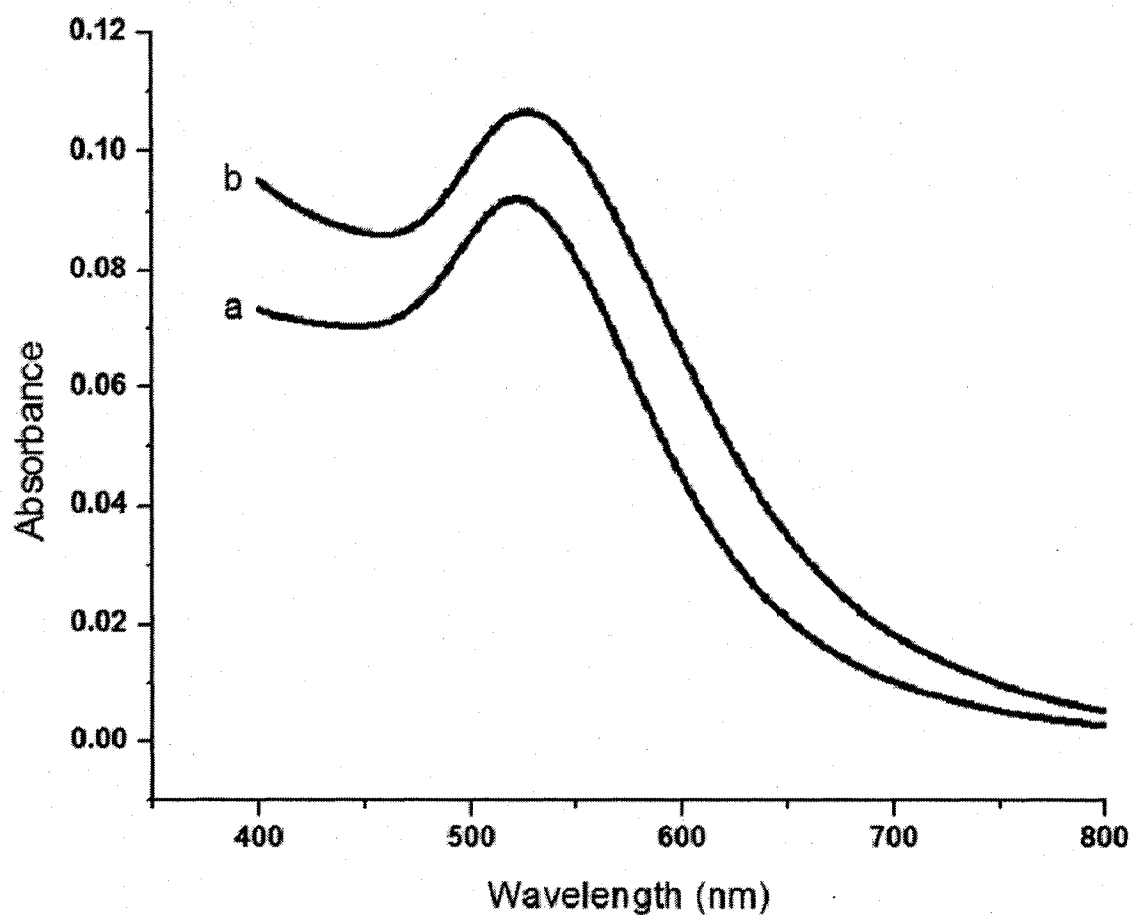


Figure 4.2 Visible absorbance spectra of gold nanoparticles on histidine-loop peptide flagella. (a) Absorbance spectrum of gold nanoparticles synthesized on flagella, showing surface plasmon resonance peak. (b) Absorbance spectrum of gold nanoparticle-flagella sample after heating to 80 °C for five minutes and cooling to room temperature.

Covalent Attachment of Gold Nanoparticles to Arginine-Lysine Loop Flagella

Covalent attachment of the pre-synthesized 3 nm Au nanoparticles by published method, (203) resulted in the formation of ca. 500 nm diameter flagella bundles with a dense layer of Au nanoparticles, as indicated in Figures 4.3 a and b. A high resolution TEM image of individual Au nanoparticles is shown in Figure 4.3 c. A schematic diagram depicting the covalent amide bond formed between the terminal amine groups of lysine residues and the outer carboxylate groups of the surface modified Au nanoparticles is shown in Figure 4.3. Amide bond formation between Au nanoparticles and flagella Arg-Lys loop peptides resulted in extensive aggregation of flagella due to the multiple attachment sites available on both the derivatized nanoparticles and flagella with Arg-Lys loops. In contrast, binding of $\text{Au}(\text{P}(\text{CH}_3))_3\text{Cl}$ on histidine imidazole groups of His-loop flagella and controlled synthesis by reduction with NaBH_4 resulted in generation of ordered arrays of Au nanoparticles and limited aggregation of flagella nanotubes. Covalent attachment of the larger 12 nm Au nanoparticles to the Arg-Lys loop flagella resulted in formation of larger, more extensive aggregates (Figure 4.3 d) than were observed for the 3 nm Au nanoparticles; these larger Au-flagellin aggregates were not stable in solution and rapidly precipitated.

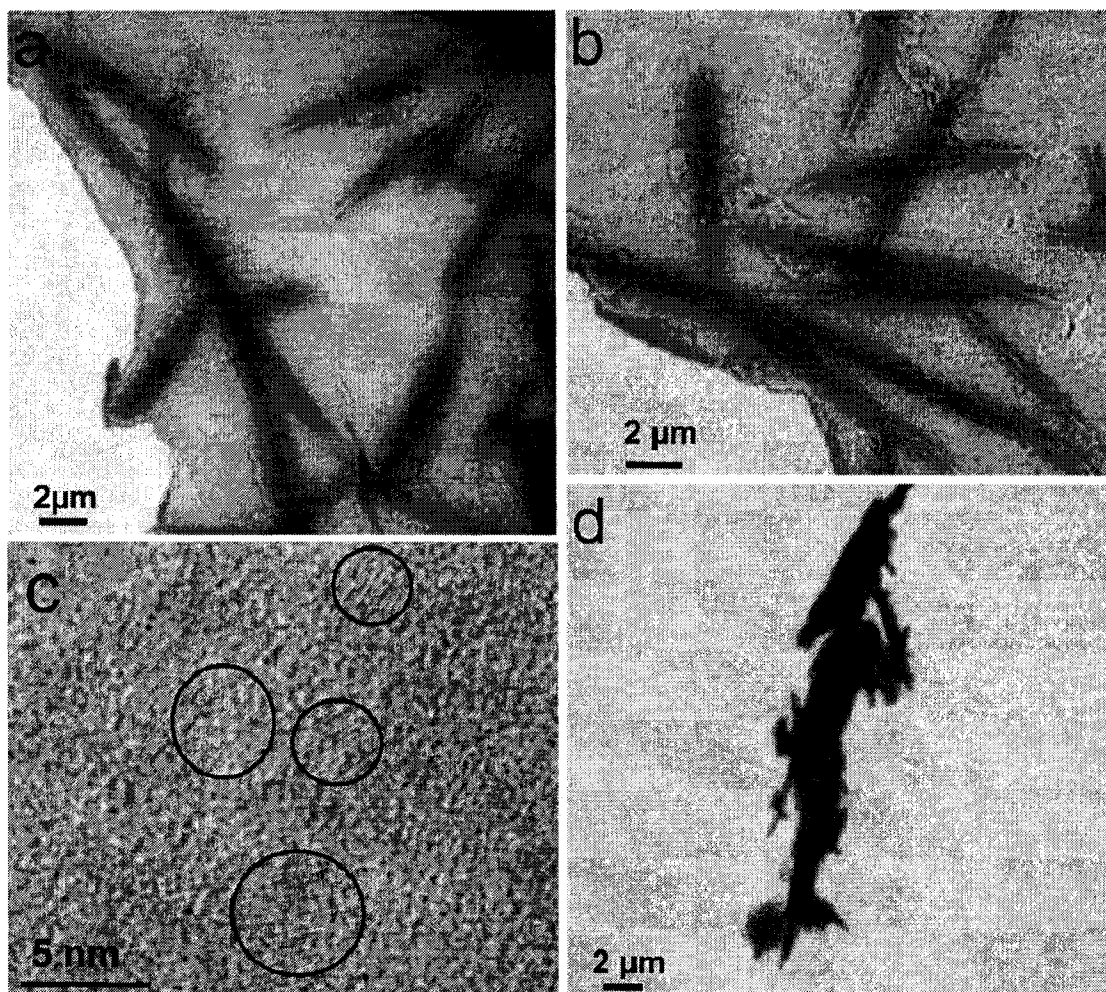


Figure 4.3 Gold nanoparticle-flagellin nanotube composite materials prepared by covalent attachment of pre-made gold nanoparticles. (a) and (b) TEM images of 3 nm gold nanoparticles attached by amine coupling to arginine-lysine peptide loop flagella. (c) High resolution TEM image of 3 nm gold nanoparticles attached to flagella. (d) TEM image of 10 nm gold nanoparticles attached by amine coupling to arginine-lysine peptide loop flagella. These images are representative of the aggregated bundles generated by this procedure.

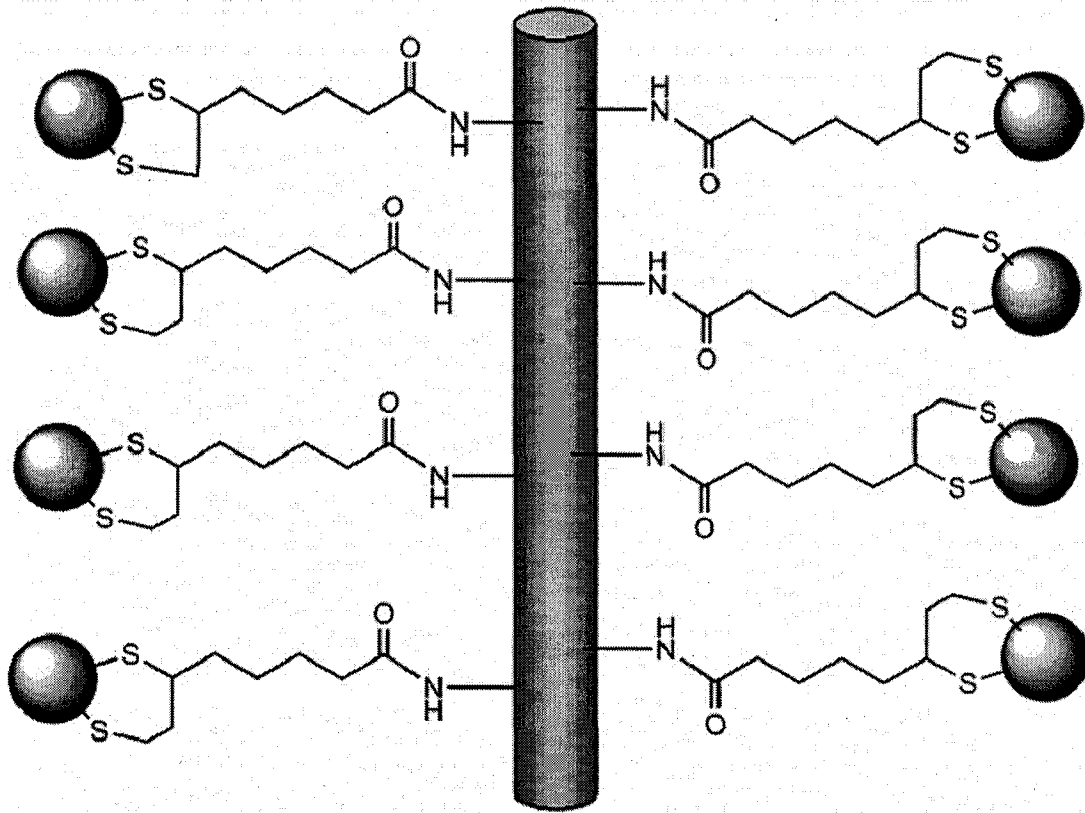


Figure 4.4 Diagram of covalent immobilization of pre-made gold nanoparticles on flagella by amide bond formation with arginine-lysine peptide loops.

Generation of Copper Nanoparticle Arrays and Nanowires on Histidine Loop Flagella

Both individual Cu nanoparticles (Figure 4.5d) and continuous Cu nanotubes (Figures 4.5a-c) could be generated on the flagella backbone when Cu(II) ions were complexed with imidazole in the His-loop peptide and reduced with 10 mM NaBH₄ in a controlled manner. A schematic of the probable mechanism of formation of Cu nanoparticles and nanotubes is given in Figure 6. The Cu nanotubes were generated by the reduction of 5 mM of Cu(II) with 100 mM NaBH₄ and their TEM images are shown in Figures 4.5a-c. It is evident from these images that the flagella nanotube has facilitated the formation of Cu nanotubes by the growth of a layer of Cu on the flagella. Most of the Cu nanotubes had a diameter of approximately 100 nm. The uniformity of growth of Cu nanotubes on the flagella templates is striking compared to Au, which resulted in formation of dense bundles. TEM images of flagella with Cu nanoparticles are shown in Figure 4.5d, with a corresponding high resolution TEM image of the Cu nanoparticles shown in Figure 5e. The flagella fibers prepared with Cu nanoparticles did not exhibit much aggregation, unlike those with Au nanoparticles. Clearly, the behavior of the two Group IB metals, Cu and Au, is quite different under the experimental conditions studied. This may be the consequence of the oxide layer formation on Cu to a greater extent compared to Au which inhibits aggregation. Only free Cu nanoparticles were obtained as seen in Figure 4.5f when wild type flagella was employed clearly indicating the role of the histidine loops in facilitating the formation of Cu nanotubes and ordered array of Cu nanoparticles.

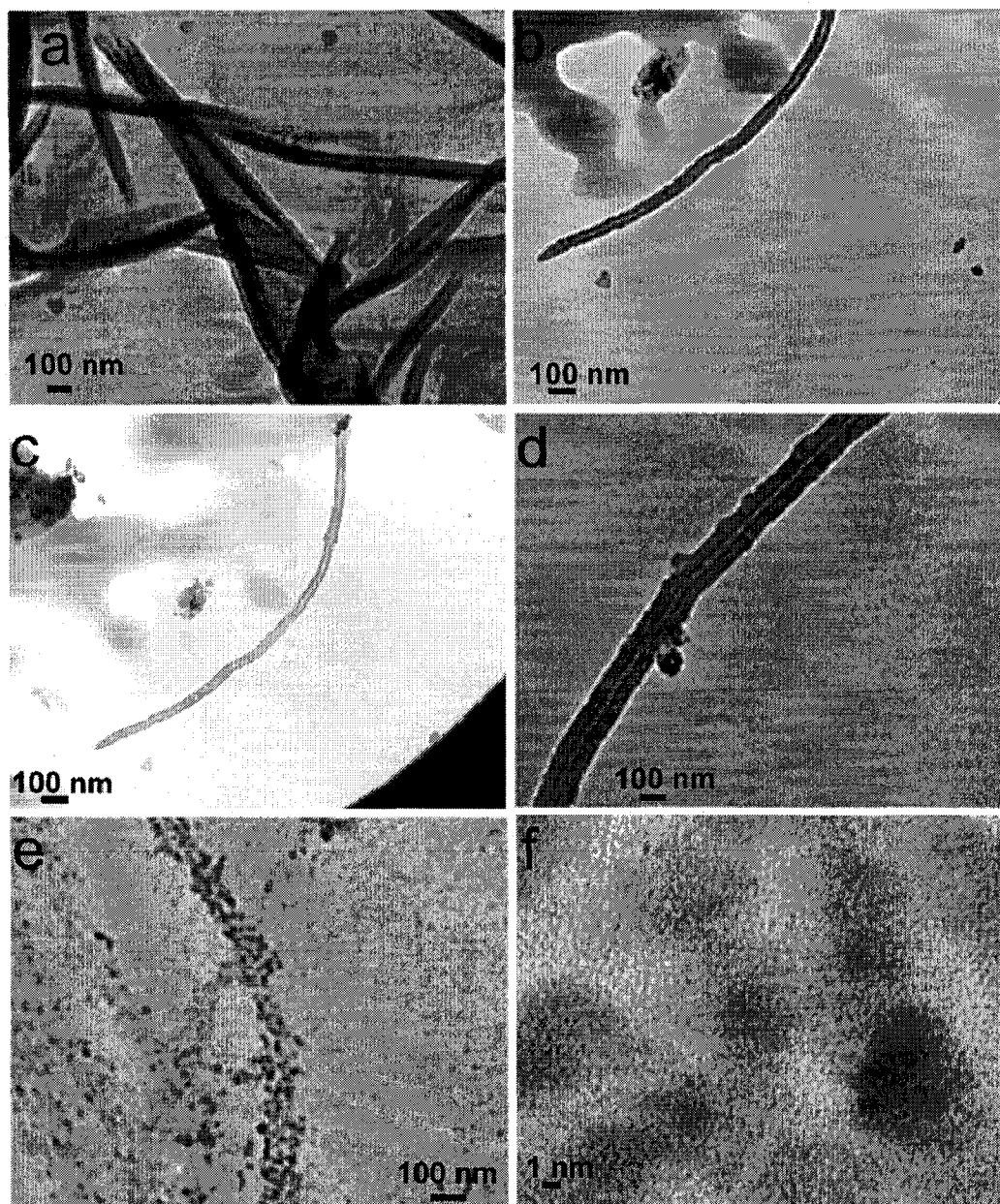


Figure 4.5 Copper-flagellin composite nanomaterials. (a), (b), and (c) TEM images of copper nanotubes synthesized by reduction of Cu(II) on histidine-loop flagella. (d) TEM image of copper nanoparticles synthesized by reduction of Cu(II) on histidine-loop flagella. (e) High resolution TEM image of copper nanoparticles synthesized on histidine-loop flagella. (f) TEM image of control experiment of the reduction of Cu(II) on wild type (without histidine loops) flagella indicating no attachment of Cu and only random distribution of Cu nanoparticles and clusters.

The formation of Cu nanoparticles and nanotubes can be rationalized by the reduction of Cu(II) complexed with histidine to form nucleating sites, on which further growth of Cu metal occurs from free Cu(II) ions in solution. When a low concentration (0.05 mM) of Cu(II) was employed, the nucleation process resulted in formation of individual nanoparticles on the flagella scaffold. When a 100X higher concentration (5.0 mM) of Cu(II) was employed, the nucleation process proceeded further, forming a continuous layer of Cu metal. The thin layer of Cu initially formed becomes the substrate for further growth of additional layers of Cu, leading to the generation of ~100 nm diameter Cu nanotubes encasing the flagella nanotube templates. Experiments are underway to remove the flagella in a controlled manner to obtain pure Cu nanotubes. Such nanotubes can be further derivatized, e.g., via thiol chemistry, to attach various functional groups. Cu nanotubes functionalized with appropriate functional groups could function as a sensor platform and have applications in molecular electronics.

Generation of Cobalt Nanoparticles on Histidine Loop Flagella

Figures 6.6a and b indicate Co nanoparticles synthesized on Asp-Glu loop peptide flagella; Figures 4.6c-e indicate Co nanoparticles synthesized on His-loop flagella. Figure 4.6e indicates that the Co nanoparticles generated with the wild type flagella leads to a mixture of the two instead of an array of nanoparticles on flagella when peptide loops are present. An ordered array of Co nanoparticles was obtained by reduction of Co(II) on Asp-Glu loop flagella (Figures 4.6a and b), while use of the His-loop flagella scaffold resulted in formation of a more dense assembly of nanoparticles on the flagella (Figures 4.6c-e). This result may be due to the higher affinity of the imidazole side chain of histidine for Co(II) transition metal ions, compared to the carboxylic side chains of glutamate and aspartate. The reduction of Co(II) was performed under ambient atmosphere; this suggests that the nanoparticle surfaces are most likely oxidized, resulting in formation of CoO, Co₂O₃, and Co₃O₄ oxide layers. Further studies are underway to characterize the nature of these nanoparticles by magnetic susceptibility measurements. We are also investigating their catalytic applications for reactions such as the Fischer-Tropsch alkane synthesis.

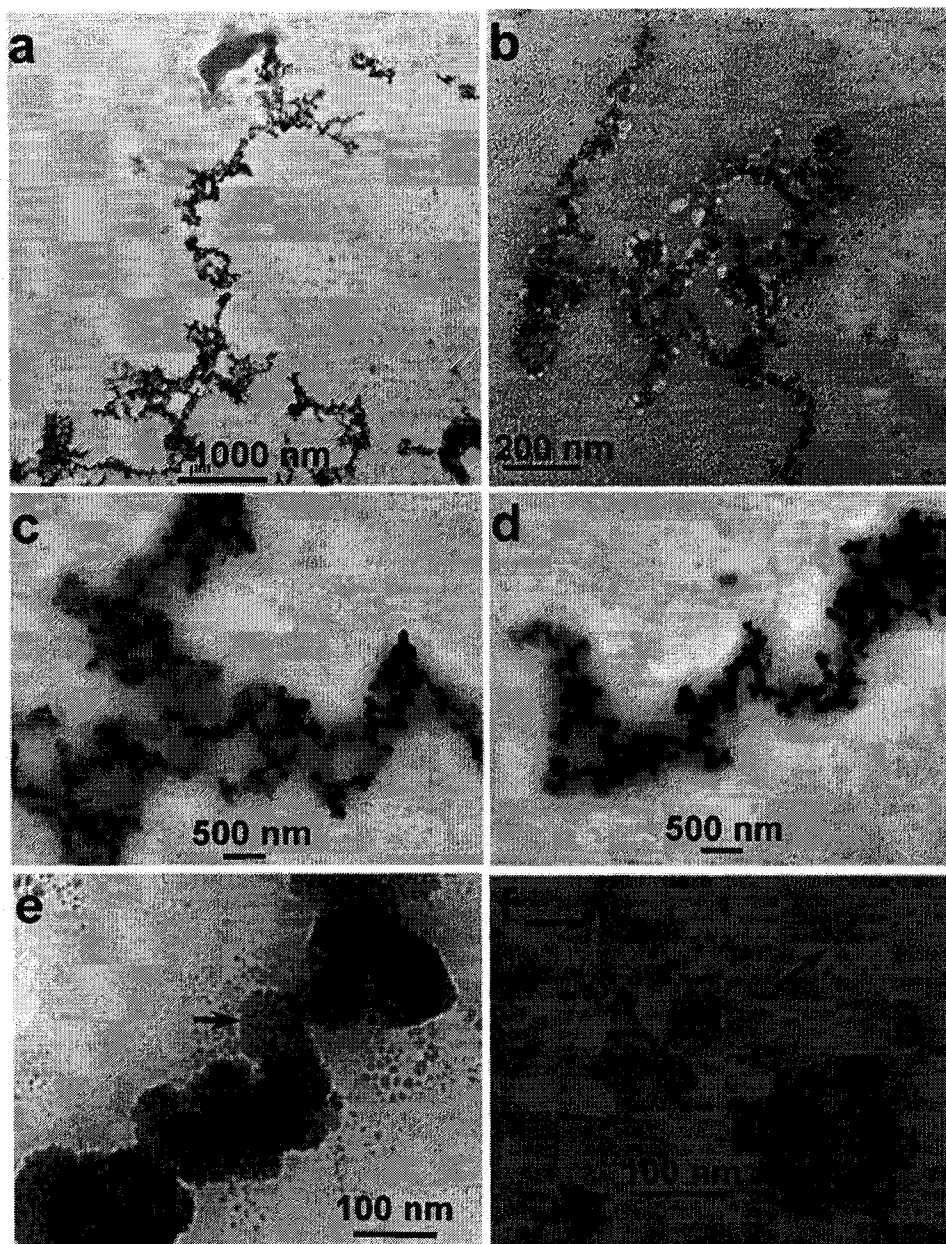


Figure 4.6 Cobalt-flagella composite nanomaterials. (a) and (b) TEM images of cobalt nanoparticles synthesized by reduction of Co(II) on glutamic acid-aspartic acid peptide loop flagella. (c), (d), and (e) TEM images of cobalt nanoparticles synthesized by reduction of Co(II) on histidine-loop flagella. Arrow indicates Co nanoparticles. (f) TEM image of control experiment of the reduction of Co(II) on wild type (without histidine loops) flagella indicating no attachment of Co and only random distribution of Co nanoparticles and clusters and flagella nanotubes. Arrows indicate the presence separately of Co nanoparticles and flagella.

Generation of Palladium and Cadmium Nanoparticles on Aspartic Acid-Glutamic Acid Loop Flagella

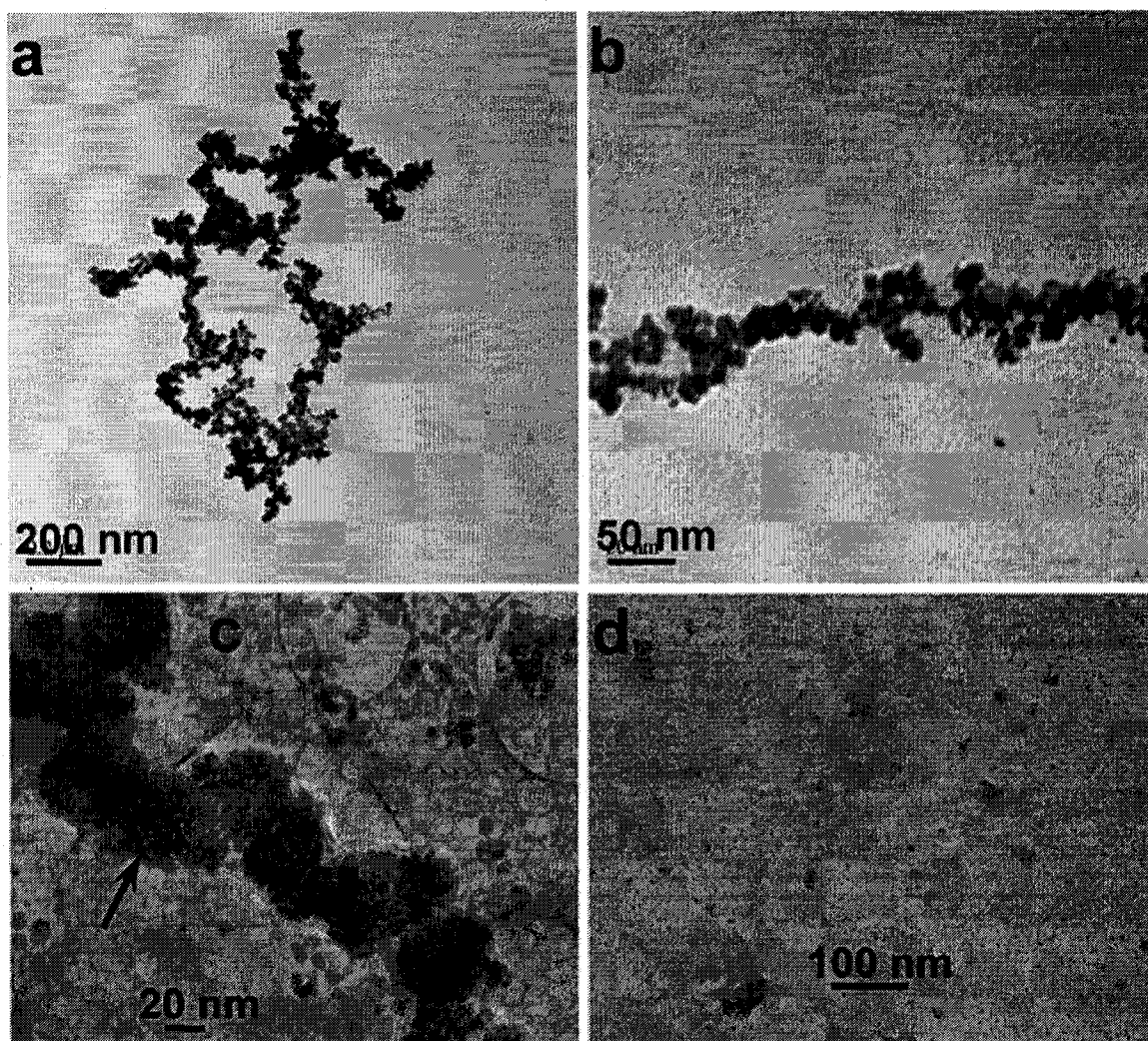


Figure 4.7 Palladium-flagellin nanocomposites. (a), (b), and (c) TEM images of palladium nanoparticles synthesized by reduction of Pd(II) on histidine-loop flagella. Arrow indicates the Pd nanoparticles. (d) TEM image of control experiment of the reduction of Pd(II) on wild type without (histidine loops) flagella indicating no attachment of Pd and only random distribution of Pd nanoparticles.

Figure Figures 4.7 a-c indicate Pd nanoparticles synthesized on His-loop flagella and Figure 8d the generation of Pd nanoparticles with the wild type flagella. Figure 9e indicates Cd nanoparticles synthesized on His-loop flagella and Figure 9f the generation of Cd nanoparticles in the presence of wild type flagella. The controlled reduction with NaBH_4 of Pd(II) and Cd(II) complexed with the His-loop flagella largely yielded nanoparticle arrays which were absent with the wild type flagella. It may be seen from Figure 8c that Pd nanoparticles are present on the His-loop flagella. The images in Figures 8a and 8b indicate that the formation of Pd nanoparticles did not result in extensive aggregation of the flagella. Some fragmentation of nanotubes resulting in a random distribution on the TEM grids was observed. Similarly, the formation of Cd nanoparticles on the His-loop peptide flagella (Figure 4.7 e) resulted in generation of an ordered array of nanoparticles and some fragmentation of the flagella and aggregation of fragments. Only random Cd nanoparticles could be detected with the wild type flagella as seen in Figure 9f.

Generation of Silver Nanowires on Aspartic Acid-Glutamic Acid Loop Flagella

The reduction of Ag(I) complexed to aspartic acid-glutamic acid peptide loops was performed with hydroquinone instead of NaBH_4 to gain better control of the generation of nanoparticles. However, even this controlled mild reduction resulted in formation of silver metal-covered flagella that were aggregated into bundles, as shown in Figures 4.8 a-c. The Ag wire structures are evident in Figures 4.8a and 4.8b; Figure 4.8c indicates heavily aggregated nanowires leading to clumps of

nanomaterials. Upon formation, the Ag nanoparticles rapidly seed the growth of further layers of Ag, analogous to our observations with higher concentrations of Cu(II). As a result, individual nanoparticles cannot be discerned and instead, arrays of nanowires resulting from the rapid growth of Ag films on the flagella were observed. Further studies with various peptide loops are underway to determine conditions that will allow the more controlled formation of Ag nanoparticles on flagella. The ease of reduction of Ag(I) compared to Cu(II) results in the observed differences in reduction after they have been bound to peptide modified flagella. This may account for the fact that in the case of Ag as shown in Figure 9d some deposition of these nanoparticles occurs even on the wild type flagella. In general, it is useful to identify conditions under which nanoparticle arrays and nanowires can be formed as the former are highly suitable for catalytic applications and the latter are more suitable for molecular electronics.

Conclusion

In summary, we have successfully demonstrated bioengineering of the FliTrx flagellin protein to generate flagella bionanotubes with high affinities for metal ions. A unique aspect of flagella is the ability to introduce peptide loops on monomers separated by 5 nm, with a high efficiency of loop peptide incorporation, resulting in evenly spaced binding sites, which make them attractive scaffolds for the generation of ordered arrays of nanoparticles and uniform nanotubes. Six different types of metal ions were complexed with the peptide loops and carefully reduced with NaBH₄ or

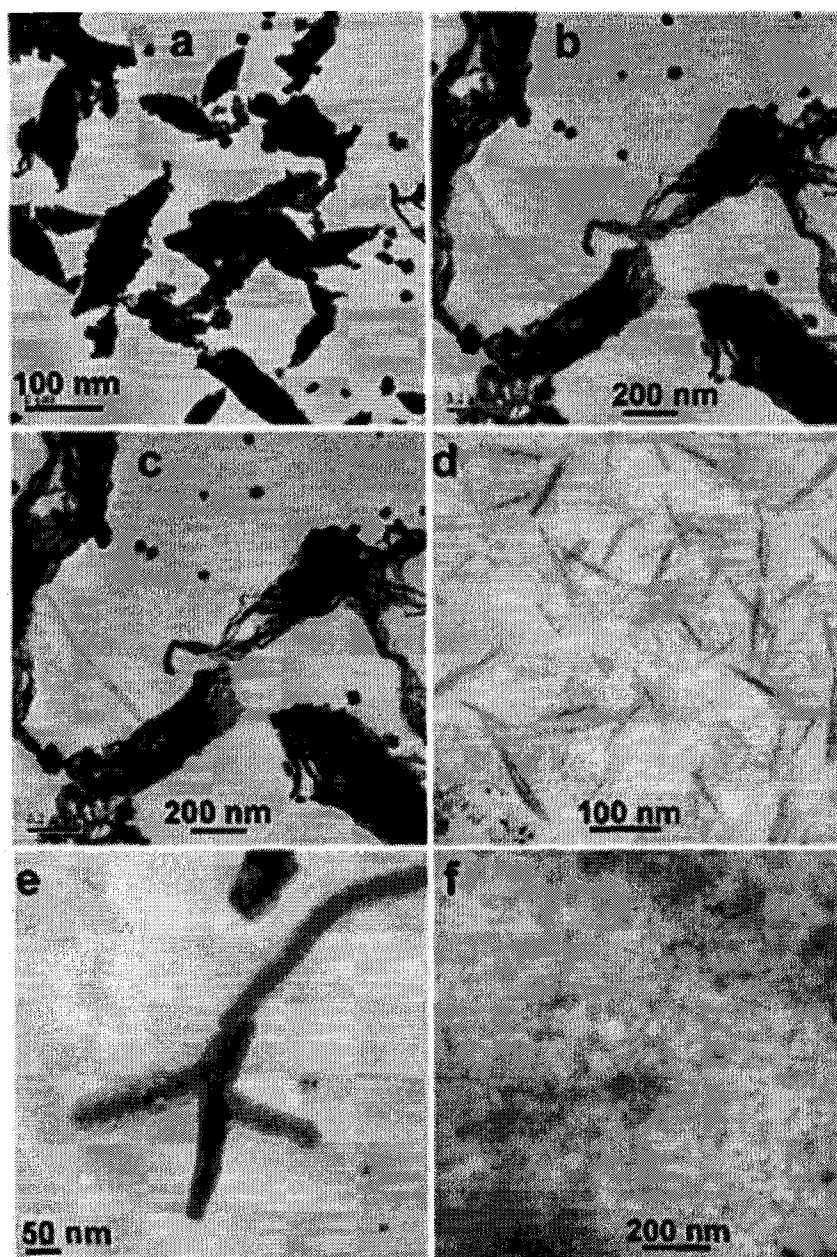


Figure 4.8 Silver-flagellin and cadmium-flagellin nanocomposite materials. (a), (b), and (c) TEM images of silver nanowires synthesized on flagella with glutamic acid-aspartic acid loop peptides. (d) TEM image of control experiment of the reduction of Ag(I) on wild type (without histidine loops) flagella indicating a weak association of Ag nanoparticles. (e) TEM image of cadmium nanoparticles synthesized on histidine-loop flagella. (f) TEM image of control experiment of the reduction of Cd(II) on wild type (without histidine loops) flagella indicating no attachment of Cd and only random distribution of Cd nanoparticles and clusters.

Table 4.1 Summary of Nanomaterials Prepared in This Study Using Engineered Flagella Nanotubes as Scaffolds.

Peptide Loop Type ^a	Metal Species	Nano-Particle Synthesis	Resulting Nanomaterial
Histidine loop ^b	Au (gold)	Synthesis of gold nanoparticles on flagella by reduction of Au(I) ions.	Linear flagella-Au nanotube bundles with discrete gold nanoparticles attached.
Arginine-lysine loop ^c	Au (gold)	Previously synthesized 3 nm and 10 nm gold nanoparticles covalently attached by amine coupling to arginine-lysine peptide loop flagella.	Aggregates of linear flagella-Au nanocomposite bundles.
Histidine loop ^b	Cu (copper)	Synthesis of discrete copper nanoparticles and continuous nanotubes on flagella by reduction of Cu(II) ions with NaBH ₄ .	Linear flagella-Cu nanotube bundles with discrete Cu nanoparticles and single linear Cu nanotubes.
a. Aspartic acid-glutamic acid loop ^d	Co (cobalt)	Synthesis of cobalt nanoparticles on flagella by reduction of Co(II) ions with NaBH ₄ .	a. Ordered array of Co nanoparticles on Asp-Glu flagella nanotubes.
b. Histidine loop ^b		Note: Cobalt oxides may be present on surface of nanoparticles.	b. Fractal-like dense assembly of flagella-Co to form nanoparticle composite on His-loop flagella nanotubes.
Histidine loop ^b	Pd (palladium)	Synthesis of palladium nanoparticles on on flagella by reduction of Pd(II) ions reduction with NaBH ₄	Single flagella-Pd nanoparticles; no extensive aggregation of the flagella.
Histidine loop ^b	Cd (cadmium)	Synthesis of cadmium nanoparticles on flagella by reduction of Cd(II) ions with NaBH ₄ .	Ordered array of nanoparticles on single and aggregated flagella nanotube fragments.
Aspartic acid-glutamic acid loop ^d	Ag (silver)	Synthesis of silver and continuous silver nanowires on flagella by reduction of Ag(I) ions with hydroquinone.	Aggregated bundles and arrays of Ag-flagella nanowires.

^a Type of genetically encoded, constrained loop peptide displayed on the surface of FliTrx flagella protein nanotubes. ^b Histidine loop peptide with 4X repeat of sequence: Gly-His-His-His-His-His (GHHHHH), peptide has 24 histidine residues with imidazole groups. ^c Arginine-lysine loop peptide with a single insert of sequence: Arg-Lys-Arg-Lys-Arg-Lys-Arg (RKRKRKR); peptide has 3 amine groups and 4 guanido groups. ^d Aspartic acid-glutamic acid loop peptide with 3X repeat of sequence: His-Asp-Glu-Asp-Glu-Asp-Glu (HDEDEDE); peptide has three imidazole and 18 carboxylate groups.

hydroquinone to obtain metal-flagellin nanocomposites. The covalent attachment of previously synthesized Au nanoparticles to the flagella scaffold was also demonstrated. In most cases, the reductive chemistry procedures resulted in generation of ordered nanoparticle arrays on the flagellin bionanotube templates, although continuous metal nanowires were also generated with Ag(I) and higher concentrations of Cu(II). These nanowires could be electrically conductive and have applications in microelectronics. They could also be further derivatized through thiol chemistry to construct sensor arrays. The resulting flagella-Au nanoparticle arrays could have sensor applications, while the flagella-Co, Co_3O_4 , and Pd nanoparticle arrays could have potential as chemical catalysts, with uniform particle sizes and high surface area to volume ratios. In general, nanoparticles, prisms, and rods would be useful for catalysis and sensor applications and nanowires for molecular electronics. These results, along with our previously reported studies on cysteine loop flagella and apatite, silica, and titania nanotube formation on flagella and polymerization of aniline bound flagella to form polyaniline bundles, are a complementary set of investigations aimed at demonstrating the efficacy of bioengineered flagella as scaffolds and substrates for the generation of novel bionanomaterials with many potentially useful applications. These studies are also complementary to other similar studies reported in the literature employing peptide nanotubes, proteins, DNA, and viral capsids.

CHAPTER V

BIOENGINEERED FLAGELLA PROTEIN NANOTUBES WITH CYSTEINE
LOOPS: SELF-ASSEMBLY AND MANIPULATION IN
AN OPTICAL TRAP

Introduction

Ordered assembly of engineered biomaterials are essential step in their applications, such as sensor materials, scaffolds for tissue engineering, and liquid crystals. Molecular recognition can be employed as a driving for ordered assembly of bionanotubes. Electrospinning and laminar flow followed by chemical cross-linking have been extensively used in macroscopic protein and peptide bundle formation (228, 229). Macroscopic bundles of self-assembled bionanotubes were proposed as scaffold for tissue repair, sensor materials and new biodegradable wound healing materials (230).

Optical trap is well understood technique and extensively used in biophysical studies of living cells and biomacromolecules. Dimension of biomacromolecules are too small to visualize by optical microscopy, so most cases biomacromolecules are attached to fluorescent polymer beads such as polystyrene for visualization by an optical microscope (231). Optical trapping exerts mechanical force of several piconewtons on biomacromolecules attached to fluorescent beads. The lateral and vertical movement of bead in an optical trap could also be used to manipulate the

biomacromolecules. In this chapter, the reversible assembly of pFliTrx bacterial flagella bundles with cysteine loop displayed on surface of flagella and their behavior in an optical trap are discussed.

Experimental Methods

Materials

All chemicals were reagent grade or better and were obtained from Sigma-Aldrich (St. Louis, MO), unless otherwise noted. Tri(2-carboxyethyl)phosphine hydrochloride (TCEP) was obtained from Fluka (Sigma-Aldrich Corp., St. Louis, MO). NanoOrange protein dye was purchased from Molecular Probes, Inc. (Eugene, OR). *E. coli* strain GI 826, the pFliTrx peptide display plasmid and all custom DNA oligonucleotides primers were obtained from Invitrogen Corp. (Carlsbad, CA). RsrII restriction enzyme, T4 DNA ligase, and alkaline phosphatase were obtained from New England Biolabs (Beverly, MA). The QuikChange® site-directed mutagenesis kit, including *PfuTurbo*® DNA polymerase, 10X reaction buffer, *Dpn* I restriction enzyme and dNTP mix, was purchased from Stratagene (La Jolla, CA). DNA gel extraction and purification kits were obtained from QIAgen, Inc. (Valencia, CA).

Electrocompetent and chemically competent *E. coli* cells were prepared using standard protocols given in the pFliTrx peptide display vector manual available online from Invitrogen. Molecular biology procedures were performed according to Sambrook and Russell (232). Synthetic DNA oligonucleotides were obtained from

Invitrogen Corp. DNA sequencing was performed by the University of Michigan DNA Sequencing Core. The following sequencing primers were used: 1. FliTrx forward primer, 5'-ATT CAC CTG ACT GAC GAC-3'; FliTrx reverse primer, 5'-CCC TGA TAT TCG TCA GCG A-3'.

Construction of FliTrx Polycysteine Loop Display Vector

The pFliTrx peptide display vector obtained from Invitrogen is not identical to that originally described by Lu, *et al.* (233) and contains a large multiple cloning site (MCS) sequence with 10 unique restriction sites intended to facilitate directional cloning (i.e., insertion) of DNA segments encoding peptides of interest. This MCS was inserted into the sequence region (denoted by *) corresponding to the middle of the thioredoxin active site, Cys₃₂-Gly₃₃-*-Pro₃₄-Cys₃₅, using the sequence numbering of wild-type *E. coli* thioredoxin. The corresponding MCS-encoded peptide, PVCWAQPARSELAAAISLARG, encodes a Cys residue (underlined), that may still be present and prone to uncontrolled oxidation and cross-linking, depending on the actual restriction sites used for cloning foreign peptides. The DNA sequence encoding this multiple cloning region was removed and the unique RsrII restriction site located in this sequence region corresponding to the original pFliTrx plasmid was restored by a series of mutations, restriction digestion and re-ligation. First, two RsrII restriction sites were introduced into regions flanking the MCS region of the plasmid by site-directed mutagenesis using the QuikChange method. The two mutagenesis primers for the first RsrII site, with mutated bases underlined, were: forward primer, 5'-GCA

GAG TGG TGC GGT CCG GTG TGC TGG GCC CAG C-3' and reverse primer, 5'-GCT GGG CCC AGC ACA CCG GAC CGC ACC ACT CTG C-3'. The two mutagenesis primers for the second RsrII site were: forward primer 5'-CCG CGA TAT CGC TAG CTC GCG GTC CGT GCA AAA TGA TCG CCC-3' and reverse primer, 5'-GGG CGA TCA TTT TGC ACG GAC CCG GAG CTA GCG ATA TCG GGG-3'. Mutations were initially identified by RsrII restriction digestion and agarose gel electrophoresis and confirmed by DNA sequencing. A 63 nucleotide fragment encoding the MCS region was removed from the pFliTrx plasmid by RsrII restriction digestion, followed by separation of the two fragments by gel electrophoresis. The large plasmid fragment was isolated by gel extraction with a QIAquick Gel Extraction Kit (Qiagen) and was ligated into circular form with T4 ligase and electrotransformed into *E. coli* GI 826 cells. Transformed cells were plated on RMG-Amp plates and isolated clones were grown in RM-Amp media. The resulting modified pFliTrx plasmid DNA encoding a single RsrII restriction site in the region corresponding to the thioredoxin active site was isolated and sequenced to confirm removal of the small fragment.

Comparison of the translated FliTrx protein sequence indicated that an additional non-native Cys₃₅₃ residue is present in the encoded FliTrx protein sequence immediately following the 3' end of the inserted *trxA* gene. This is probably a Gly→Cys mutation that occurred during construction of the original FliTrx library. Therefore, the Cys₃₅₃→Ser mutation was also introduced via the QuikChange method to prevent unwanted formation of disulfide bonds with this lone Cys residue.

The two mutagenesis primers for the Cys353Ser mutation (with mutated bases underlined) were: forward primer: 5'-CCT CGA CGC TAA CCT GGC CTC TGC CGC CAG TTC TCC AAC CG-3' and reverse primer, 5'-CGG TTG GAG AAC TGG CGG CAG AGG CCA GGT TAG CGT CGA GG-3'.

Construction of FliTrx Peptide Loop Variants

The modified pFliTrx plasmid was digested with RsrII and treated with alkaline phosphatase to remove the terminal 5' phosphates and prevent self-ligation. The following two synthetic oligonucleotides were designed to encode a one histidine, six cysteine loop peptide ("Cys-loop") containing thiol side chains, -His-Cys-Cys-Cys-Cys-Cys-, encoded by the forward oligo, 5'-GT CAC TGT TGC TGT TGC TGT TGC G-3' and reverse oligo, 5'-G ACC GCA ACA GCA ACA GCA ACA GT-3'. A double-stranded DNA cassette was prepared by annealing the two oligonucleotides in annealing buffer: 10 mM Tris HCl (pH 7.5), 100 mM NaCl and 1.0 mM EDTA. The DNA cassette was then inserted into the RsrII-cut pFliTrx plasmid and ligated with T4 ligase. The molar ratio of the inserted cassette to plasmid DNA can be varied to allow possible insertion of multiple cassette fragments into the single RsrII restriction site. The same procedure was followed to insert a one glycine, six histidine loop peptide ("His-loop") containing imidazole side chains, -Gly-His-His-His-His-His-, encoded by the forward oligo, 5'-GTC ATC ACC ATC ACC ATC ACG-3'; and reverse oligo, 5'-GAC CGT GAT GGT GAT GGT GAT-3'), an anionic three glutamic acid, three aspartic acid, one glycine loop peptide ("Glu-Asp loop"), -

Asp-Glu-Asp-Glu-Asp-Glu-Gly-, encoded by the forward oligo, 5'-GTC GCA AGC GTA AGC GCA AGC-3' and reverse oligo 5'-GAC GCT TGC GCT TAC GCT TGC-3', and a cationic four arginine, three lysine loop peptide ("Arg-Lys loop"), -Arg-Lys-Arg-Lys-Arg-Lys-Arg-, encoded by the (forward oligo, 5'-GTC GCA AGC GTA AGC GCA AGC-3' and reverse oligo, 5'-GAC GCT TGC GCT TAC GCT TGC-3'. The resulting plasmids were electrotransformed into GI 826 *E. coli* cells, single colonies were picked and cultured and plasmid DNA was isolated and sequenced. Due to the nature of the single RsrII restriction/insertion site and self-complementary ends of cassettes encoding loop peptides, both single and multiple loop peptide inserts were isolated in the resulting plasmids. The presence of one or more loop inserts in the expressed FliTrx protein was also verified in a qualitative manner by sodium dodecyl sulfate-polyacrylamide gel electrophoresis (SDS-PAGE) analysis of post-induction whole cell lysates (234).

FliTrx Flagellin Protein Expression and Purification

Engineered pFliTrx plasmids were transformed into *E. coli* GI 724 or GI 826 cells and plated on RMG-Amp plates. Individual colonies were picked with toothpicks and were grown in 50 mL IMC-Amp media at 30 °C with shaking (225 rpm) for 16 h (overnight). The 50 mL cultures were used to inoculate one liter of IMC-Amp media and grown at 30 °C with shaking (225 rpm). Cultures were grown to an optical density at 550 nm (OD₅₅₀) of 0.5 and induced with L-tryptophan (100

mg/L) at 37 °C with shaking (225 rpm) for 3 h. Cells were harvested by centrifugation at 3000 x g for 10 min at 4 °C and suspended in 3 ml of pH 7.5 phosphate buffered saline solution. Flagella were sheared from the cells by vortexing for 3 min at maximum speed. The cells were then pelleted by centrifugation at 10,000 x g for 15 min. The clarified flagellin-enriched supernatant solution was used to prepare samples for initial transmission electron microscopy (TEM) imaging. Clarified solutions of Cys-loop flagella were further centrifuged at 50,000 x g for one h to pellet the flagella. Disulfide bond reduction was carried out in freshly prepared TCEP-HCl solution keeping its final concentration 50 mM at 37 °C for times of 1 h and 12 h. Flagellin samples were prepared for TEM imaging by placing 10 µL of reduced solution on a formvar/carbon-400 mesh copper grid (Electron Microscope Science, Hatfield, PA) for 1 min, blotting off excess solution with filter paper, negative staining with 2% neutral phosphotungstic acid for one min, followed by blotting off excess solution and allowing the sample grid to air dry. TEM images were taken with JEOL 3011 electron microscope operated at 300 kV.

Fluorescence Imaging and Laser Tweezer Manipulation of Flagella Bundle

A volume of 50 µL of Cys-loop flagella bundle solution in phosphate saline buffer was placed on a concave microscope slide and mixed with 3 µL of 500X NanoOrange fluorescence dye stock solution. Fluorescence images were taken with an epifluorescence microscope (Nikon TE 2000) using an FM 143 filter cube with a 480/30x (465-495 nm) excitation band pass filter and a 515-555 nm emission band

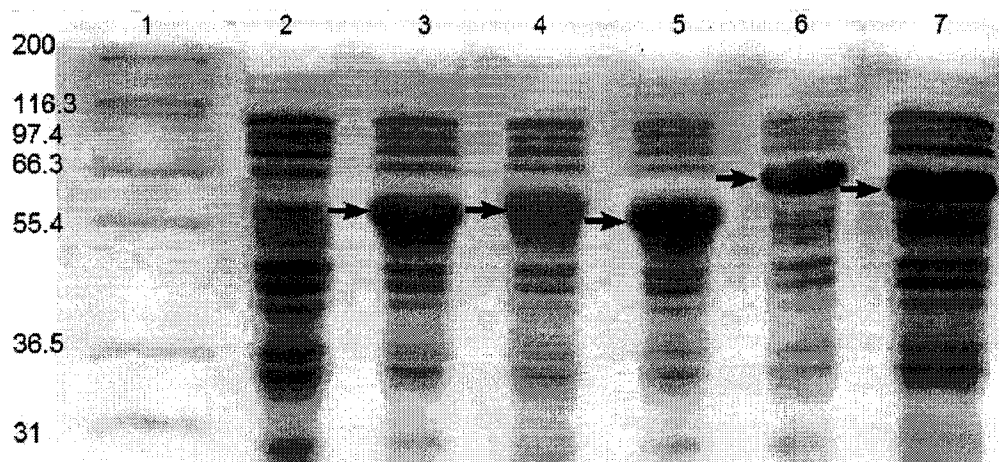


Figure 5.1 SDS-PAGE (15%) analysis FliTrx loop variant protein expression and export in GI 826 *E. coli* cells. (a) Lane 1, Mark-12 molecular weight marker; Lane 2, Whole-cell lysate before FliTrx expression; Lane 3, Post-induction whole-cell lysate of six cysteine loop variant (1X insert); Lane 4, Post-induction whole-cell lysate of twelve cysteine loop variant (2X insert); Lane 5, Post-induction whole-cell lysate of four arginine and three lysine loop variant (1X insert); Lane 6, Post-induction whole-cell lysate of nine aspartic and nine glutamic acid loop variant (3X insert); Lane 7, Post-induction whole-cell lysate of twenty four histidine loop variant (4X insert).

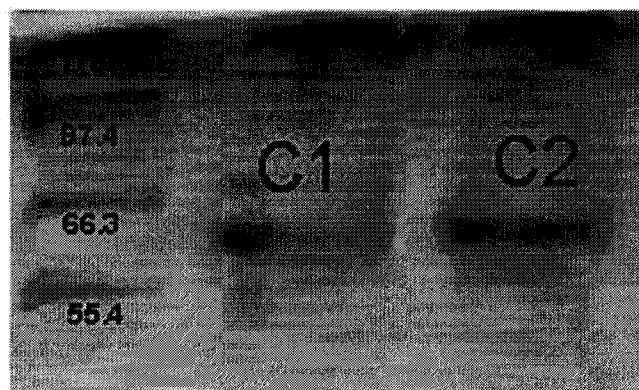


Figure 5.2 Lane 1, Mark-12 molecular weight marker; Lane 2, Post-induction exported sheared flagella of six cysteine loop variant (1X insert); Lane 3, Post-induction exported sheared flagella of twelve cysteine loop variant (2X insert).

pass filter (Chroma Technology Corp., Rockingham, VT). Optical manipulation of flagella bundles was performed using a Bioryx 200 laser tweezer instrument (Arroyo, Chicago, IL) with a 1064 nm wavelength Nd:YAG laser source coupled with a Nikon TE 2000 inverted epifluorescence microscope.

Isolation and Expression Tolerance of Flagellin Loop Variants

FliTrx loop variants with 1-3 inserts of the Cys-loop variant, 1-6 inserts of the His-loop variant, one insert of the cationic Arg-Lys loop variant and 1-4 inserts of the anionic Glu-Asp loop were successfully identified by DNA sequencing and confirmed by SDS-PAGE analysis of the expressed proteins in whole cell lysates. Many of the engineered FliTrx loop variants were expressed at very high levels in both GI 724 and GI 826 strains of *E. coli*, as indicated by SDS-PAGE analysis of pre- and post-induction cell lysates (Figure 5.1). However, some of the loop variants had very low levels of expressed protein and consequently, did not yield functional flagella. Both single and double insert Cys-loop FliTrx variants were successfully expressed at high levels and were exported and assembled into functional flagella fibers (Figure 5.2). These Cys-loop flagella then further self-assembled into flagellin bundles, as indicated by TEM imaging (Fig. 2). Cys-loop variants with more than two inserted copies of the Cys-loop peptide were not expressed at significant levels and failed to form measurable quantities of flagella in both GI 724 and GI 826 strains. Thus, there appears to be a biological limit in the export pathway to the number and size of

cysteine residues that can be inserted into the FliTrx protein, in contrast to many other larger peptides that are successfully exported in both GI 826 and GI 724 strains, including the large number of random 12-mer peptides encoded in the original FliTrx peptide library (233). This result is not surprising, as Cys residues were not observed in any of the peptides previously isolated from the FliTrx random library panning procedure against several antibodies (233, 235). The two Cys residues in the thioredoxin active site of FliTrx proteins may rapidly form a stable, intrachain disulfide bond in the oxidizing environment of the bacterial periplasm or possibly during or after extracellular export. The presence of additional Cys residues may result in formation of covalently cross-linked FliTrx protein complexes that are too large and/or inflexible to be exported by the flagellar type III secretion system (236) that is part of the basal motor complex of the flagella.

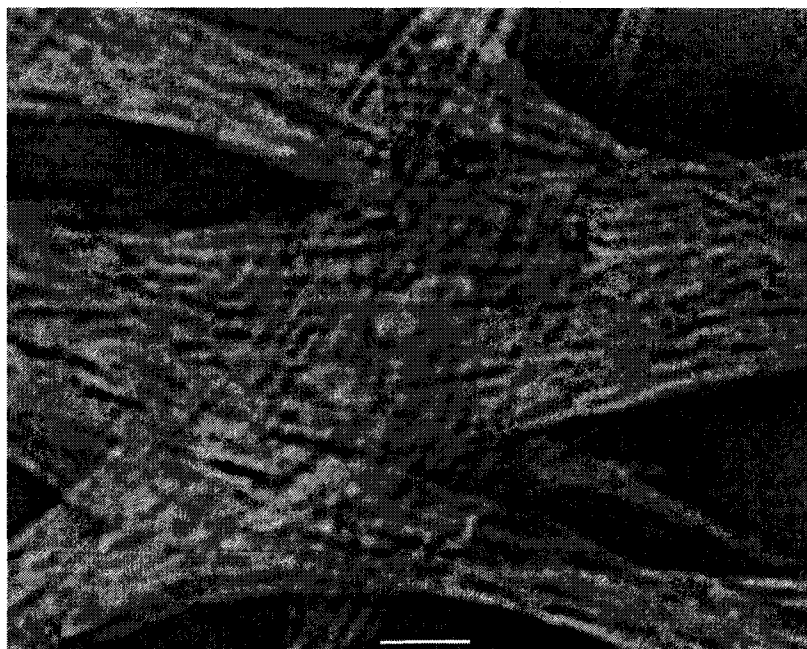


Figure 5.3 TEM imaging of disulfide cross-linked cysteine-loop FliTrx flagellin bundles. Stained with 2% phosphotungstic acid (pH 7.5) (scale 100 nm).

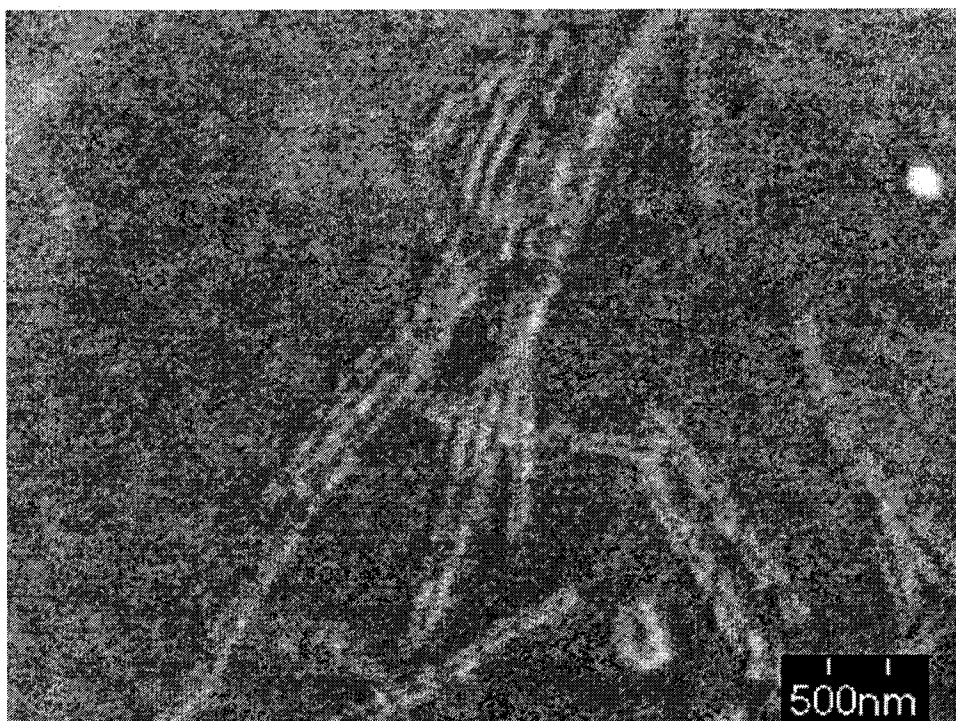


Figure 5.4 SEM image of Cys-loop flagella bundles on carbon grid (500 nm).

Purification of cysteine-tagged proteins is challenging, due to aggregation and inclusion body formation. Intra- and intermolecular disulfide bond formation of proteins is not possible in the reducing environment of the *E. coli* cytoplasm, but generally occurs in the periplasmic space. However, a number of the engineered FliTrx variants, including several that contain polycysteine peptide loops, were expressed at high levels and were successfully exported and assembled into flagella fibers in both GI 724 and GI 826 strains of *E. coli*. While the other His-loop, Arg-Lys loop and Glu-Asp loop variants were isolated as monomeric flagella fibers, the Cys-loop variant fibers aggregated and self-assembled into larger cross-linked bundles in the oxidizing environment outside the cell. These Cys-loop bundles were easily

harvested by shearing them from bacterial cells as self-assembled microscopic flagella bundles, without lysing the cells and releasing large numbers of other contaminating proteins. The GI 826 *E. coli* strain was previously engineered so that the rotary motor is no longer functional, (233) however, typical growth conditions of 150 rpm shaking and subsequent pelleting of cells by centrifugation still resulted in collision and disulfide-mediated bundle assembly. Disulfide bond formation between cysteine residues of flagella is the driving force of this polyfiber self-assembly process that is mediated by dissolved oxygen in the growth media. The cysteine loop is present in the solvent-accessible D3 domain of flagellin and can form intermolecular disulfide bonds without any steric hindrance. These inserted peptide loops are flexible and may allow for changes in their orientation and conformation. These flagella bundles can be disassembled by reduction of disulfide bridges between flagella tubes by use of reducing agents such as dithiothreitol or TCEP, as shown in the schematic of Fig. 3. We observed flagella bundles up to 10 μm in length and 200 nm in diameter with an average length of 8 μm . Individual flagella and their parallel orientation in bundles are distinctly visible (Figure 5.3). Overnight (12 h) reduction with 50 mM TCEP resulted in complete separation of flagella bundles to form single flagella nanotubes (Figure 5.6).

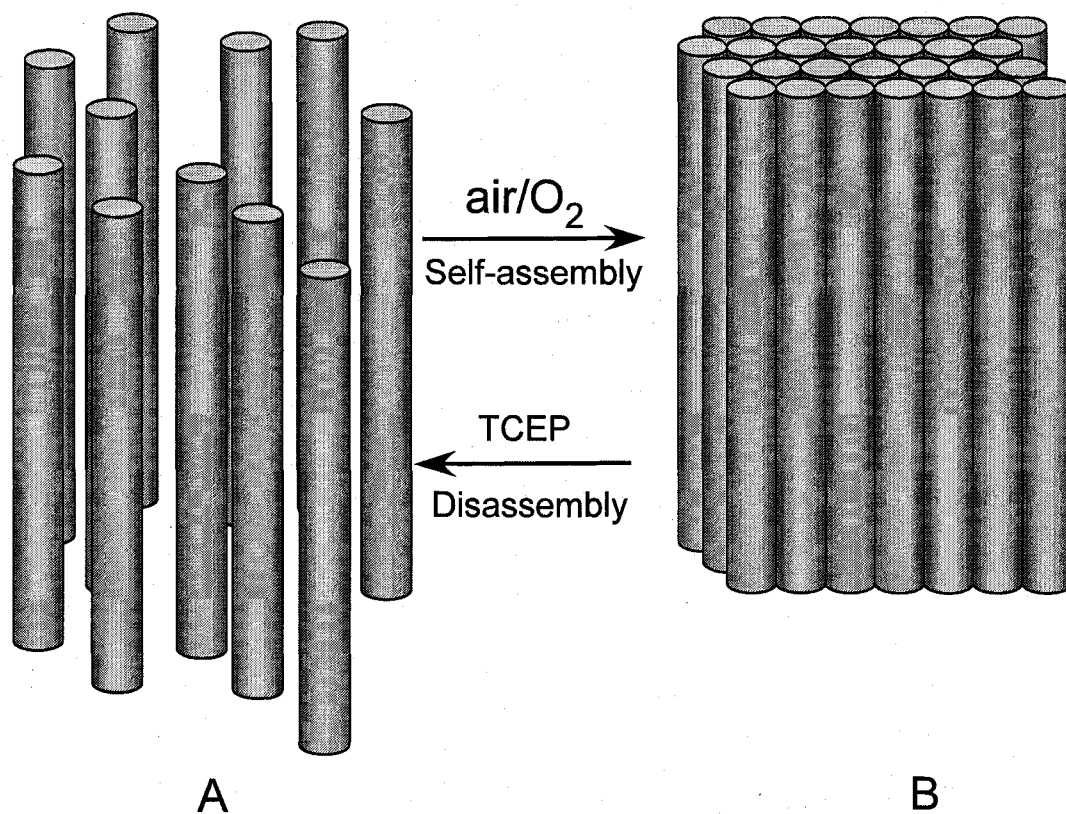
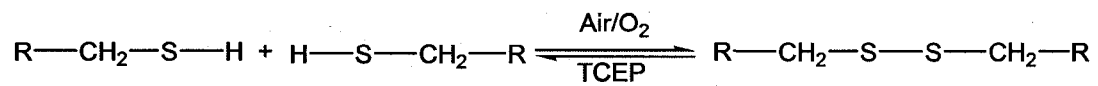


Figure 5.5 Formation of disulfide bonds between cysteine loops in the presence of oxygen. (b) Flagella nanotube bundle formation upon oxidative disulfide bond formation and disassembly upon addition of a reducing agent.

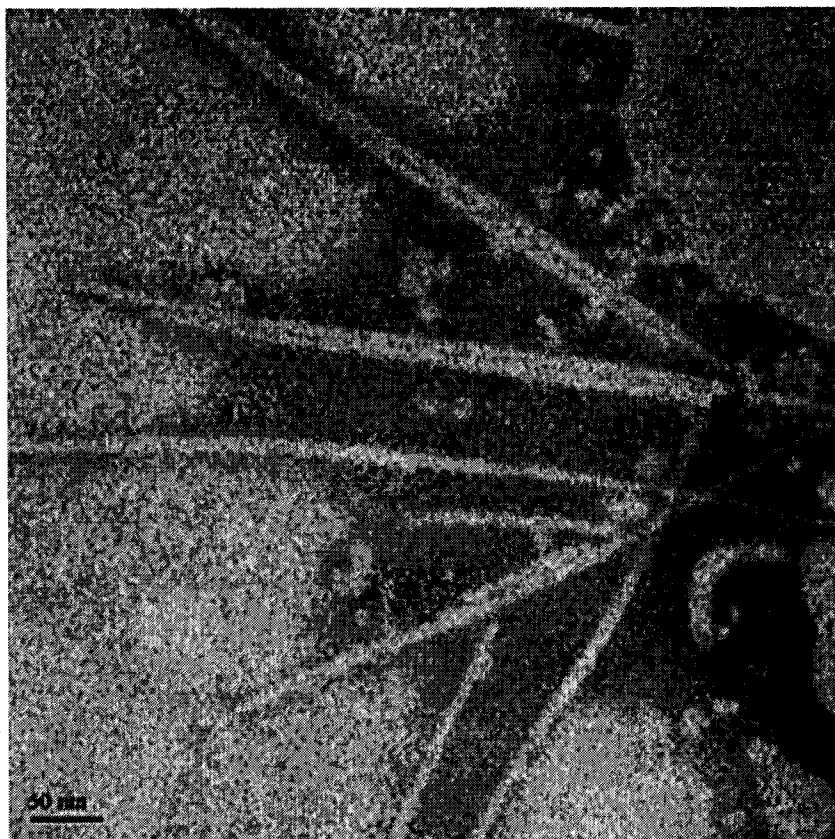


Figure 5.6 TEM images of cysteine loop FliTrx flagella monomeric fibers after 12 h incubation with 50 mM TCEP.

For comparison, loop-less FliTrx and His loop flagella were also bioengineered and isolated. TEM imaging indicated only single fibers for these other types of engineered flagella, which did not show any bundle formation under similar conditions. The properties and interactions of these other engineered loop variants with other nanomaterials will be addressed in a later publication. Fluorescence microscopy of NanoOrange labeled protein samples showed flagella bundles that ranged in length from 4-10 μm (Figure 5.7). NanoOrange is protein-specific dye that, when bound to protein and excited at 470-490 nm wavelengths of light, fluoresces at

wavelengths of 570-590 nm; otherwise it is non-fluorescent in water. The flagella bundles had a strong tendency to adsorb to glass surfaces, which was minimized by the addition of 0.01% Triton X-100 nonionic detergent.

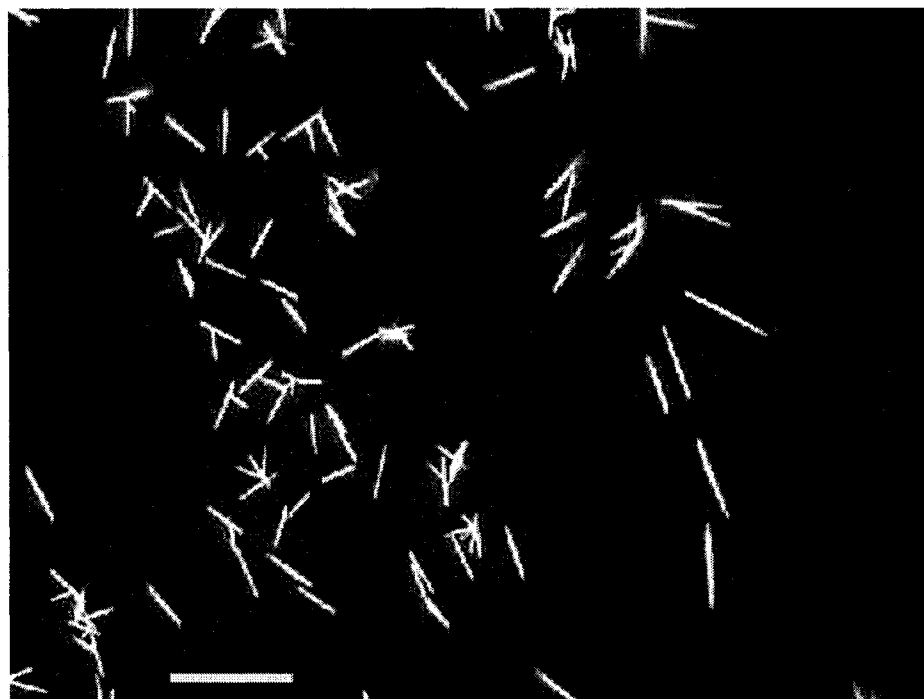


Figure 5.7 Fluorescence image of Cys-loop flagella bundles adsorbed on surface of glass slide (scale bar 10 μm). Flagella bundles were stained with NanoOrange dye.

Optical Trapping of Flagella Bundles

We attempted to trap flagella bundles using a biologically compatible infrared wavelength (1064 nm) laser tweezer (optical trap) with various laser output power levels ranging from 0.2 W to 2.0 W. The flagella bundles were visualized using a 465-495 nm excitation band pass filter and an emission cut-off filter for wavelengths below 570 nm. Unexpectedly, fluorescently labeled flagella bundles in solution were

rapidly repelled by the laser beam; rather than being held in place by tweezing action, they were repeatedly observed to move in a downward direction parallel to the laser beam and disappear from focus (see appendix for an example movie of attempted capture of a flagella bundle by the laser optical trap).

The movie indicates an attempt to trap a Cys-loop flagella bundle of approximately 10 μm length and 300 nm diameter (diameter is an estimate based on the diffraction limit of the emission wavelength region) by the maximum power of 2 W of the 1064 nm laser. The movie clearly depicts the movement of the flagella bundle in the optical trap and its eventual escape. It also depicts repeated unsuccessful attempts to trap the bundle. The Cys-loop bundle, due to its size, acts like a lens that refracts the rays of light and redirects the momentum of the photons. This draws the bundle to the high flux region of photons in the trap which is the focus of the trapping laser beam (237, 238). Initially this causes the bundle to align lengthwise along the optical axis, as we have observed for other systems such as bacterial *E. coli* cells (239). Once in the trap, the flagella nanotubes absorb the momentum from the photons in the beam. This momentum transfer is to some extent aided by the weak absorbance that the Cys-loop flagella have at 1064 nm that was observed by near-IR absorbance spectrophotometry. Weak absorbance with conventional light sources can become significant in a tightly focused energetic laser beam. The momentum transfer drives the flagella bundle down the optical axis, aiding its escape from the optical trap, as evident from the movie. Clearly the behavior of the Cys-loop flagella in the

optical trap is complex and warrants further investigation; further studies are in progress.

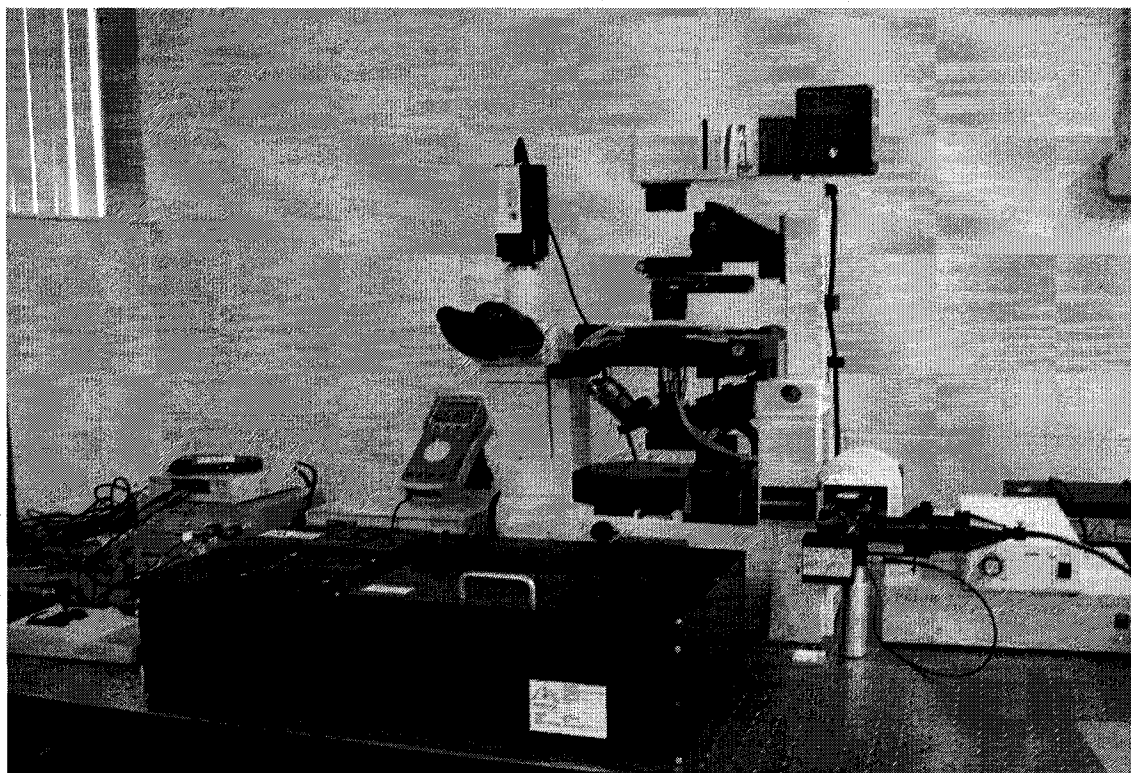


Figure 5.8 Image of lasers tweezers with inverted microscope.

Conclusion

We have demonstrated that FliTrx flagella nanotubes with rationally designed surface functionalities can be engineered and isolated from bacterial *E. coli* cells, including flagella bundles formed by Cys-loop variants. These 4-10 μm long bundles represent a novel bioengineered fibrous material that is readily visualized by fluorescence microscopy, can be immobilized on glass surfaces by simple adsorption

procedures, may have useful elastic and tensile strength properties and could also serve as a template for biomineralization of larger structures and labeling via standard thiol chemistries. Furthermore, given that flagellins from different species can be combined and assembled *in vitro* into heterogeneous flagella through interactions of the highly conserved N- and C-terminal domains, (34-36, 240) the Cys-loop FliTrx protein can be considered as a thiol cross-linking building block that can be combined with other flagellin monomers that have other functionalities. For example, Cys-loop FliTrx variants could be combined *in vivo* or *in vitro* with other FliTrx engineered loop variants that have other specific molecular recognition properties, such as the transition metal-binding His-loop peptide, the cationic Arg-Lys loop and the anionic Glu-Asp loop, to produce multifunctional protein nanotube bundles that are stabilized by cross-links (69-71).

CHAPTER VI

LAYER BY LAYER ASSEMBLY OF BIOENGINEERED FLAGELLA
NANOTUBE FILM AND BIOMINERALIZATION

Introduction

Applications of layer-by-layer assembly as versatile technique for fabrication of thin layers and coatings have increased dramatically over the last two decades; layer-by-layer assembly of polycations and polyanions was first proposed by Decher in the early 1990s (241, 242). Electrostatic interaction, hydrogen bonding, van der Waal's forces, and covalent bond formation between layers were used to hold multiple layers together (243). Organic polymers (244), nanoparticles (245) and biological molecules such as enzymes (246), DNA (247), peptides (248, 249), proteins (250), chitosan (251), and viruses (252) have been demonstrated as building blocks in multilayer construction and employed as biosensors, supports for cell adhesion, templates for biomineralization, in controlled release of drugs, and as antibacterial coatings. Layer-by-layer assembly of viral protein cage architecture was reported by Young and coworkers (253), where streptavidin-biotin molecular recognition was used. Biological molecules provide genetically controlled natural building blocks, which can be used in the "bottom-up" construction of nano to micro structures, to overcome the inherent limitations of traditional "top-down" assembly approaches such as photolithography.

In this paper, we discuss the layer-by-layer assembly of an engineered fusion protein of bacterial flagellin and thioredoxin, termed FliTrx, as a functionalized bionanotube. The functionalization was achieved by display of peptide loops on the surface of flagella and chemical modification of the side chains of the proteins. The bacterial flagella is a whip-like structure that extends from the surface bound motor complex, followed by a universal joint hook structure and the stem, and an elongated fiber, which is composed of the protein flagellin (FliC). The flagellin protein is helically self-assembled to form the flagella nanotube, consisting of 11 subunits of flagellin per turn and the distal end of the fiber is capped with a lid complex formed from a protein heptamer called FliD or Hap2 (254, 255). Extensive details of bacterial flagella structure have been reviewed elsewhere (56, 69-71, 73). Our research program involves the development of engineered mesophilic and hyperthermophilic bacterial flagella nanotubes for the fabrication of hybrid nanomaterials and bionanotube systems. Recently, we demonstrated a computational model for a thermophilic bacterial flagellin protein (256) and followed this by functional characterization of the D3 domain deletion library of *Salmonella* flagella (239). Furthermore, the FliTrx system of *E.coli* was used to display multiple polypeptides on the flagella surface with various functional side chains such as cysteine, arginine, lysine, histidine, aspartic acid, glutamic acid and tyrosine. These functionalized flagella were used to make covalently bonded flagella bundles (73), and for the complexation and reduction of metal ions on functional groups of flagella to form uniform metal nanotube and nanoparticles on the surface of flagella (69), directed

assembly and polymerization of aniline to form conductive nanotubes (71), biomineralization leading to the formation of SiO₂ and TiO₂ nanotubes and hydroxyapatite crystals (16), and assembly and synthesis of semiconductor quantum dots in an ordered array where exciton energy transfer between small and large size quantum dots was demonstrated (70). This paper discusses the continuation of our research and demonstrates the possible application of engineered flagella in surface fabrication using layer-by-layer assembly, with the assistance of electrostatic interactions and molecular recognition. Finally, we discuss potential applications of a surface assembled bionanotube system as a template for the biomineralization of calcium carbonate.

Experimental Procedures

Materials

Polyethylene glycol (PEG) 750 (MW 750), polyethylenimine (MW 2000), streptavidin, and 3-(2-(2-aminoethylamino)ethylamino)propyl-trimethoxysilane were obtained from Sigma-Aldrich (St. Louis, MO). 11-amino-undecanethiol was obtained from Dojindo Molecular Technologies, Inc. (Gaithersburg, MD), NanoThinks ethanolic solutions of n-octane thiol (5 mM) and n-octane thiol (5 mM) were obtained from Sigma-Aldrich. The NHS-PEG₄-biotin and NHS-PEG₄-biotin were obtained from Pierce Biotechnology, Inc. (Rockford, IL). Gold-plated mica was obtained

from Molecular Probes, (Eugene, OR). Dialysis membrane 50 kDa molecular weight cutoff cellulose was obtained from Membrane Filtration Products Inc. (Seguin, Texas). Atomic force microscopy of samples was performed using an Agilent 5500 AFM/SPM Microscope (Agilent Technologies, Tempe, AZ) with model FESP AFM tips (Veeco, Santa Barbara, CA), using “tapping” mode force feed-back control for imaging biological samples.

Preparation of amine terminated mixed self-assembled monolayers on Au(111) surface

A calculated weight of 11-amino-undecanethiol (Dujindo Chemicals) was mixed with an ethanolic solution of n-octane thiol (5 mM, Nanothinks 8, Sigma) to form a 2 mM solution with an amine thiol: alkyl thiol ratio of 2:5. Self-assembled monolayers (SAMs) were prepared by incubating gold-plated mica plates in thiol solution for 16 h and cleaned by thoroughly washing with ethanol, followed by rinsing with deionized (DI) water with a resistivity of 18 Mohm.

Biotinylation of thiol self assembled monolayers

Thiolated gold-plated mica plates were placed in a 1 mM solution of NHS-PEG₄-biotin in 100 mM phosphate buffer (pH 7.2) for 2 h. Biotinylated plates were cleaned with DI water.

Biotinylation of flagella

A 5 mL solution of 1 mg/mL flagella in 200 mM NaCl and 10 mM at pH 7.2 (10 mM phosphate buffer) was mixed with 1 mL of 5 mg/ml solution of NHS-PEG₄-biotin in at pH 7.2 (10 mM phosphate buffer) and stored at 4 °C for 5 h. This was followed by addition of another 1 mL of biotin solution and stored at 4 °C for another 2 h. Excess NHS-PEG₄-biotin and other soluble reaction byproducts were removed by dialyzing the flagella sample against 200 mM NaCl, at pH 7.2 (10 mM phosphate buffer) for 36 hours using a 50 kDa molecular weight cutoff cellulose membrane with a buffer change performed every 12 h.

Layer-by-Layer Assembly of Streptavidin and Flagella

Biotinylated gold-plated mica plates were placed in a solution of 0.5 mg/mL streptavidin dissolved in 50 mM phosphate (pH 7.2) buffer solution for 10 minutes and washed three times with a 0.1% (wt./vol.) PEG 750 solution in 50 mM phosphate buffer (pH 7.2), followed by rinsing with phosphate buffer and DI water. The resulting streptavidin-coated plates were air dried for 10 min and AFM images were collected using the tapping mode. For assembly of a flagella layer, the streptavidin-coated mica plates were placed for 20 minutes in a 0.5 mg/mL flagella solution in 200 mM NaCl and 50 mM phosphate buffer and washed three times with a 0.1% PEG 750 solution, followed by rinsing with 50 mM phosphate buffer and DI water. AFM

images were recorded after air-drying for 10 min. The same procedures were followed to prepare additional layers of streptavidin and biotinylated flagella nanotubes immobilized on the second streptavidin layer.

Layer-by-Layer Assembly of Polyamines and Flagella

Quartz plates with dimensions of 8 cm X 2 cm X 2 mm were cleaned with piranha solution (3:1 conc. H_2SO_4 : 30% H_2O_2) and washed 3 times with DI water. Cleaned and dried quartz plates were placed in a 50 mM solution of 3-(2-(2-aminoethylamino)ethylamino)propyl-trimethoxysilane (AEPTS) in absolute ethanol for 4 h and washed twice with absolute ethanol, followed by rinsing with DI water and pH 7.2, 50 mM phosphate buffer. The resulting quartz plates were immersed in a 0.5 mg/mL solution of glutamic-acid-aspartic acid (Glu-Asp) loop peptide) flagella, described previously (69, 71), in 100 mM NaCl at pH 7.0 (pH was adjusted with 0.01 M HCl/0.01 M NaOH) for 5 min and washed with DI water 3 times by dipping. AFM images were recorded after the plates were air dried for 10 min and the UV-visible absorbance spectrum was recorded with a Lambda 20 spectrophotometer (Perkin-Elmer, Wellesley, MA). The resulting plates were immersed in a pH 7.0, 0.01% solution of polyethylenimine in water for 5 minutes and washed three times with DI water. Each polyethylenimine-coated plate was immersed in the Glu-ASp loop flagella solution for 5 min, followed by AFM imaging and absorbance measurements were recorded. The same procedure was repeated for additional cycles to prepare

multiple layers of the anionic flagella-cationic polymer composite material on the mica slides.

CaCO₃ Mineralization on Flagella

Low density of flagella were deposited on an AEPTS-coated quartz plate by immersing the plate in a 0.5 mg/mL solution of Glu-Asp-loop flagella in 100 mM NaCl at pH 7.0 for one min. A 0.5mg/mL flagella solution in 75 mL of 5 mM CaCl₂ solution in 100 mL beaker and then beaker was placed in sealed container containing solid (NH₄)₂CO₃ for 4 h. Each quartz plate was air-dried and AFM images were recorded in tapping mode.

Results and Discussion

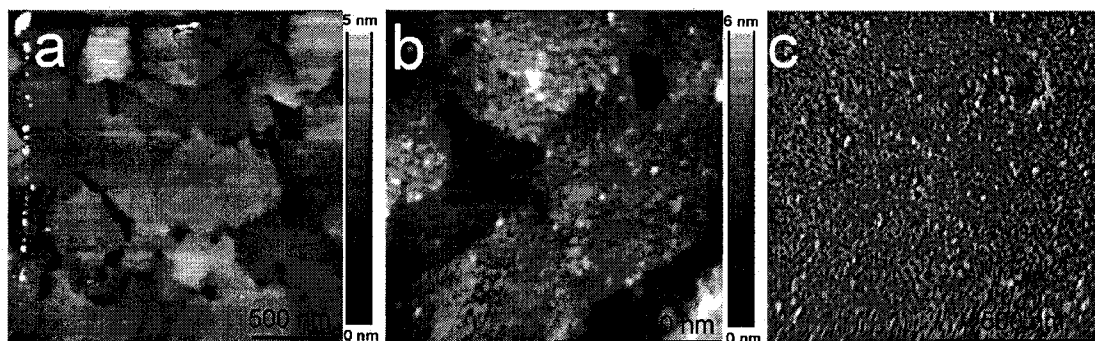


Figure 6.1 AFM images of a biotin-functionalized gold surface and a subsequent streptavidin assembled surface.

Mixed thiol SAMs on a gold surface with alkyl- and amine-terminated groups were used to generate a biotin-functionalized Au(111) surface for the assembly of a

first layer of streptavidin. In this case, the alkyl-terminated thiol was used to reduce the surface density of the resulting biotin SAM; furthermore, alkyl groups have a very low affinity for proteins, thus minimizing nonspecific binding of streptavidin. Washing treated plates with dilute PEG solutions and DI water also removed nonspecifically-bound protein from the surface. AFM images of a biotin-functionalized gold surface and a subsequent streptavidin assembled surface are shown in Figures 6.1(a), (b) and (c). In Figure 1(a), gold granules with step edges are clearly indicated and densely packed streptavidin molecules are indicated in Figures 6.1(b) and 1(c). Streptavidin is associated to from a cubictetramer with two pairs of biotin binding sites on opposite faces. Therefore, each streptavidin molecule immobilized on the biotinylated surface has a second pair of available biotin binding sites on the solvent-exposed surface of the protein. These available biotin binding sites were used to assemble a second protein layer of biotinylated flagella on the surface of streptavidin layer. AFM images of the assembled flagella layer are shown in Figures 6.2(a) and 6.2(b). Flagella with inserted peptides containing three lysine residues alternatively composed along with three arginine residues in a surface-displayed loop peptide were chemically coupled to biotin molecules via a 2.9 nm long polyethylene oxide spacer arm; theoretically each flagellin molecule may have three or more biotin molecules covalently linked to its surface. EDC coupling was used and the spacer arm was used to prevent any steric hindrance of biotin for binding with streptavidin. Functional biotin molecules are available on the flagella surface, and another layer of streptavidin was assembled on flagella using the exposed functional

biotin. AFM images of the streptavidin layer assembled on flagella are indicated in Figures 6.3(a) and 3(b). In a phase image of Figure 6.3(b), assembly of streptavidin was clearly indicated compared to a phase image of flagella in Figure 6.2(b). Another biotinylated flagella layer was assembled on the streptavidin layer and AFM images were recorded as indicated in Figure 6.2(c). The Figure 6.4 indicates a schematic representation of layer-by-layer assembly of biotinylated flagella nanotubes.

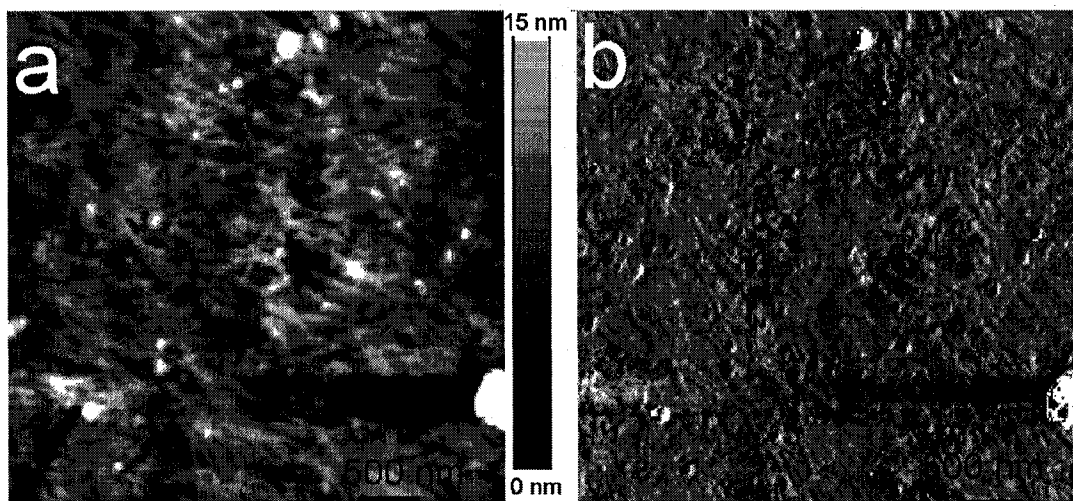


Figure 6.2 AFM images of the assembled flagella layer.

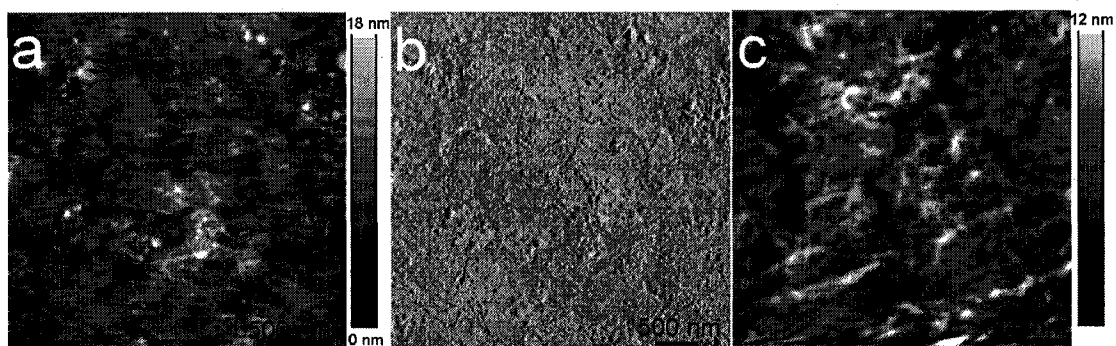


Figure 6.3 AFM images of the streptavidin layer assembled on flagella.

Electrostatic interactions were also used to prepare a layer-by-layer assembly of negatively charged bioengineered flagella nanotubes. In this case, flagella were assembled on positively charged quartz surface coated with AEPTS. At pH values below 9, the amine groups are protonated and generate a positive charge. Positively-charged polyethylenimine was used to electrostatically bind the negatively charged flagella. Figures 6.5(a), (b), (c), and (d) indicated each step in electrostatic layer-by-layer assembly of flagella. The Figure 6.6 is a schematic illustration of electrostatic layer-by-layer assembly. Absorbance spectra were recorded with each step in the assembly process and the raw absorbance data are indicated in Figure 6.7. Increase in absorbance in the visible region of the spectrum, where protein does not absorb could be attributed to light scattering, by multiple layers of protein nanotubes. Absorbance increase in the uv region is due to the amino acid residues in the protein. By comparison, the first layer of flagella generated by electrostatic interaction was more tightly packed than the flagella assembled with biotin-streptavidin linkages. This can be easily seen by difference between Figures 6.2(a), 2(b) and Figures 6.5(a) and 6.5(b). Electrostatic interaction occurred over the entire flagella bionanotube surface with surface-functionalized quartz, but biotin-streptavidin interactions resulted in only partial binding and assembly of flagella on the surface. This suggests that electrostatic interactions are more suitable for generating nanomaterial surfaces with smaller and fewer pores and a more tightly packed flagella monolayer, while the opposite holds for flagella monolayer assembled via molecular complementarity.

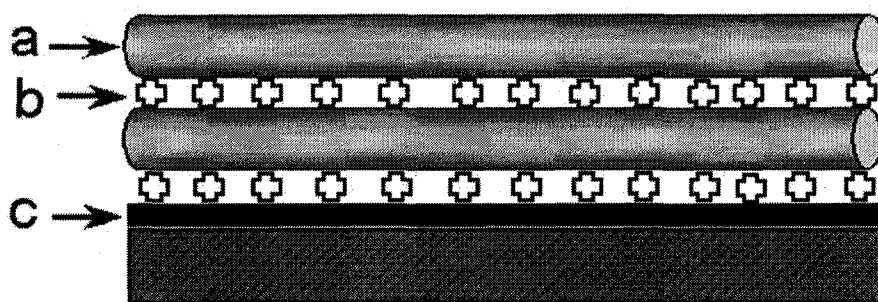


Figure 6.4 schematic representation of layer-by-layer assembly of biotinylated flagella nanotubes.

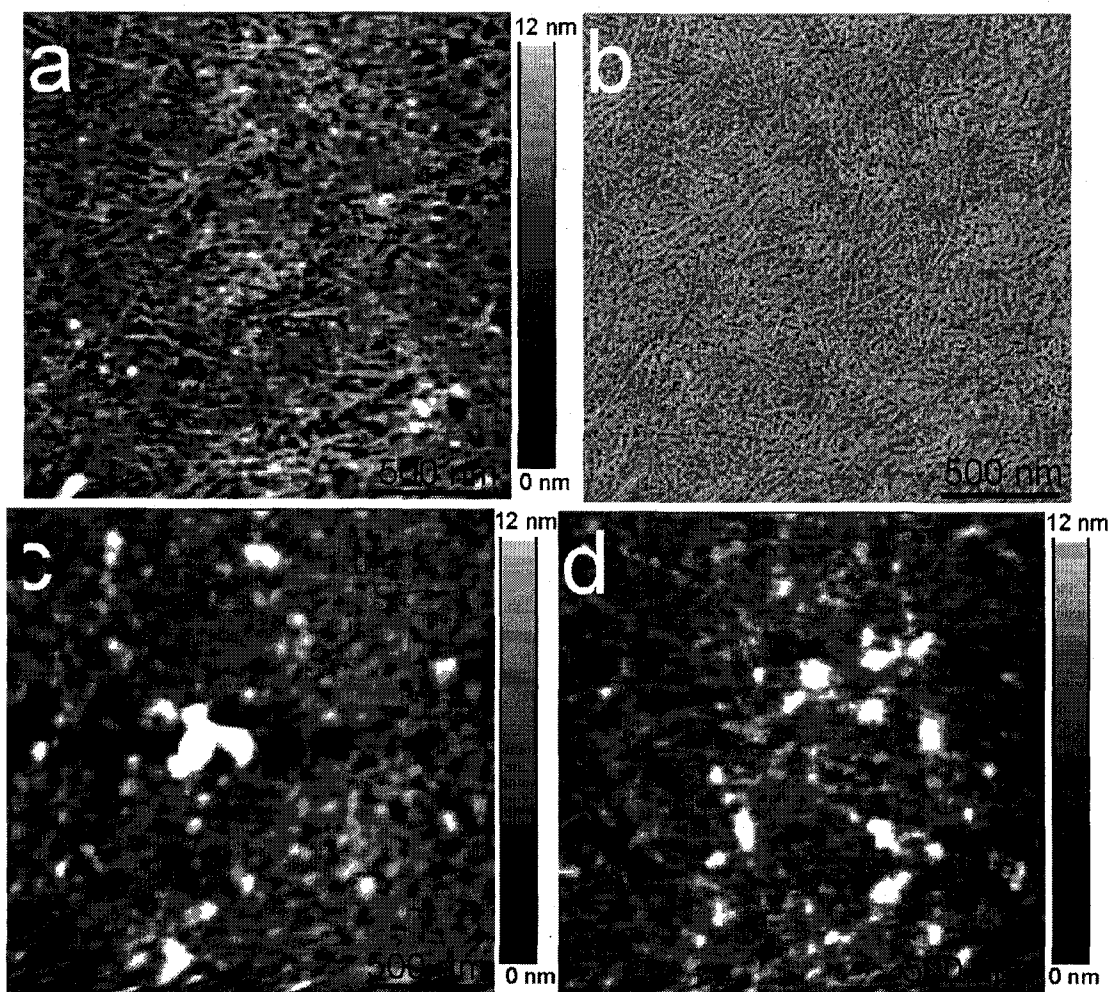


Figure 6.5 Electrostatic layer-by-layer assembly of flagella electrostatic layer-by-layer assembly of flagella.

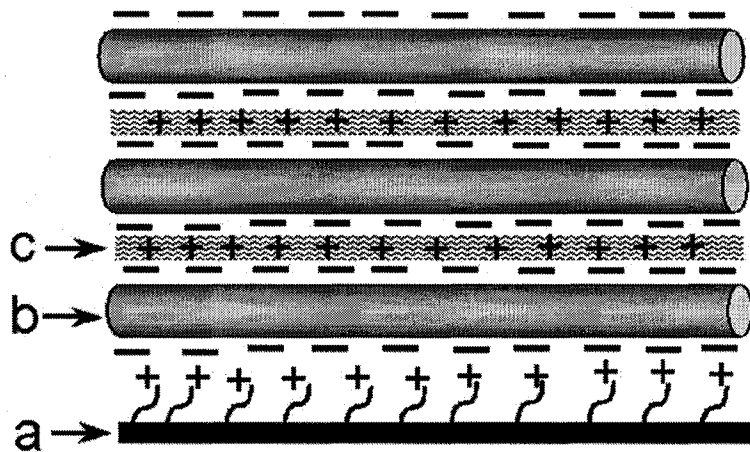


Figure 6.6 schematic illustration of electrostatic layer-by-layer assembly (a) thiolated gold surface (b) flagella (c) polyamine.

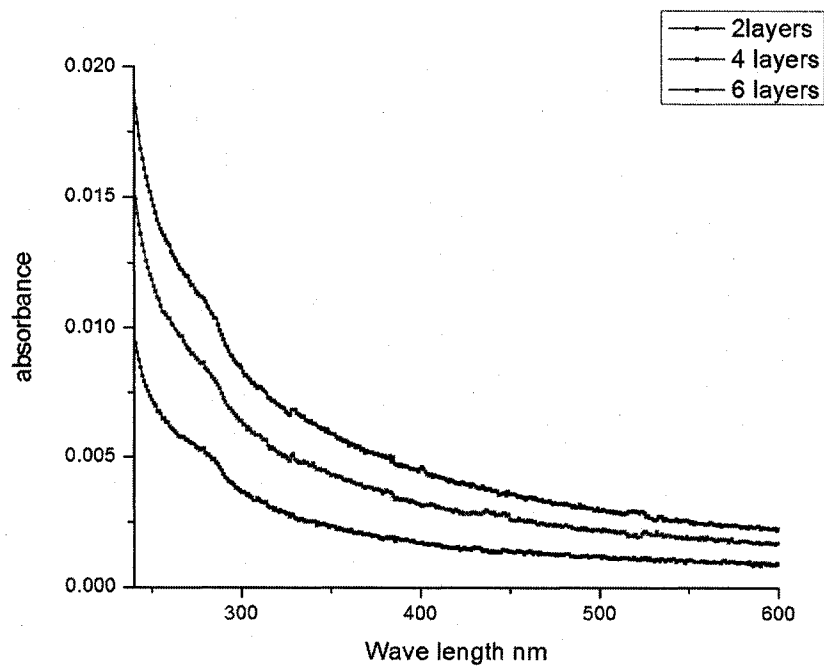


Figure 6.7 Absorbance spectra of electrostatic assembly of flagella on quartz.

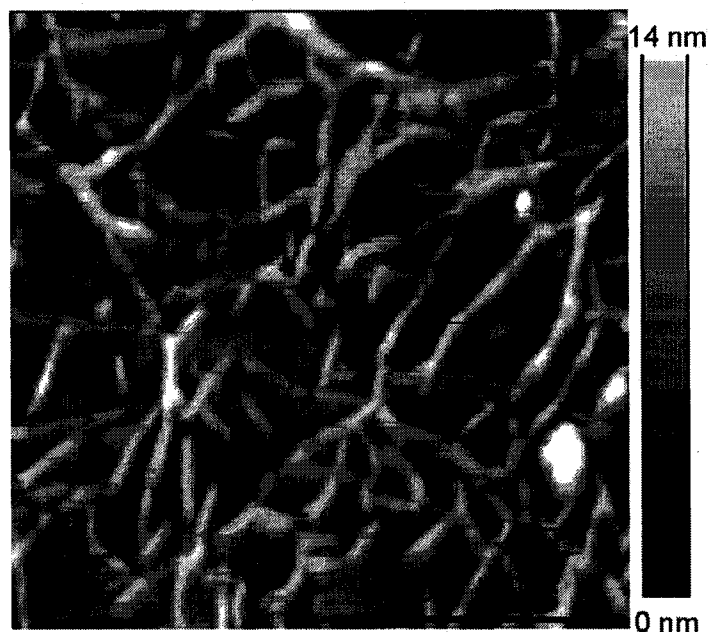


Figure 6.8 AFM images of CaCO_3 mineralized on flagella.

As a final demonstration of bottom-up assembly of a potentially biocompatible nanomaterial scaffold, calcium carbonate mineralization was carried out on flagella assembled on positively-charged quartz plates. Well-separated low density of Glu-Asp loop peptide flagella layer was assembled on quartz with brief exposure to the flagella solution. In the biomineralization process, Ca^{2+} ions are thought to bind to the carboxylate side chains of the aspartic acid and glutamic acid residues, which may assist in initiating nucleation of CaCO_3 mineralization by generation of a region of local supersaturation with diffusion of $\text{CO}_2(\text{CO}_3^{2-})$ to the vicinity of flagella. AFM images of CaCO_3 mineralized on flagella are indicated in Figure 6.8.

CHAPTER VII

FUTURE DIRECTIONS

The previous work described in this study represents a series of preliminary investigations in which the preparation of a number of different nanomaterials was demonstrated for the first time with bacterial flagella. A number of potential future research directions for further exploration and development of hybrid flagella nanomaterials are discussed below.

Assembly of Multifunctional Bio-Nanotubes and Their Applications

Flagella with multiple surface functionality can be achieved by sequential self-assembly of flagellin protein monomers with different engineered functions. These multifunctional flagella can then be used to generate multifunctional nanomaterials using their differential affinity for inorganic materials. For example, histidine-loop flagellin subunits displaying imidazole groups can be used to assemble semiconductor quantum dot nanoparticles, while glutamic acid peptide loops displaying carboxylate groups incorporated into the same flagella can be used to assemble avidin-conjugated ferritin particles. Gold binding peptides and silver binding peptides can be displayed on the surface of flagellins and flagella; resulting mixed polymeric flagella can be used to assemble gold and silver nanoparticle in same flagella.

Display of Gold, Silver, and Titanium Binding Peptides and Generation of Gold Nanowires

Metal-binding peptides, such as gold-binding peptides and silver-binding peptides, can be displayed on the surface of flagella (257). These peptide-displaying flagella can then be used to assemble appropriate metal nanoparticles into highly ordered arrays that could have sensor applications, as demonstrated in Chapter X??? of this thesis with gold nanoparticles, etc.. Furthermore, metal nanowires can be synthesized by a process of electrode-free metal deposition on metal nanoparticles previously assembled on flagella (258). Conductive atomic force microscopy and gold electrodes cast on a glass surface can be used to measure the electrical conductivity of the resulting nanowires (259, 260). Copper nanowires synthesized on flagella scaffold can be used as self-reducing and sacrificial template for synthesis of metal nanotubes such as platinum and palladium (261).; the compatibility and affinity of different precious metals for each other is well known, as indicated by the frequent occurrence of certain metals together in naturally occurring mineral deposits, e.g. mixtures of gold, silver and copper, and alloys of platinum, palladium.

Synthesis and Applications of Transition Metal Alloy Nanoparticles on Flagella Scaffold

Bimetallic nanoparticles can be synthesized on a flagella scaffold which can be used as a type of inorganic catalyst (262). The composition of peptide loops can be used to tune the composition and functional performance of metallic nanoparticles, hence

catalytic activity can be enhanced by varying the composition of materials attached or synthesized on flagella nanotubes.

Application of Self-Assembled Nanoparticles on Flagella as an Optical Waveguide System

An ordered assembly of uniform semiconductor quantum dots on a flagella scaffold could potentially be used as an optical wave guide (155, 263). Engineered flagella displaying the desired types of peptide loops can be assembled on an appropriate surface, e.g., quartz, glass, silica, or gold, and quantum dots can then be assembled on the immobilized flagella. The interparticle distance between quantum dots and consequently, the fluorescence energy transfer properties can be tuned by varying the His-loop flagellin composition in flagella. An assembled quantum dot-flagellin protein system could be further stabilized by chemical cross-linking of flagella and forming a thin??? silica layer on top of the quantum dot-flagella nanocomposite.

Synthesis of Doped Semiconductor Quantum Dots on Flagella Scaffold and Study of Their Properties with Fluorescence and Electron Spin Resonance

Semiconductor quantum dots such as CdS and ZnS can be synthesized on bacterial flagella and these nanoparticles can be doped with magnetic metal ions such as Mn^{2+} and Co^{3+} (70). Electromagnetic properties and optical properties of these composite nanoparticles can be studied with electron spin resonance (ESR) spectroscopy and fluorescence spectroscopy. There are several well-known examples of small peptides

that are known to function as templates for nucleation and directed self-assembly of semiconductor nanostructures with thermodynamically unfavorable lattice structures at room temperature (141). The lattice structure of any resulting flagellin-nanomaterial composites can be studied by X-ray diffraction and electron diffraction techniques, which yield characteristic diffraction patterns for different types of lattice structures. Any change in the lattice structure will result in a change in the electron spin splitting; furthermore, doped magnetic nuclei can also be used as probes to measure changes in the lattice structure. A possible change in the crystal lattice of quantum dots can be studied by enzymatic degradation of the flagella protein scaffold and detergent-based unfolding of flagella.

Fluorescence Detection of Flagella Self-Assembly Process and Use of Dye and Quantum Dots Labeled Flagella as Antenna for Harvesting Solar Light

Peptides containing single cysteine residues with reactive thiol side chains can be introduced into the multiple cloning site of the FliTrx flagellin protein by cassette mutagenesis. The resulting thiol-displaying flagellin can then be labeled with Cy3 and Cy5 donor and acceptor fluorophore dyes that have reactive mono-functional maleimides (www.piercenet.com/www.amershambiosciences.com) specific for the sulfhydryl (-SH) group of cysteine. Following controlled self-assembly of the two dye-labeled flagellin monomers into a 1:1 ratio mixture, the resulting hybrid flagella should show strong FRET from the Cy3 donor to the Cy5 acceptor. An increase in the FRET efficiency can be used as a measure as a function of rate of flagellin self

assembly (264, 265). This would be similar to the use of either fluorescence quenching or an increase in fluorescence intensity due to changes in FRET, used to monitor the polymerase chain reaction in the “real-time” PCR technique.

Generation of Millimeter Length Flagella Wires with a Microfluidic System and Characterization of its Mechanical Properties

Several techniques can be employed to generate macroscopic covalently bonded flagella bundles. In the first method, a solution of concentrated, reduced cysteine-loop flagella can be passed through a narrow tube, using a solution flow rate and viscosity that will ensure laminar flow in the tube. The parabolic distribution of fluid shear forces accord the diameter of the tube will result in alignment of any rod-like flagella structures with the direction of fluid flow; this approach is used to manufacture Kevlar fibers used in “bullet-proof” materials.. Disulfide bonds can be generated between aligned flagella by introduction of oxidant at some location near the midpoint of the tube with out disturbing the laminar flow pattern. In the second method, lysine-loop flagella can be aligned in a flow system and an amine-reactive chemical cross-linking agent such as glutaraldehyde can be introduced to form chemical cross-links (266). Mechanical properties of the resulting fibers, such as tensile strength, can be measured with appropriate instrumental set-up (267). Finally, higher order structures of assembled flagella bundles might be generated by optical trapping of the fibers and generation of multiple point and/or line traps with laser

tweezer instrument, such as the BioRyx 200 instrument present in the W. M. Keck Nanotechnology facility at WMU.

REFERENCES

1. Nanotechnology Research and Computation CenterWu, L. Q., and Payne, G. F., Biofabrication: Using Biological Materials and Biocatalysts to Construct Nanostructured Assemblies, *Trends Biotechnol*, 22, 593 (2004).
2. Martin, C. R., and Kohli, P., The Emerging Field of Nanotube Biotechnology, *Nat Rev Drug Discov*, 2, 29 (2003).
3. Kohli, P., and Martin, C. R., Smart Nanotubes for Biotechnology, *Curr Pharm Biotechnol*, 6, 35 (2005).
4. Matsui, H., Pan, S., and Douberlt, G. E., Fabrication of Nanocrystal Tube Using Peptide Tubule as Template and Its Application as Signal-Enhancing Cuvette, *J. Phys. Chem. B*, 105, 1683 (2001).
5. Lopez, C. F., Nielsen, S. O., Moore, P. B., and Klein, M. L., Understanding Nature's Design for a Nanosyringe, *Proc Natl Acad Sci U S A*, 101, 4431 (2004).
6. Srinivasan, U., Iyer, G. H., Przybycien, T. A., Samsonoff, W. A., and Bell, J. A., Crystine: Fibrous Biomolecular Material from Protein Crystals Cross-Linked in a Specific Geometry, *Protein Eng*, 15, 895 (2002).
7. Mao, C., Solis, D. J., Reiss, B. D., Kottmann, S. T., Sweeney, R. Y., Hayhurst, A., Georgiou, G., Iverson, B., and Belcher, A. M., Virus-Based Toolkit for the Directed Synthesis of Magnetic and Semiconducting Nanowires, *Science*, 303, 213 (2004).
8. Ipsita A. banerjee, L. Y., and Hiroshi Matsui, Cu Nanocystal Growth on Peptide Nanotubes by Biomineralization: Size Control of Cu Nanocrystals by Tuning Peptide Conformation, *Proc Natl Acad Sci U S A*, 100, 14678 (2003).
9. Matsui, H., Pan, S., Gologan, B., and Jonas, S. H., Bolaamphiphile Nanotube-Templated Metallized Wires, *J. Phys. Chem. B*, 104, 9576 (2000).
10. Zhang, S., Emerging Biological Materials through Molecular Self-Assembly, *Biotechnol Adv*, 20, 321 (2002).
11. Nam, K. T., Peelle, B. R., Lee, S.-W., and Belcher, A. M., Genetically Driven Assembly of Nanorings Based on the M13 Virus, *Nano Letters*, 4, 23 (2003).
12. Lin, C. C., Yeh, Y. C., Yang, C. Y., Chen, C. L., Chen, G. F., Chen, C. C., and Wu, Y. C., Selective Binding of Mannose-Encapsulated Gold Nanoparticles to Type 1 Pili in Escherichia Coli, *J Am Chem Soc*, 124, 3508 (2002).
13. Audette, G. F., van Schaik, E. J., Hazes, B., and Irvin, R. T., DNA-Binding Protein Nanotubes: Learning from Nature's Nanotech Examples, *Nano Letters*, 4, 1897 (2004).
14. Fernandez-Lopez, S., Kim, H. S., Choi, E. C., Delgado, M., Granja, J. R., Khasanov, A., Kraehenbuehl, K., Long, G., Weinberger, D. A., Wilcoxon, K. M., and Ghadiri, M. R., Antibacterial Agents Based on the Cyclic D,L-Alpha-Peptide Architecture, *Nature*, 412, 452 (2001).

15. Hartgerink, J. D., Beniash, E., and Stupp, S. I., Self-Assembly and Mineralization of Peptide-Amphiphile Nanofibers, *Science*, *294*, 1684 (2001).
16. Yemini, M., Reches, M., Rishpon, J., and Gazit, E., Novel Electrochemical Biosensing Platform Using Self-Assembled Peptide Nanotubes, *Nano Lett*, *5*, 183 (2005).
17. Beniash, E., Hartgerink, J. D., Storrie, H., Stendahl, J. C., and Stupp, S. I., Self-Assembling Peptide Amphiphile Nanofiber Matrices for Cell Entrapment, *Acta Biomater*, *1*, 387 (2005).
18. Zhang, S., Gelain, F., and Zhao, X., Designer Self-Assembling Peptide Nanofiber Scaffolds for 3d Tissue Cell Cultures, *Semin Cancer Biol*, *15*, 413 (2005).
19. Davis, M. E., Motion, J. P., Narmoneva, D. A., Takahashi, T., Hakuno, D., Kamm, R. D., Zhang, S., and Lee, R. T., Injectable Self-Assembling Peptide Nanofibers Create Intramyocardial Microenvironments for Endothelial Cells, *Circulation*, *111*, 442 (2005).
20. Mao, C., Flynn, C. E., Hayhurst, A., Sweeney, R., Qi, J., Georgiou, G., Iverson, B., and Belcher, A. M., Viral Assembly of Oriented Quantum Dot Nanowires, *Proc Natl Acad Sci U S A*, *100*, 6946 (2003).
21. Lee, S. W., Mao, C., Flynn, C. E., and Belcher, A. M., Ordering of Quantum Dots Using Genetically Engineered Viruses, *Science*, *296*, 892 (2002).
22. Huang, Y., Chiang, C. Y., Lee, S. K., Gao, Y., Hu, E. L., De Yoreo, J., and Belcher, A. M., Programmable Assembly of Nanoarchitectures Using Genetically Engineered Viruses, *Nano Lett*, *5*, 1429 (2005).
23. Tseng, R. J., Tsai, C., Ma, L., Ouyang, J., Ozkan, C. S., and Yang, Y., Digital Memory Device Based on Tobacco Mosaic Virus Conjugated with Nanoparticles, *Nat. Nano.*, *1*, 72 (2006).
24. Fujikawa, S., and Kunitake, T., Surface Fabrication of Hollow Nanoarchitectures of Ultrathin Titania Layers from Assembled Latex Particles and Tobacco Mosaic Viruses as Templates, *Langmuir*, *19*, 6545 (2003).
25. Yamashita, I., Suzuki, H., and Namba, K., Multiple-Step Method for Making Exceptionally Well-Oriented Liquid-Crystalline Sols of Macromolecular Assemblies, *J Mol Biol*, *278*, 609 (1998).
26. Nam, K. T., Kim, D. W., Yoo, P. J., Chiang, C. Y., Meethong, N., Hammond, P. T., Chiang, Y. M., and Belcher, A. M., Virus-Enabled Synthesis and Assembly of Nanowires for Lithium Ion Battery Electrodes, *Science*, *312*, 885 (2006).
27. Schlick, T. L., Ding, Z., Kovacs, E. W., and Francis, M. B., Dual-Surface Modification of the Tobacco Mosaic Virus, *J. Am. Chem. Soc.*, *127*, 3718 (2005).
28. Westerlund-Wikstrom, B., Tanskanen, J., Virkola, R., Hacker, J., Lindberg, M., Skurnik, M., and Korhonen, T. K., Functional Expression of Adhesive Peptides as Fusions to Escherichia Coli Flagellin, *Protein Eng.*, *10*, 1319 (1997).

29. Tanskanen, J., Korhonen, T. K., and Westerlund-Wikstrom, B., Construction of a Multihybrid Display System: Flagellar Filaments Carrying Two Foreign Adhesive Peptides., *Appl. Environ. Microbiol.*, 66, 4152 (2000).
30. Westerlund-Wikstrom, B., Peptide Display on Bacterial Flagella: Principles and Applications., *Int. J. Med. Microbiol.*, 290, 223 (2000).
31. Lu, Z., Murray, K. S., Van Cleave, V., LaVallie, E. R., Stahl, M. L., and McCoy, J. M., Expression of Thioredoxin Random Peptide Libraries on the Escherichia Coli Cell Surface as Functional Fusions to Flagellin: A System Designed for Exploring Protein-Protein Interactions., *Biotechnology (N Y)*, 13, 366 (1995).
32. Lu, Z., Tripp, B. C., and McCoy, J. M., Displaying Libraries of Conformationally Constrained Peptides on the Surface of Escherichia Coli as Flagellin Fusions, *Meth. Mol. Biol.*, 87, 265 (1998).
33. Minamino, T., and Namba, K., Self-Assembly and Type Iii Protein Export of the Bacterial Flagellum, *J. Mol. Microbiol. Biotechnol.*, 7, 5 (2004).
34. Asakura, S., and Iino, T., Polymorphism of Salmonella Flagella as Investigated by Means of in Vitro Copolymerization of Flagellins Derived from Various Strains, *J. Mol. Biol.*, 64, 251 (1972).
35. Kamiya, R., Asakura, S., and Yamaguchi, S., Formation of Helical Filaments by Copolymerization of Two Types of 'Straight' Flagellins, *Nature*, 286, 628 (1980).
36. Lawn, A. M., Comparison of the Flagellins from Different Flagellar Morphotypes of Escherichia Coli, *J. Gen. Microbiol.*, 101, 112 (1977).
37. Jones, C. J., and Aizawa, S. I., The Bacterial Flagellum and Flagellar Motor: Structure, Assembly and Function., *Adv. Microb. Physiol.*, 32, 109 (1991).
38. Jones, C. J., and Aizawa, S., The Bacterial Flagellum and Flagellar Motor: Structure, Assembly and Function, *Adv Microb Physiol*, 32, 109 (1991).
39. Moens, S., and Vanderleyden, J., Functions of Bacterial Flagella, *Crit Rev Microbiol*, 22, 67 (1996).
40. Bardy, S. L., Ng, S. Y., and Jarrell, K. F., Prokaryotic Motility Structures, *Microbiology*, 149, 295 (2003).
41. Metlina, A. L., Bacterial and Archaeal Flagella as Prokaryotic Motility Organelles, *Biochemistry (Mosc)*, 69, 1203 (2004).
42. Berg, H. C., The Rotary Motor of Bacterial Flagella, *Annu Rev Biochem*, 72, 19 (2003).
43. Berry, R. M., and Armitage, J. P., The Bacterial Flagella Motor, *Adv Microb Physiol*, 41, 291 (1999).
44. DeRosier, D. J., The Turn of the Screw: The Bacterial Flagellar Motor, *Cell*, 93, 17 (1998).
45. Samatey, F. A., Matsunami, H., Imada, K., Nagashima, S., Shaikh, T. R., Thomas, D. R., Chen, J. Z., Derosier, D. J., Kitao, A., and Namba, K., Structure of the Bacterial Flagellar Hook and Implication for the Molecular Universal Joint Mechanism, *Nature*, 431, 1062 (2004).

46. Shaikh, T. R., Thomas, D. R., Chen, J. Z., Samatey, F. A., Matsunami, H., Imada, K., Namba, K., and Derosier, D. J., A Partial Atomic Structure for the Flagellar Hook of Salmonella Typhimurium, *Proc Natl Acad Sci U S A*, *102*, 1023 (2005).
47. Flores, H., Lobaton, E., Mendez-Diez, S., Tlupova, S., and Cortez, R., A Study of Bacterial Flagellar Bundling, *Bull Math Biol*, *67*, 137 (2005).
48. Yonekura, K., Maki, S., Morgan, D. G., DeRosier, D. J., Vonderviszt, F., Imada, K., and Namba, K., The Bacterial Flagellar Cap as the Rotary Promoter of Flagellin Self-Assembly, *Science*, *290*, 2148 (2000).
49. Yonekura, K., Maki-Yonekura, S., and Namba, K., Growth Mechanism of the Bacterial Flagellar Filament, *Res Microbiol*, *153*, 191 (2002).
50. Macnab, R. M., How Bacteria Assemble Flagella, *Annu Rev Microbiol*, *57*, 77 (2003).
51. Yonekura, K., Maki-Yonekura, S., and Namba, K., Complete Atomic Model of the Bacterial Flagellar Filament by Electron Cryomicroscopy, *Nature*, *424*, 643 (2003).
52. Macnab, R. M., Type Iii Flagellar Protein Export and Flagellar Assembly, *Biochim Biophys Acta*, *1694*, 207 (2004).
53. Minamino, T., and Namba, K., Self-Assembly and Type Iii Protein Export of the Bacterial Flagellum, *J Mol Microbiol Biotechnol*, *7*, 5 (2004).
54. Maki-Yonekura, S., Yonekura, K., and Namba, K., Domain Movements of Hap2 in the Cap-Filament Complex Formation and Growth Process of the Bacterial Flagellum, *Proc Natl Acad Sci U S A*, *100*, 15528 (2003).
55. Dioszeghy, Z., Zavodszky, P., Namba, K., and Vonderviszt, F., Stabilization of Flagellar Filaments by Hap2 Capping, *FEBS Lett*, *568*, 105 (2004).
56. Namba, K., and Vonderviszt, F., Molecular Architecture of Bacterial Flagellum, *Q Rev Biophys*, *30*, 1 (1997).
57. Fedorov, O. V., and Efimov, A. V., Flagellin as an Object for Supramolecular Engineering, *Protein Eng*, *3*, 411 (1990).
58. Tripp, B. C., Lu, Z., Bourque, K., Sookdeo, H., and McCoy, J. M., Investigation of the 'Switch-Epitope' Concept with Random Peptide Libraries Displayed as Thioredoxin Loop Fusions, *Protein Eng*, *14*, 367 (2001).
59. Samatey, F. A., Imada, K., Nagashima, S., Vonderviszt, F., Kumasaka, T., Yamamoto, M., and Namba, K., Structure of the Bacterial Flagellar Protofilament and Implications for a Switch for Supercoiling, *Nature*, *410*, 331 (2001).
60. Yonekura, K., Maki-Yonekura, S., and Namba, K., Building the Atomic Model for the Bacterial Flagellar Filament by Electron Cryomicroscopy and Image Analysis, *Structure (Camb)*, *13*, 407 (2005).
61. Fischer, J. E., Chemical Doping of Single-Wall Carbon Nanotubes, *Acc Chem Res*, *35*, 1079 (2002).
62. Hu, H., Zhao, B., Hamon, M. A., Kamaras, K., Itkis, M. E., and Haddon, R. C., Sidewall Functionalization of Single-Walled Carbon Nanotubes by Addition of Dichlorocarbene, *J Am Chem Soc*, *125*, 14893 (2003).

63. Lu, J., Nagase, S., Yu, D., Ye, H., Han, R., Gao, Z., Zhang, S., and Peng, L., Amphoteric and Controllable Doping of Carbon Nanotubes by Encapsulation of Organic and Organometallic Molecules, *Phys Rev Lett*, *93*, 116804 (2004).
64. Kavan, L., and Dunsch, L., Ionic Liquid for in Situ Vis/Nir and Raman Spectroelectrochemistry: Doping of Carbon Nanostructures, *Chemphyschem*, *4*, 944 (2003).
65. Kavan, L., Kalbac, M., Zukalova, M., Krause, M., and Dunsch, L., Electrochemical Doping of Double-Walled Carbon Nanotubes: An in Situ Raman Spectroelectrochemical Study, *Chemphyschem*, *5*, 274 (2004).
66. Lammert, P. E., Crespi, V. H., and Rubio, A., Stochastic Heterostructures and Diodium in B/N-Doped Carbon Nanotubes, *Phys Rev Lett*, *87*, 136402 (2001).
67. Kang, H. S., Organic Functionalization of Sidewall of Carbon Nanotubes, *J Chem Phys*, *121*, 6967 (2004).
68. Conn, M. M., and Rebek, J., Jr., Self-Assembling Capsules, *Chem Rev*, *97*, 1647 (1997).
69. Kumara, M. T., Tripp, B. C., and Muralidharan, S., Self-Assembly of Metal Nanoparticles and Nanotubes on Bioengineered Flagella Scaffolds, *Chem Mater*, *19*, 2056 (2007).
70. Kumara, M. T., Tripp, B. C., and Muralidharan, S., Exciton Energy Transfer in Self-Assembled Quantum Dots on Bioengineered Bacterial Flagella, *J Phys. Chem. C*, *111*, 5276 (2007).
71. Kumara, M. T., Muralidharan, S., and Tripp, B. C., Generation and Characterization of Inorganic and Organic Nanotubes on Bioengineered Flagella of Mesophilic Bacteria, *J. Nanosci. Nanotechnol*, *7*, 2260 (2007).
72. Yang, G., Cecconi, C., Baase, W. A., Vetter, I. R., Breyer, W. A., Haack, J. A., Matthews, B. W., Dahlquist, F. W., and Bustamante, C., Solid-State Synthesis and Mechanical Unfolding of Polymers of T4 Lysozyme, *Proc Natl Acad Sci U S A*, *97*, 139 (2000).
73. Kumara, M. T., Srividya, N., Muralidharan, S., and Tripp, B. C., Bioengineered Flagella Protein Nanotubes with Cysteine Loops: Self-Assembly and Manipulation in an Optical Trap, *Nano Lett.*, *6*, 2121 (2006).
74. Martin-Jezequel, V., Hildebrand, M., and Brzezinski, M. A., Silicon Metabolism in Diatoms: Implications for Growth, *J. Phycol.*, *36*, 821 (2000).
75. Poulsen, N., and Kroger, N., Silica Morphogenesis by Alternative Processing of Silaffins in the Diatom *Thalassiosira Pseudonana*, *J Biol Chem*, *279*, 42993 (2004).
76. Sumper, M., Brunner, E., and Lehmann, G., Biomineralization in Diatoms: Characterization of Novel Polyamines Associated with Silica, *FEBS Lett.*, *579*, 3765 (2005).
77. Lenoci, L., and Camp, P. J., Self-Assembly of Peptide Scaffolds in Biosilica Formation: Computer Simulations of a Coarse-Grained Model, *J Am Chem Soc*, *128*, 10111 (2006).
78. Gautier, C., Lopez, P. J., Hemadi, M., Livage, J., and Coradin, T., Biomimetic Growth of Silica Tubes in Confined Media, *Langmuir*, *22*, 9092 (2006).

79. Schroder, H. C., Brandt, D., Schlossmacher, U., Wang, X., Tahir, M. N., Tremel, W., Belikov, S. I., and Muller, W. E., Enzymatic Production of Biosilica Glass Using Enzymes from Sponges: Basic Aspects and Application in Nanobiotechnology (Material Sciences and Medicine), *Naturwissenschaften*, *94*, 339 (2007).
80. Brott, L. L., Naik, R. R., Pikas, D. J., Kirkpatrick, S. M., Tomlin, D. W., Whitlock, P. W., Clarson, S. J., and Stone, M. O., Ultrafast Holographic Nanopatterning of Biocatalytically Formed Silica, *Nature*, *413*, 291 (2001).
81. Kroger, N., Deutzmann, R., and Sumper, M., Polycationic Peptides from Diatom Biosilica That Direct Silica Nanosphere Formation, *Science*, *286*, 1129 (1999).
82. Lutz, K., Groger, C., Sumper, M., and Brunner, E., Biomimetic Silica Formation: Analysis of the Phosphate-Induced Self-Assembly of Polyamines, *Phys. Chem. Chem. Phys.*, *7*, 2812 (2005).
83. Vrieling, E. G., Beelen, T. P. M., van Santen, R. A., and Gieskes, W. W. C., Mesophases of (Bio)Polymer-Silica Particles Inspire a Model for Silica Biomineralization in Diatoms, *Angew. Chem. Int. Ed.*, *41*, 1543 (2002).
84. Vrieling, E. G., Sun, Q., Beelen, T. P., Hazelaar, S., Gieskes, W. W., van Santen, R. A., and Sommerdijk, N. A., Controlled Silica Synthesis Inspired by Diatom Silicon Biomineralization, *J. Nanosci. Nanotechnol.*, *5*, 68 (2005).
85. Foo, C. W. P., Patwardhan, S. V., Belton, D. J., Kitchel, B., Anastasiades, D., Huang, J., Naik, R. R., Perry, C. C., and Kaplan, D. L., Novel Nanocomposites from Spider Silk-Silica Fusion (Chimeric) Proteins, *Proc. Natl. Acad. Sci. USA*, *103*, 9428 (2006).
86. Sumper, M., and Brunner, E., Learning from Diatoms: Nature's Tools for the Production of Nanostructured Silica, *Adv. Func. Mat.*, *16*, 17 (2006).
87. Gautier, C., Lopez, P. J., Livage, J., and Coradin, T., Influence of Poly-L-Lysine on the Biomimetic Growth of Silica Tubes in Confined Media, *J. Colloid Interface Sci.*, *309*, 44 (2007).
88. Fujikawa, S., Takaki, R., and Kunitake, T., Nanocopying of Individual DNA Strands and Formation of the Corresponding Surface Pattern of Titania Nanotube, *Langmuir*, *21*, 8899 (2005).
89. Sumerel, J. L., Yang, W., Kisailus, D., Weaver, J. C., Choi, J. H., and Morse, D. E., Biocatalytically Templated Synthesis of Titanium Dioxide, *Chem. Mater.*, *15*, 4804 (2003).
90. Ji, Q., and Shimizu, T., Chemical Synthesis of Transition Metal Oxide Nanotubes in Water Using an Iced Lipid Nanotube as a Template, *Chem. Commun. (Camb)*, 4411 (2005).
91. Law, M., Greene, L. E., Johnson, J. C., Saykally, R., and Yang, P., Nanowire Dye-Sensitized Solar Cells, *Nat. Mater.*, *4*, 455 (2005).
92. Varghese, O. K., Paulose, M., Shankar, K., Mor, G. K., and Grimes, C. A., Water-Photolysis Properties of Micron-Length Highly-Ordered Titania Nanotube-Arrays, *J. Nanosci. Nanotechnol.*, *5*, 1158 (2005).

93. Mor, G. K., Shankar, K., Paulose, M., Varghese, O. K., and Grimes, C. A., Enhanced Photocleavage of Water Using Titania Nanotube Arrays, *Nano Lett.*, *5*, 191 (2005).
94. Mor, G. K., Shankar, K., Paulose, M., Varghese, O. K., and Grimes, C. A., Use of Highly-Ordered TiO₂ Nanotube Arrays in Dye-Sensitized Solar Cells, *Nano Lett.*, *6*, 215 (2006).
95. Varghese, O. K., Mor, G. K., Grimes, C. A., Paulose, M., and Mukherjee, N., A Titania Nanotube-Array Room-Temperature Sensor for Selective Detection of Hydrogen at Low Concentrations, *J. Nanosci. Nanotechnol.*, *4*, 733 (2004).
96. Gao, X., Zhu, H., Pan, G., Ye, S., Lan, Y., Wu, F., and Song, D., Preparation and Electrochemical Characterization of Anatase Nanorods for Lithium-Inserting Electrode Material, *J. Phys. Chem. B*, *108*, 2868 (2004).
97. Quan, X., Yang, S., Ruan, X., and Zhao, H., Preparation of Titania Nanotubes and Their Environmental Applications as Electrode, *Environ. Sci. Technol.*, *39*, 3770 (2005).
98. Stupp, S. I., Hanson, J. A., Eurell, J. A., Ciegler, G. W., and Johnson, A., Organoapatites: Materials for Artificial Bone. Iii. Biological Testing, *J. Biomed. Mater. Res.*, *27*, 301 (1993).
99. Aoba, T., Shimazu, Y., Taya, Y., Soeno, Y., Sato, K., and Miake, Y., Fluoride and Apatite Formation in Vivo and in Vitro, *J. Electr. Microsc. (Tokyo)*, *52*, 615 (2003).
100. Zhao, B., Hu, H., Mandal, S. K., and Haddon, R. C., A Bone Mimic Based on the Self-Assembly of Hydroxyapatite on Chemically Functionalized Single-Walled Carbon Nanotubes, *Chem. Mater.*, *17*, 3235 (2005).
101. Wang, Z. H., Scherr, E. M., MacDiarmid, A. G., and Epstein, A. J., Transport and Epr Studies of Polyaniline: A Quasi-One-Dimensional Conductor with Three-Dimensional "Metallic" States, *Phys. Rev. B. Condensed Matter.*, *45*, 4190 (1992).
102. Nagarajan, R., Liu, W., Kumar, J., Tripathy, S. K., Bruno, F. F., and Samuelson, L. A., Manipulating DNA Conformation Using Intertwined Conducting Polymer Chains, *Macromolecules*, *34*, 3921 (2001).
103. Lee, K., Cho, S., Park, S. H., Heeger, A. J., Lee, C. W., and Lee, S. H., Metallic Transport in Polyaniline, *Nature*, *441*, 65 (2006).
104. Feng, X., Mao, C., Yang, G., Hou, W., and Zhu, J. J., Polyaniline/Au Composite Hollow Spheres: Synthesis, Characterization, and Application to the Detection of Dopamine, *Langmuir*, *22*, 4384 (2006).
105. Ma, Y., Zhang, J., Zhang, G., and He, H., Polyaniline Nanowires on Si Surfaces Fabricated with DNA Templates, *J. Am. Chem. Soc.*, *126*, 7097 (2004).
106. Dawn, A., and Nandi, A. K., Simple Method for the Preparation of DNA-Poly(O-Methoxyaniline) Hybrid: Structure, Morphology, and Uncoiling of Poly(O-Methoxyaniline) on the DNA Surface, *Langmuir*, *22*, 3273 (2006).
107. Holmgren, A., Thioredoxin, *Annu. Rev. Biochem.*, *54*, 237 (1985).

108. Lu, Z., LaVallie, E. R., and McCoy, J. M., Using Bio-Panning of Flitrx Peptide Libraries Displayed on E. Coli Cell Surface to Study Protein-Protein Interactions, *Meth. Mol. Biol.*, 205, 267 (2003).
109. LaVallie, E. R., DiBlasio, E. A., Kovacic, S., Grant, K. L., Schendel, P. F., and McCoy, J. M., A Thioredoxin Gene Fusion Expression System That Circumvents Inclusion Body Formation in the E. Coli Cytoplasm, *Biotechnology (N Y)*, 11, 187 (1993).
110. LaVallie, E. R., DiBlasio-Smith, E. A., Collins-Racie, L. A., Lu, Z., and McCoy, J. M., Thioredoxin and Related Proteins as Multifunctional Fusion Tags for Soluble Expression in E. Coli, *Meth. Mol. Biol.*, 205, 119 (2003).
111. Zhao, S., and Lee, E. Y. C., A Protein Phosphatase-1-Binding Motif Identified by the Panning of a Random Peptide Display Library, *J. Biol. Chem.*, 272, 28368 (1997).
112. Xu, H., Zhang, P., Liu, L., and Lee, M. Y., A Novel PcnA-Binding Motif Identified by the Panning of a Random Peptide Display Library, *Biochemistry*, 40, 4512 (2001).
113. Brown, C. K., Modzelewski, R. A., Johnson, C. S., and Wong, M. K., A Novel Approach for the Identification of Unique Tumor Vasculature Binding Peptides Using an E. Coli Peptide Display Library, *Ann Surg Oncol*, 7, 743 (2000).
114. Thai, C. K., Dai, H., Sastry, M. S., Sarikaya, M., Schwartz, D. T., and Baneyx, F., Identification and Characterization of Cu(2)O- and Zn-Binding Polypeptides by Escherichia Coli Cell Surface Display: Toward an Understanding of Metal Oxide Binding, *Biotechnol Bioeng*, 87, 129 (2004).
115. Nickels, P., Dittmer, W. U., Beyer, S., Kotthaus, J. P., and Simmel, F. C., Polyaniline Nanowire Synthesis Templated by DNA, *Nanotechnology*, 15, 1524 (2004).
116. Noll, F., Sumper, M., and Hampp, N., Nanostructure of Diatom Silica Surfaces and of Biomimetic Analogues, *Nano Lett.*, 2, 91 (2002).
117. Coradin, T., and Lopez, P. J., Biogenic Silica Patterning: Simple Chemistry or Subtle Biology? *ChemBiochem.*, 4, 251 (2003).
118. Yee, N., Phoenix, V. R., Konhauser, K. O., Benning, L. G., and Ferris, F. G., The Effect of Cyanobacteria on Silica Precipitation at Neutral Ph: Implications for Bacterial Silicification in Geothermal Hot Springs, *Chem. Geol.*, 199, 83 (2003).
119. Wenzl, S., Deutzmann, R., Hett, R., Hochmuth, E., and Sumper, M., Quaternary Ammonium Groups in Silica-Associated Proteins, *Angew. Chem. Int. Ed. Engl.*, 43, 5933 (2004).
120. Sun, J., Gao, L. A., and Zhang, Q. H., TiO₂ Tubes Synthesized by Using Ammonium Sulfate and Carbon Nanotubes as Templates, *J. Mater. Sci. Lett.*, 22, 339 (2003).
121. Sainsbury, T., and Fitzmaurice, D., Templated Assembly of Semiconductor and Insulator Nanoparticles at the Surface of Covalently Modified Multiwalled Carbon Nanotubes, *Chem. Mater.*, 16, 3780 (2004).

122. Zhao, J., Wang, X., Sun, T., and Li, L., In Situ Templated Synthesis of Anatase Single-Crystal Nanotube Arrays, *Nanotechnology*, *16*, 2450 (2005).
123. Ji, Q., Kamiya, S., and Shimizu, T., Confined Sol–Gel Reaction Using a Neutral Glycolipid Nanotube as a Template: Aqueous Fabrication of Titania Rod Structures, *Chemistry Lett.*, *35*, 394 (2006).
124. Knez, M., Kadri, A., Wege, C., Gosele, U., Jeske, H., and Nielsch, K., Atomic Layer Deposition on Biological Macromolecules: Metal Oxide Coating of Tobacco Mosaic Virus and Ferritin, *Nano Lett.*, *6*, 1172 (2006).
125. Bauerlein, E., Biomineralization of Unicellular Organisms: An Unusual Membrane Biochemistry for the Production of Inorganic Nano- and Microstructures, *Angew. Chem. Int. Ed. Engl.*, *42*, 614 (2003).
126. Küther, J., Seshadri, R., Knoll, W., and Tremel, W., Templated Growth of Calcite, Vaterite and Aragonite Crystals Onself-Assembled Monolayers of Substituted Alkylthiols on Gold, *J. Mater. Chem.*, *8*, 641 (1998).
127. Fu, G., Valiyaveetil, S., Wopenka, B., and Morse, D. E., Caco3 Biomineralization: Acidic 8-Kda Proteins Isolated from Aragonitic Abalone Shell Nacre Can Specifically Modify Calcite Crystal Morphology, *Biomacromol.*, *6*, 1289 (2005).
128. Tsuchiya, H., Macak, J. M., Muller, L., Kunze, J., Muller, F., Greil, P., Virtanen, S., and Schmuki, P., Hydroxyapatite Growth on Anodic TiO₂ Nanotubes, *J. Biomed. Mater. Res. A*, *77*, 534 (2006).
129. Aryal, S., Bahadur, K. C. R., Dharmaraj, N., Kim, K.-W., and Kim, H. Y., Synthesis and Characterization of Hydroxyapatite Using Carbon Nanotubes as a Nano-Matrix, *Scripta Materialia*, *54*, 131 (2006).
130. Akasaka, T., Watari, F., Sato, Y., and Tohji, K., Apatite Formation on Carbon Nanotubes, *Mater. Sci. Eng. C*, *26*, 675 (2006).
131. Nickels, P., Dittmer, W. U., Beyer, S., Kotthaus, J. P., and Simmel, F. C., Polyaniline Nanowire Synthesis Templated by DNA, *Nanotech.*, *15*, 1524 (2004).
132. Xia, H., Chan, H. S. O., Xiao, C., and Cheng, D., Self-Assembled Oriented Conducting Polyaniline Nanotubes, *Nanotechnology*, *15*, 1807 (2004).
133. Dawn, A., and Nandi, A. K., Biomolecular Hybrid of a Conducting Polymer with DNA: Morphology, Structure, and Doping Behavior, *Macromol. Biosci.*, *5*, 441 (2005).
134. Dawn, A., and Nandi, A. K., Slow Doping Rate in DNA-Poly(O-Methoxyaniline) Hybrid: Uncoiling of Poly(O-Methoxyaniline) Chain on DNA Template, *Macromolecules*, *38*, 10067 (2005).
135. Niu, Z., Bruckman, M., Kotakadi, V. S., He, J., Emrick, T., Russell, T. P., Yang, L., and Wang, Q., Study and Characterization of Tobacco Mosaic Virus Head-to-Tail Assembly Assisted by Aniline Polymerization, *Chem. Commun.*, 3019 (2006).
136. Steinmetz, N. F., Lomonossoff, G. P., and Evans, D. J., Cowpea Mosaic Virus for Material Fabrication: Addressable Carboxylate Groups on a Programmable Nanoscaffold, *Langmuir*, *22*, 3488 (2006).

137. Yu, Y., Zhihuai, S., Chen, S., Bian, C., Chen, W., and Xue, G., Facile Synthesis of Polyaniline-Sodium Alginate Nanofibers, *Langmuir*, *22*, 3899 (2006).
138. Konyushenko, E. N., Stejskal, J., Sedenkova, I., Trchova, M., Sapurina, I., Cieslar, M., and Prokes, J., Polyaniline Nanotubes: Conditions of Formation, *Polym. Int.*, *55*, 31 (2006).
139. Huang, Y., Chiang, C. Y., Lee, S. K., Gao, Y., Hu, E. L., De Yoreo, J., and Belcher, A. M., Programmable Assembly of Nanoarchitectures Using Genetically Engineered Viruses, *Nano Lett.*, *5*, 1429 (2005).
140. Mao, C., Flynn, C. E., Hayhurst, A., Sweeney, R., Qi, J., Georgiou, G., Iverson, B., and Belcher, A. M., Viral Assembly of Oriented Quantum Dot Nanowires, *Proc. Natl. Acad. Sci. USA*, *100*, 6946 (2003).
141. Banerjee, I. A., Yu, L., and Matsui, H., Room-Temperature Wurtzite ZnS Nanocrystal Growth on Zn Finger-Like Peptide Nanotubes by Controlling Their Unfolding Peptide Structures, *J. Am. Chem. Soc.*, *127*, 16002 (2005).
142. Prozorov, T., Mallapragada, S. K., Narasimhan, B., Wang, L., Palo, P., Nilsen-Hamilton, M., Williams, T. J., Bazyliniski, D. A., Prozorov, R., and Canfield, P. C., Protein-Mediated Synthesis of Uniform Superparamagnetic Magnetite Nanocrystals, *Advanced Functional Materials*, *17*, 951 (2007).
143. Chan, W. C., and Nie, S., Quantum Dot Bioconjugates for Ultrasensitive Nonisotopic Detection, *Science*, *281*, 2016 (1998).
144. Chen, F., and Gerion, D., Fluorescent CdSe/ZnS Nanocrystal-Peptide Conjugates for Long-Term, Nontoxic Imaging and Nuclear Targeting in Living Cells, *Nano Lett.*, *4*, 1827 (2004).
145. Goldman, E. R., Medintz, I. L., Whitley, J. L., Hayhurst, A., Clapp, A. R., Uyeda, H. T., Deschamps, J. R., Lassman, M. E., and Mattoussi, H., A Hybrid Quantum Dot-Antibody Fragment Fluorescence Resonance Energy Transfer-Based TNT Sensor, *J. Am. Chem. Soc.*, *127*, 6744 (2005).
146. Huffaker, D. L., Park, G., Zou, Z., Shchekin, O. B., and Deppe, D. G., 1.3 μm Room-Temperature GaAs-Based Quantum-Dot Laser, *Applied Physics Letters*, *73*, 2564 (1998).
147. Medintz, I. L., Clapp, A. R., Mattoussi, H., Goldman, E. R., Fisher, B., and Mauro, J. M., Self-Assembled Nanoscale Biosensors Based on Quantum Dot FRET Donors, *Nat. Mater.*, *2*, 630 (2003).
148. Medintz, I. L., Uyeda, H. T., Goldman, E. R., and Mattoussi, H., Quantum Dot Bioconjugates for Imaging, Labelling and Sensing, *Nat Mater*, *4*, 435 (2005).
149. Achermann, M., Petruska, M. A., Koleske, D. D., Crawford, M. H., and Klimov, V. I., Nanocrystal-Based Light-Emitting Diodes Utilizing High-Efficiency Nonradiative Energy Transfer for Color Conversion, *Nano Lett*, *6*, 1396 (2006).
150. Achermann, M., Petruska, M. A., Kos, S., Smith, D. L., Koleske, D. D., and Klimov, V. I., Energy-Transfer Pumping of Semiconductor Nanocrystals Using an Epitaxial Quantum Well, *Nature*, *429*, 642 (2004).

151. Coe, S., Woo, W. K., Bawendi, M., and Bulovic, V., Electroluminescence from Single Monolayers of Nanocrystals in Molecular Organic Devices, *Nature*, *420*, 800 (2002).
152. Huang, Y., Duan, X., Cui, Y., Lauhon, L. J., Kim, K. H., and Lieber, C. M., Logic Gates and Computation from Assembled Nanowire Building Blocks, *Science*, *294*, 1313 (2001).
153. Huynh, W. U., Dittmer, J. J., and Alivisatos, A. P., Hybrid Nanorod-Polymer Solar Cells, *Science*, *295*, 2425 (2002).
154. Tseng, R. J., Tsai, C., Ma, L., Ouyang, J., Ozkan, C. S., and Yang, Y., Digital Memory Device Based on Tobacco Mosaic Virus Conjugated with Nanoparticles, *Nature Nanotechnology*, *1*, 72 (2006).
155. Wang, C. J., Huang, L., Parviz, B. A., and Lin, L. Y., Subdiffraction Photon Guidance by Quantum-Dot Cascades, *Nano Lett.* (2006).
156. Beermann, P. A. G., McGarvey, B. R., Muralidharan, S., and Sung, R. C. W., Epr Spectra of Mn²⁺-Doped Zns Quantum Dots, *Chem. Mater.*, *16*, 915 (2004).
157. Beermann, P. A. G., Synthesis and Spectroscopic Characterization of Zinc Sulfide Quantum Dot Nanocrystals, in *Chemistry*, Western Michigan University, Kalamazoo (2005).
158. Beermann, P. A. G., McGarvey, B. R., Skadtchenko, B. O., Muralidharan, S., and Sung, C. W., Cationic Substitution Sites in Mn²⁺-Doped Zns Nanoparticles, *J. Nanoparticle Res.*, *8*, 235 (2006).
159. Zhang, H., Gilbert, B., Huang, F., and Banfield, J. F., Water-Driven Structure Transformation in Nanoparticles at Room Temperature, *Nature*, *424*, 1025 (2003).
160. Gaponik, N., Talapin, D. V., Rogach, A. L., Hoppe, K., Shevchenko, E. V., Kornowski, A., Eychmuller, A., and Weller, H., Thiol-Capping of Cdte Nanocrystals: An Alternative to Organometallic Synthetic Routes, *J. Phys. Chem. B*, *106*, 7177 (2002).
161. Koole, R., Liljeroth, P., de Mello Donega, C., Vanmaekelbergh, D., and Meijerink, A., Electronic Coupling and Exciton Energy Transfer in Cdte Quantum-Dot Molecules, *J. Am. Chem. Soc.* (2006).
162. Bayer, M., Hawrylak, P., Hinzer, K., Fafard, S., Korkusinski, M., Wasilewski, Z. R., Stern, O., and Forchel, A., Coupling and Entangling of Quantum States in Quantum Dot Molecules, *Science*, *291*, 451 (2001).
163. Chung, J. H., Ah, C. S., and Jang, D. J., Formation and Distinctive Decay Times of Surface- and Lattice-Bound Mn²⁺ Impurity Luminescence in Zns Nanoparticles, *J. Phys. Chem. B*, *105*, 4128 (2001).
164. Osovsky, R., Shavel, A., Gaponik, N., Amirav, L., Eychmuller, A., Weller, H., and Lifshitz, E., Electrostatic and Covalent Interactions in Cdte Nanocrystalline Assemblies, *J. Phys. Chem. B*, *109*, 20244 (2005).
165. Franzl, T., Koktysh, D. S., Klar, T. A., Rogach, A. L., Feldmann, J., and Gaponik, N., Fast Energy Transfer in Layer-by-Layer Assembled Cdte Nanocrystal Bilayers, *Appl. Phys. Lett.*, *84*, 2904 (2004).

166. Wuister, S. F., Koole, R., de Mello Donega, C., and Meijerink, A., Temperature-Dependent Energy Transfer in Cadmium Telluride Quantum Dot Solids, *J. Phys. Chem. B*, *109*, 5504 (2005).
167. Tang, Z., Zhang, Z., Wang, Y., Glotzer, S. C., and Kotov, N. A., Self-Assembly of Cdte Nanocrystals into Free-Floating Sheets, *Science*, *314*, 274 (2006).
168. Micic, O. I., Ahrenkiel, S. P., and Nozik, A. J., Synthesis of Extremely Small Inp Quantum Dots and Electronic Coupling in Their Disordered Solid Films, *Appl. Phys. Lett.*, *78*, 4022 (2001).
169. Wargnier, R., Baranov, A. V., Maslov, V. G., Stsiapura, V., Artemyev, M., Pluot, M., Sukhanova, A., and Nabiev, I., Energy Transfer in Aqueous Solutions of Oppositely Charged Cdse/Zns Core/Shell Quantum Dots and in Quantum Dot-Nanogold Assemblies, *Nano Lett.*, *4*, 451 (2004).
170. Achermann, M., Petruska, M. A., Crooker, S. A., and Klimov, V. I., Picosecond Energy Transfer in Quantum Dot Langmuir-Blodgett Nanoassemblies, *J. Phys. Chem. B*, *107*, 13782 (2003).
171. Kagan, C. R., Murray, C. B., and Bawendi, M. G., Long-Range Resonance Transfer of Electronic Excitations in Close-Packed Cdse Quantum-Dot Solids, *Phys. Rev. B Condens. Matter*, *54*, 8633 (1996).
172. Crooker, S. A., Hollingsworth, J. A., Tretiak, S., and Klimov, V. I., Spectrally Resolved Dynamics of Energy Transfer in Quantum-Dot Assemblies: Towards Engineered Energy Flows in Artificial Materials, *Phys. Rev. Lett.*, *89*, 186802 (2002).
173. Kagan, C. R., Murray, C. B., Nirmal, M., and Bawendi, M. G., Electronic Energy Transfer in Cdse Quantum Dot Solids, *Phys. Rev. Lett.*, *76*, 1517 (1996).
174. Zhao, X., and Zhang, S., Fabrication of Molecular Materials Using Peptide Construction Motifs, *Trends Biotechnol.*, *22*, 470 (2004).
175. Wu, L. Q., and Payne, G. F., Biofabrication: Using Biological Materials and Biocatalysts to Construct Nanostructured Assemblies, *Trends Biotechnol.*, *22*, 593 (2004).
176. Sidhu, S. S., Engineering M13 for Phage Display, *Biomol. Eng.*, *18*, 57 (2001).
177. Szardenings, M., Phage Display of Random Peptide Libraries: Applications, Limits, and Potential, *J. Recept. Signal Transduct. Res.*, *23*, 307 (2003).
178. Kehoe, J. W., and Kay, B. K., Filamentous Phage Display in the New Millennium, *Chem. Rev.*, *105*, 4056 (2005).
179. Whaley, S. R., English, D. S., Hu, E. L., Barbara, P. F., and Belcher, A. M., Selection of Peptides with Semiconductor Binding Specificity for Directed Nanocrystal Assembly, *Nature*, *405*, 665 (2000).
180. Sanghvi, A. B., Miller, K. P., Belcher, A. M., and Schmidt, C. E., Biomaterials Functionalization Using a Novel Peptide That Selectively Binds to a Conducting Polymer, *Nat. Mater.*, *4*, 496 (2005).

181. Nam, K. T., Peelle, B. R., Lee, S.-W., and Belcher, A. M., Genetically Driven Assembly of Nanorings Based on the M13 Virus, *Nano Lett.*, *4*, 23 (2003).
182. Lee, S. K., Yun, D. S., and Belcher, A. M., Cobalt Ion Mediated Self-Assembly of Genetically Engineered Bacteriophage for Biomimetic Co-Pt Hybrid Material, *Biomacromol.*, *7*, 14 (2006).
183. Scheibel, T., Parthasarathy, R., Sawicki, G., Lin, X. M., Jaeger, H., and Lindquist, S. L., Conducting Nanowires Built by Controlled Self-Assembly of Amyloid Fibers and Selective Metal Deposition, *Proc. Natl. Acad. Sci. USA*, *100*, 4527 (2003).
184. Mertig, M., Kirsch, R., and Pompe, W., Biomolecular Approach to Nanotube Fabrication, *Appl. Phys. A*, *66*, S723 (1998).
185. Banerjee, I. A., Yu, L., and Matsui, H., Cu Nanocrystal Growth on Peptide Nanotubes by Biomineralization: Size Control of Cu Nanocrystals by Tuning Peptide Conformation, *Proc. Natl. Acad. Sci. USA*, *100*, 14678 (2003).
186. Banerjee, I. A., Yu, L., and Matsui, H., Application of Host-Guest Chemistry in Nanotube-Based Device Fabrication: Photochemically Controlled Immobilization of Azobenzene Nanotubes on Patterned Alpha-Cd Monolayer/Au Substrates Via Molecular Recognition, *J. Am. Chem. Soc.*, *125*, 9542 (2003).
187. Banerjee, I. A., Yu, L., and Matsui, H., Room-Temperature Wurtzite Zns Nanocrystal Growth on Zn Finger-Like Peptide Nanotubes by Controlling Their Unfolding Peptide Structures, *J. Am. Chem. Soc.*, *127*, 16002 (2005).
188. Matsui, H., Gologan, B., Pan, S., and Douberly Jr, G. E., Controlled Immobilization of Peptide Nanotube-Templated Metallic Wires on Au Surfaces, *Eur. Phys. J. D*, *16*, 403 (2001).
189. Djalali, R., Chen, Y. F., and Matsui, H., Au Nanowire Fabrication from Sequenced Histidine-Rich Peptide, *J. Am. Chem. Soc.*, *124*, 13660 (2002).
190. Banerjee, I. A., Yu, L., and Matsui, H., Location-Specific Biological Functionalization on Nanotubes: Attachment of Proteins at the Ends of Nanotubes Using Au Nanocrystal Masks, *Nano Lett.*, *3*, 283 (2003).
191. Li, L.-S., and Stupp, S. I., One-Dimensional Assembly of Lipophilic Inorganic Nanoparticles Templated by Peptide-Based Nanofibers with Binding Functionalities, *Angew. Chem. Int. Ed.*, *44*, 1833 (2005).
192. Fu, X., Wang, Y., Huang, L., Sha, Y., Gui, L., Lai, L., and Tang, Y., Assemblies of Metal Nanoparticles and Self-Assembled Peptide Fibrils-Formation of Double Helical and Single-Chain Arrays of Metal Nanoparticles, *Adv. Mater.*, *15*, 902 (2003).
193. Ellis, A. V., Vijayamohanan, K., Goswami, R., Chakrapani, N., Ramanathan, L. S., Ajayan, P. M., and Ramanath, G., Hydrophobic Anchoring of Monolayer-Protected Gold Nanoclusters to Carbon Nanotubes, *Nano Lett.*, *3*, 279 (2003).
194. Ou, Y. Y., and Huang, M. H., High-Density Assembly of Gold Nanoparticles on Multiwalled Carbon Nanotubes Using 1-Pyrenemethylamine as Interlinker, *J. Phys. Chem. B*, *110*, 2031 (2006).

195. Han, L., Wu, W., Kirk, F. L., Luo, J., Maye, M. M., Kariuki, N. N., Lin, Y., Wang, C., and Zhong, C. J., A Direct Route toward Assembly of Nanoparticle-Carbon Nanotube Composite Materials, *Langmuir*, *20*, 6019 (2004).
196. Li, C. P., Sun, X. H., Wong, N. B., Lee, C. S., Lee, S. T., and Teo, B. K., Silicon Nanowires Wrapped with Au Film, *J. Phys. Chem. B*, *106*, 6980 (2002).
197. Hassenkam, T., Moth-Poulsen, K., Stuhr-Hansen, N., Norgaard, K., Kabir, M. S., and Bjornholm, T., Self-Assembly and Conductive Properties of Molecularly Linked Gold Nanowires, *Nano Lett.*, *4*, 19 (2004).
198. Ravi Kumar, M. N., Sameti, M., Mohapatra, S. S., Kong, X., Lockey, R. F., Bakowsky, U., Lindenblatt, G., Schmidt, H., and Lehr, C. M., Cationic Silica Nanoparticles as Gene Carriers: Synthesis, Characterization and Transfection Efficiency in Vitro and in Vivo, *J Nanosci Nanotechnol*, *4*, 876 (2004).
199. Balmes, O., Bovin, J. O., and Malm, J. O., Self-Healing and Self-Organized Gold Nanoparticle Films at a Water/Organic Solvent Interface, *J. Nanosci. Nanotechnol.*, *6*, 130 (2006).
200. Dujardin, E., Peet, C., Stubbs, G., Culver, J. N., and Mann, S., Organization of Metallic Nanoparticles Using Tobacco Mosaic Virus Templates, *Nano Lett.*, *3*, 413 (2003).
201. Radloff, C., Vaia, R. A., Brunton, J., Bouwer, G. T., and Ward, V. K., Metal Nanoshell Assembly on a Virus Bioscaffold, *Nano Lett.*, *5*, 1187 (2005).
202. Storhoff, J. J., Lazarides, A. A., Mucic, R., Mirkin, C., Letsinger, R., and Schatz, G. C., What Controls the Optical Properties of DNA-Linked Gold Nanoparticle Assemblies? *J. Am. Chem. Soc.*, *122*, 4640 (2000).
203. Harnack, O., Ford, W. E., Yasuda, A., and Wessels, J. M., Tris(Hydroxymethyl)Phosphine-Capped Gold Particles Templated by DNA as Nanowire Precursors, *Nano Lett.*, *2*, 919 (2002).
204. Zheng, J., Constantinou, P. E., Micheel, C., Alivisatos, A. P., Kiehl, R. A., and Seeman, N. C., Two-Dimensional Nanoparticle Arrays Show the Organizational Power of Robust DNA Motifs, *Nano Lett.*, *6*, 1502 (2006).
205. Lisiecki, I., Filankembo, A., Sack-Kongehl, H., Weiss, K., Pileni, M. P., and Urban, J., Structural Investigations of Copper Nanorods by High-Resolution Tem, *Phys. Rev. B*, *61*, 4968 (2000).
206. Jiang, X., Herricks, T., and Xia, Y., Cuo Nanowires Can Be Synthesized by Heating Copper Substrates in Air, *Nano Lett.*, *2*, 1333 (2002).
207. Liu, Z., and Bando, Y., A Novel Method for Preparing Copper Nanorods and Nanowires, *Adv. Mater.*, *15*, 303 (2003).
208. Gonzalez, J. C., Rodrigues, V., Bettini, J., Rego, L. G. C., Rocha, A. R., Coura, P. Z., Dantas, S. O., Sato, F., Galvao, D. S., and Ugarte, D., Indication of Unusual Pentagonal Structures in Atomic-Size Cu Nanowires, *Phys. Rev. Lett.*, *93*, 126103 (2004).
209. Li, N., Li, X., Yin, X., Wang, W., and Qiu, S., Electroless Deposition of Open-End Cu Nanotube Arrays, *Solid State Commun.*, *132*, 841 (2004).

210. Luo, Y. H., Huang, J., Jin, J., Peng, X., Schmitt, W., and Ichinose, I., Formation of Positively Charged Copper Hydroxide Nanostrands and Their Structural Characterization, *Chem. Mater.*, *18*, 1795 (2006).
211. Setlur, A. A., Lauerhaas, J. M., Dai, J. Y., and Chang, R. P. H., A Method for Synthesizing Large Quantities of Carbon Nanotubes and Encapsulated Copper Nanowires, *Appl. Phys. Lett.*, *69*, 345 (1996).
212. Ziegler, K. J., Harrington, P. A., Ryan, K. M., Crowley, T., Holmes, J. D., and Morris, M. A., Supercritical Fluid Preparation of Copper Nanotubes and Nanowires Using Mesoporous Templates, *J. Phys. Condens. Matter*, *15*, 8303 (2003).
213. Monson, C. F., and Woolley, A. T., DNA-Templated Construction of Copper Nanowires, *Nano Lett.*, *3*, 359 (2003).
214. Ren, L., Guo, L., Wark, M., and Hou, Y., Self-Integration of Aligned Cobalt Nanoparticles into Silica Nanotubes, *Appl. Phys. Lett.*, *87*, 212503 (2005).
215. Bezemer, G. L., Bitter, J. H., Kuipers, H. P. C. E., Oosterbeek, H., Holewijn, J. E., Xu, X., Kapteijn, F., vanDillen, A. J., and deJong, K. P., Cobalt Particle Size Effects in the Fischer-Tropsch Reaction Studied with Carbon Nanofiber Supported Catalysts, *J. Am. Chem. Soc.*, *128*, 3956 (2006).
216. Yu, S., Welp, U., Hua, L. Z., Rydh, A., Kwok, W. K., and Wang, H. H., Fabrication of Palladium Nanotubes and Their Application in Hydrogen Sensing, *Chem. Mater.*, *17*, 3445 (2005).
217. Ye, X.-R., Lin, Y., Wang, C., Engelhard, M. H., Wang, Y., and Wai, C. M., Supercritical Fluid Synthesis and Characterization of Catalytic Metal Nanoparticles on Carbon Nanotubes, *J. Mater. Chem.*, *14*, 908 (2004).
218. Hull, R. V., Li, L., Xing, Y., and Chusuei, C. C., Pt Nanoparticle Binding on Functionalized Multiwalled Carbon Nanotubes, *Chem. Mater.*, *18*, 1780 (2006).
219. Richter, J., Seidel, R., Kirsch, R., Mertig, M., Pompe, W., Plaschke, J., and Schackert, H. K., Nanoscale Palladium Metallization of DNA, *Adv. Mater.*, *12*, 507 (2000).
220. Behrens, S., Rahn, K., Habicht, W., Böhm, K.-J., Rösner, H., Dinjus, E., and Unger, E., Nanoscale Particle Arrays Induced by Highly Ordered Protein Assemblies, *Adv. Mater.*, *14*, 1621 (2002).
221. Song, Y., Challa, S. R., Medforth, C. J., Qiu, Y., Watt, R. K., Peña, D., Miller, J. E., van Swol, F., and A., S. J., Synthesis of Peptide-Nanotube Platinum-Nanoparticle Composites, *Chem. Commun. (Camb.)*, 1044 (2004).
222. Barbic, M., Mock, J. J., Smith, D. R., and Schultz, S., Single Crystal Silver Nanowires Prepared by the Metal Amplification Method, *J. Appl. Phys.*, *91*, 9341 (2002).
223. Sioss, J. A., and Keating, C. D., Batch Preparation of Linear Au and Ag Nanoparticle Chains Via Wet Chemistry, *Nano Lett.*, *5*, 1779 (2005).
224. Braun, E., Eichen, Y., Sivan, U., and Ben-Yoseph, G., DNA-Templated Assembly and Electrode Attachment of a Conducting Silver Wire, *Nature*, *391*, 775 (1998).

225. Carny, O., Shalev, D. E., and Gazit, E., Fabrication of Coaxial Metal Nanocables Using a Self-Assembled Peptide Nanotube Scaffold, *Nano Lett.* (2006).
226. Gao, P., Zhan, C., and Liu, M., Controlled Synthesis of Double- and Multiwall Silver Nanotubes with Template Organogel from a Bolaamphiphile, *Langmuir*, 22, 775 (2006).
227. Hutter, E., and Fendler, J. H., Size Quantized Formation and Self-Assembly of Gold Encased Silver Nanoparticles, *Chem. Commun. (Camb)*, 378 (2002).
228. Lee, S. W., and Belcher, A. M., Virus-Based Fabrication of Micro- and Nanofibers Using Electrospinning, *Nano Lett.*, 4, 387 (2004).
229. Matsui, H., and Douberly, G. E., Organization of Peptide Nanotubes into Macroscopic Bundles, *Langmuir*, 17, 7918 (2001).
230. Gao, X., and Matsui, H., Peptide-Based Nanotubes and Their Applications in Bionanotechnology, *Adv. Mater.*, 17, 2037 (2005).
231. Khalil, A. S., Ferrer, J. M., Brau, R. R., Kottmann, S. T., Noren, C. J., Lang, M. J., and Belcher, A. M., Single M13 Bacteriophage Tethering and Stretching, *Proc Natl Acad Sci U S A*, 104, 4892 (2007).
232. Sambrook, J., and Russell, D., *Molecular Cloning: A Laboratory Manual*, Cold Spring Harbor Laboratory Press, Cold Spring Harbor, NY (2001).
233. Lu, Z., Murray, K. S., Van Cleave, V., LaVallie, E. R., Stahl, M. L., and McCoy, J. M., Expression of Thioredoxin Random Peptide Libraries on the Escherichia Coli Cell Surface as Functional Fusions to Flagellin: A System Designed for Exploring Protein-Protein Interactions, *Biotechnology (N Y)*, 13, 366 (1995).
234. Tripp, B. C., 15% Cross-Linked Sds-Page Gels Were Prepared and Run Using a Bio-Rad (Hercules, Ca) Mini-Protean 3 Gel Apparatus. Gels Were Run at Constant Current with an Initial Voltage of 130 Volts for 1.5 H and Were Stained with Coomassie Brilliant Blue R-250 Dye. (2006).
235. Tripp, B. C., Lu, Z., Bourque, K., Sookdeo, H., and McCoy, J. M., Investigation of the 'Switch-Epitope' Concept with Random Peptide Libraries Displayed as Thioredoxin Loop Fusions, *Protein Eng.*, 14, 367 (2001).
236. Macnab, R. M., Type Iii Flagellar Protein Export and Flagellar Assembly, *Biochim. Biophys. Acta*, 1694, 207 (2004).
237. Ashkin, A., Optical Trapping and Manipulation of Neutral Particles Using lasers, *Proc Natl Acad Sci U S A*, 94, 4853 (1997).
238. Bushuk, S. B., Kruchenok, A. J. V., Kurilo, A. G. I., Nemkovich, A. N. A., and Rubinov, A. A. N., Orientation of Erythrocytes in the Fringes of an Interference Laser Field, *J. Opt A: P Appl. Opt.*, 8, 1464 (2005).
239. Malapaka, R. R., Adebayo, L. O., and Tripp, B. C., A Deletion Variant Study of the Functional Role of the Salmonella Flagellin Hypervariable Domain Region in Motility, *J Mol Biol* (2006).
240. Jones, C. J., and Aizawa, S., The Bacterial Flagellum and Flagellar Motor: Structure, Assembly and Function, *Adv. Microb. Physiol.*, 32, 109 (1991).

241. Decher, G., Hong, J. D., and J. S., Buildup of Ultrathin Multilayer Films by a Self-Assembly Process: Iii. Consecutively Alternating Adsorption of Anionic and Cationic Polyelectrolytes on Charged Surfaces, *Thin Solid Films*, 210-211, 831 (1992).
242. Decher, G., Fuzzy Nanoassemblies: Toward Layered Polymeric Multicomposites, *Science*, 277, 1232 (1997).
243. R, V. K., Internal Structure of Polyelectrolyte Multilayer Assemblies, *Phys Chem Chem Phys*, 8, 5012 (2006).
244. Li, Q., Quinn, J. F., Wang, Y., and Caruso, F., Preparation of Nanoporous Polyelectrolyte Multilayer Films Via Nanoparticle Templating, *Chem. Mater.*, 18, 5480 (2006).
245. C. Jiang, V. V. T., Freestanding Nanostructures Via Layer-by-Layer Assembly, *Advanced Materials*, 18, 829 (2006).
246. Rauf, S., Zhou, D., Abell, C., Klenerman, D., and Kang, D.-J., Building Three-Dimensional Nanostructures with Active Enzymes by Surface Templated Layer-by-Layer Assembly, *Chemical Communications*, 1721 (2006).
247. Serizawa, T., Yamaguchi, M., and Akashi, M., Time-Controlled Desorption of Ultrathin Polymer Films Triggered by Enzymatic Degradation, *Angew Chem Int Ed Engl*, 42, 1115 (2003).
248. Kokkoli, E., Mardilovich, A., Wedekind, A., Rexeisen, E. L., Garg, A., and Craig, J. A., Self-Assembly and Applications of Biomimetic and Bioactive Peptide-Amphiphiles, *Soft Matter*, 2, 1015 (2006).
249. Haynie, D. T., Zhang, L., Rudra, J. S., Zhao, W., Zhong, Y., and Palath, N., Polypeptide Multilayer Films, *Biomacromolecules*, 6, 2895 (2005).
250. Tian, Y., He, Q., Cui, Y., and Li, J., Fabrication of Protein Nanotubes Based on Layer-by-Layer Assembly, *Biomacromolecules*, 7, 2539 (2006).
251. Serizawa, T., Yamaguchi, M., and Akashi, M., Alternating Bioactivity of Polymeric Layer-by-Layer Assemblies: Anticoagulation Vs Procoagulation of Human Blood, *Biomacromolecules*, 3, 724 (2002).
252. Yoo, P. J., Nam, K. T., Qi, J., Lee, S. K., Park, J., Belcher, A. M., and Hammond, P. T., Spontaneous Assembly of Viruses on Multilayered Polymer Surfaces, *Nat Mater*, 5, 234 (2006).
253. Suci, P. A., Klem, M. T., Arce, F. T., Douglas, T., and Young, M., Assembly of Multilayer Films Incorporating a Viral Protein Cage Architecture, *Langmuir*, 22, 8891 (2006).
254. Vonderviszt, F., Imada, K., Furukawa, Y., Uedaira, H., Taniguchi, H., and Namba, K., Mechanism of Self-Association and Filament Capping by Flagellar Hap2, *J Mol Biol*, 284, 1399 (1998).
255. Yonekura, K., Maki-Yonekura, S., and Namba, K., Structure Analysis of the Flagellar Cap-Filament Complex by Electron Cryomicroscopy and Single-Particle Image Analysis, *J Struct Biol*, 133, 246 (2001).

256. Malapaka, V. R., and Tripp, B. C., A Theoretical Model of Aquifex Pyrophilus Flagellin: Implications for Its Thermostability, *J Mol Model*, *12*, 481 (2006).
257. Park, T. J., Lee, S. Y., Lee, S. J., Park, J. P., Yang, K. S., Lee, K. B., Ko, S., Park, J. B., Kim, T., Kim, S. K., Shin, Y. B., Chung, B. H., Ku, S. J., Kim, D. H., and Choi, I. S., Protein Nanopatterns and Biosensors Using Gold Binding Polypeptide as a Fusion Partner, *Anal. Chem.*, *78*, 7197 (2006).
258. Scheibel, T., Parthasarathy, R., Sawicki, G., Lin, X. M., Jaeger, H., and Lindquist, S. L., Conducting Nanowires Built by Controlled Self-Assembly of Amyloid Fibers and Selective Metal Deposition, *Proc Natl Acad Sci U S A*, *100*, 4527 (2003).
259. Hersam, M. C., Hoole, A. C. F., Shea, S. J. O., and Welland, M. E., Potentiometry and Repair of Electrically Stressed Nanowires Using Atomic Force Microscopy, *Applied Physics Letters*, *72*, 915 (1998).
260. Ziegler, K. J., Polyakov, B., Kulkarni, J. S., Crowley, T. A., Ryan, K. M., Morris, M. A., Erts, D., and Holmes, J. D., Conductive Films of Ordered Nanowire Arrays, *Journal of Materials Chemistry*, *14*, 585 (2004).
261. Zhou, G., Lu, M., and Yang, Z., Aqueous Synthesis of Copper Nanocubes and Bimetallic Copper/Palladium Core-Shell Nanostructures, *Langmuir*, *22*, 5900 (2006).
262. Slocik, J. M., Tam, F., Halas, N. J., and Naik, R. R., Peptide-Assembled Optically Responsive Nanoparticle Complexes, *Nano Lett.*, *7*, 1054 (2007).
263. Huang, L., Wang, C. J., and Lin, L. Y., Comparison of Cross-Talk Effects between Colloidal Quantum Dot and Conventional Waveguides, *Opt Lett*, *32*, 235 (2007).
264. Hohng, S., Joo, C., and Ha, T., Single-Molecule Three-Color FRET, *Biophys J*, *87*, 1328 (2004).
265. Lee, N. K., Kapanidis, A. N., Koh, H. R., Korlann, Y., Ho, S. O., Kim, Y., Gassman, N., Kim, S. K., and Weiss, S., Three-Color Alternating-Laser Excitation of Single Molecules: Monitoring Multiple Interactions and Distances, *Biophys J*, *92*, 303 (2007).
266. C.-Y. Chiang, J., C. M. M., G. E. C., C. M. S. K., Van Vliet, J., and Belcher, A. M., Weaving Genetically Engineered Functionality into Mechanically Robust Virus Fibers, *Adv. Mater.*, *19*, 826 (2007).
267. Khalil, A. S., Ferrer, J. M., Brau, R. R., Kottmann, S. T., Noren, C. J., Lang, M. J., and Belcher, A. M., Single M13 Bacteriophage Tethering and Stretching, *Proc Natl Acad Sci U S A*, *104*, 4892 (2007).

APPENDIX**DNA Primers AND Resulted DNA Sequences**

Multiple cloning site CYS₃₂-GLY₃₃- PEPTIDEPVCWAQPARSELAAAISLARG,-
 PRO₃₄-CYS₃₅

Peptide removed from multiple cloning site

PEPTIDEPVCWAQPARSELAAAISLARG

DNA primers used to generate RsrII restriction digestion sites

RsrII site one

Foreword primer

5'-GCA GAG TGG TGC GGT CCG GTG TGC TGG GCC CAG C-3'

Reversed primer

5'-GCT GGG CCC AGC ACA CCG GAC CGC ACC ACT CTG C-3'

RsrII site two

Foreword primer

5'-CCG CGA TAT CGC TAG CTC GCG GTC CGT GCA AAA TGA TCG CCC-3'

Reversed primer

5'-GGG CGA TCA TTT TGC ACG GAC CGC GAG CTA GCG ATA TCG GGG-
 3'.

Primers used to mutate unwanted cysteine (CYS353SER mutation) to serine

Forward primer

5'-CCT CGA CGC TAA CCT GGC CTC TGC CGC CAG TTC TCC AAC CG-3'

Reverse primer

5'-CGG TTG GAG AAC TGG CGG CAG AGG CCA GGT TAG CGT CGA GG-3'

DNA primers used to generate cysteine loops

Forward primer

5'-GT CAC TGT TGC TGT TGC TGT TGC G-3

Reverse primer

5'-G ACC GCA ACA GCA ACA GCA ACA GT-3'

DNA primes used to generate histidine loops

Forward primer

5'-GTC ATC ACC ATC ACC ATC ACG-3'

Reverse primer

5'-GAC CGT GAT GGT GAT GGT GAT-3'

DNA primes used to generate acid loops

Forward primer

5'-GTC GCA AGC GTA AGC GCA AGC-3'

Reverse primer

5'-GAC GCT TGC GCT TAC GCT TGC-3'

DNA primes used to generate arginine-lysine loops

Forward primer

5'-GTC GCA AGC GTA AGC GCA AGC-3'

Reverse primer

5'-GAC GCT TGC GCT TAC GCT TGC-3'

DNA primes used to generate tyrosine loops

Forward primer

5'-GTC ACT ATA GCT ACG GTT ACT CCT ACG GCT ACT CTT ATG-3'

Reverse primer

5'-GAC CAT AAG AGT AGC CGT AGG AGT AAC CGT AGC TAT AGT-3'

Primers used to mutate tryptophan to tyrosine(Trp272Tyr, Trp275Tyr)

First mutation (Trp272Tyr)

Forward primer

5' GAT CCT CGT CGA TTT CTA CGC AGA GTG GTG CGG TC 3'

Reverse primer

5' GAC CGC ACC ACT CTG CGT AGA AAT CGA CGA GGA TC 3'

Second mutation (Trp275Tyr)

Forward primer

5' GATTTCTACGCAGAGTACTGCGGTCATCACCATC 3'

Reverse primer

5' GATGGTGATGACCGCAGTACTCTGCGTAGAAATC 3'

1 Cys-Loop

GATGTA CTCAAAGCGGACGGGGCGATCCTCGTCGATTTCTGGGCAGAGTG
 GTGCGGTC ACTGTTGCTGTTGCTGTTGCGGTCCGTGCAAAATGATCGCCCC
 GATTCTGGATGAAATCGCTGACGAATATCAGGGCAA ACTGACCGTTGCAA
 AACTGAACATCGATCAA AACCTGGCACTGCGCCGAAATATGGCATCCGT

2 Cys-Loop

GATGTA CTCAAAGCGGACGGGGCGATCCTCGTCGATTTCTGGGCAGAGTG
 GTGCGG TCACTGTTGCTGTTGCTGTTGCGG TCACTGTTGCTGTTGCTGTTG
 CGGTCCGTGCAA AATGATCGCCCCGATTCTGGATGAAATCGCTGACGAAT
 ACAGGGCAA ACTGACCGTTGCAA AACTGAACATCGATCAA AACCTGGC
 ACTGCGCCGAA ATATGGCATCCGTGGTATCCCGACTCTGCTGCTGTTCAA
 AAACGGTGA AGTGGCGGCAACCAAAGTGGGTGCACTGTCTAAAGGTCAG
 TTGAAAGAGTTCCTCGACGCTAACCTGGCCTCTGCCGCCAGTTCTCCAACC
 GCGGTCAA ACTGGGCGGAGATGATGGCAA AACAGAAGTGGTCGATATTG
 ATGGTAA AACATACGATTCTGCCGATTTAAATGGCGGTAATCTGCAAACA
 GGTTTGACT

His loops(24H)

GGG GCG ATC CTC GTC GAT TTC TGG GCA GAG TGG TGC GGT CAT
 CAC CAT CAC CAT CAC GGT CAT CAC CAT CAC CAT CAC GGT CAT
 CAC CAT CAC CAT CAC GGT CAT CAC CAT CAC CAT CAC GGT CCG
 TGC AAA ATG ATC GCC CCG ATT CTG GAT GAA ATC GCT GAC GAA
 TAT CAG GGC AAA CTG ACC GTT GCA AAA CTG AAC ATC GAT CAA
 AAC CCT GGC ACT GCG CCG AAA TAT GGC ATC CGT GGT ATC CCG
 ACT CTG CTG CTG TTC AAA AAC GGT GAA GTG GCG GCA ACC AAA
 GTG GGT GCA CTG TCT AAA GGT CAG TTG AAA GAG TTC CTC GAC

Acid loop

GGG GCG ATC CTC GTC GAT TTC TGG GCA GAG TGG TGC GGT CAC
GAC GAA GAT GAG GAC GAA GGT CAC GAC GAA GAT GAG GAC GAA
GGT CAC GAC GAA GAT GAG GAC GAA GGT CCG TGC AAA ATG ATC
GCC CCG ATT CTG GAT GAA ATC GCT GAC GAA TAT CAG GGC AAA
CTG ACC GTT GCA AAA CTG AAC ATC GAT CAA AAC CCT GGC ACT
GCG CCG AAA TAT GGC ATC CGT GGT ATC CCG ACT CTG CTG CTG
TTC AAA AAC GGT GAA GTG GCG GCA ACC AAA GTG GGT GCA CTG
TCT AAA GGT CAG TTG AAA GAG TTC CTC GAC GCT AAC CTG GCC

Arg-lys loop

GGG GCG ATC CTC GTC GAT TTC TGG GCA GAG TGG TGC GGT CGC
AAG CGT AAG CGC AAG CGT CCG TGC AAA ATG ATC GCC CCG ATT
CTG GAT GAA ATC GCT GAC GAA TAT CAG GGC AAA CTG ACC GTT
GCA AAA CTG AAC ATC GAT CAA AAC CCT GGC ACT GCG CCG AAA
TAT GGC ATC CGT GGT ATC CCG ACT CTG CTG CTG TTC AAA AAC
GGT GAA GTG GCG GCA ACC AAA GTG GGT GCA CTG TCT AAA GGT
CAG TTG AAA GAG TTC CTC GAC GCT AAC CTG GCC TCT GCC GCC